Characterisation of Brainstem Lateral Line Neurons in Goldfish, *Carassius auratus*: Frequency Selectivity, Spatial Excitation Patterns and Flow Sensitivity

Dissertation

Zur
Erlangung der Doktorgrades (Dr. rer. nat.)
der
Mathematisch-Naturwissenschaftlichen Fakultät
der
Rheinischen Friedrich-Wilhelms-Universität

vorgelegt von
Silke Künzel
aus Linnich

Bonn Oktober 2009

Angefertigt mit Genehmigung der Mathematisch-Naturwissenschaftlichen Fakultät der Rheinischen Friedrich-Wilhelms-Universität Bonn

1. Gutachter: PD Dr. J. Mogdans
2. Gutachter: Prof. Dr. H. Bleckmann

Tag der Promotion: 21.12.2009

Erscheinungsjahr: 2010

ABSTRACT

In the present study lateral line units in the medial octavolateral nucleus (MON) in the brainstem in goldfish, *Carassius auratus,* were extracellulary recorded. The aim of the work was to investigate and characterize the response behaviour of these units to different hydrodynamic stimuli to learn more about central processing of lateral line information. It was investigated how MON units respond to a vibrating sphere in terms of different frequencies, locations, and sphere vibration directions. The spatial excitation patterns of Mon units were described and finally the response behaviour to water flow in different directions and velocities.

The responses of MON units to a vibrating sphere presented with various vibration frequencies were analyzed and described. Most of the units exhibited a change in discharge rate and/or phase-locking to at least one of the applied stimulation frequencies (90.4 %). Three groups of units were distinguished. Units from Group 1 (9.6 %) responded with a change in discharge rate and/or a phase coupling to only one, units from Group 2 responded to two (25.5 %), and units from Group 3 (55.3 %) responded to all three applied stimulation frequencies. Eighty-six out of ninety-four units responded to any of the applied frequencies with an increase or a decrease in discharge rate and/or with phase coupling. Eight units did not respond to any of the presented stimuli. The current findings demonstrate that response behaviour, patterns of discharge and frequency response characteristics of brainstem lateral line units are much more diverse than those of primary afferents. Most MON units responded preferentially to one particular stimulus frequency. 45 % of the units showed their strongest response in terms of discharge rate (increase or decrease) and/or phase locking to the 50 Hz stimulus, 42 % in response to 100 Hz, and 13 % to 20 Hz. Thus, many MON units exhibited band-pass, high-pass, or low-pass characteristics.

Theoretical data suggest that information on the position of a vibrating source is linearly coded in the spatial characteristics of the excitation pattern of pressure gradients distributed along the lateral line (Curcic-Blake and van Netten 2006). The theoretical predictions were confirmed by neurophysiologic experiments performed

on single fibres in the posterior lateral line nerve of goldfish, demonstrating that the location and separation of peaks and troughs in the neuronal responses change in a predictable way with location and vibration angle of a dipole, i.e., sinusoidally vibrating sphere. If a central unit would receive input from peripheral receptors then this central unit would directly encode for object location. It was searched for such units in medial octavolateralis nucleus in the fish brainstem by systematically investigating spatial excitation properties with a sinusoidally vibrating sphere. Spike activity evoked by the sphere was recorded as function of sphere location alongside the fish and different angles of sphere vibration (0°=parallel to the fish, 90°=perpendicular to the fish, 45° and 135°). The current data show that MON units exhibit very variable spatial excitation patterns. Excitation patterns with single excitatory or inhibitory areas were found as well as excitation patterns with two or more excitatory or inhibitory areas. Further excitation patterns exhibited broad areas of increased or decreased discharge rate along a big part of the fish's body as response to stimulation. The observed effects were different from those predicted for primary afferent fibres. Units with a distinct stimulation direction preference were not observed. Nevertheless, most of the MON units showed different responses to the given vibration directions. The changes were not that regularly or predictable like in primary afferent fibres. In most of the units the generally shape of their excitation patterns stayed nearly stable at the different vibration directions. The differences insisted in shifts of the excitation patterns flanks. Some other units changed number or location of the response peaks. These data suggest that pressure gradient patterns are not represented by MON units as they are by the lateral line periphery. This implies that information about the sinusoidally vibrating sphere may be inferred from brainstem excitation patterns. For the first time is shown that there are effects of sphere vibration angle on the excitation pattern shape and size on lateral line units in the fish brainstem.

Literature suggests that fluctuations within a water flow may be used to determine flow direction and flow velocity by comparing inputs from an array of peripheral receptors. To test, this hypothesis, we recorded the activity from brainstem units in response to water flow. We analyzed the response characteristics with special respect to directional sensitivity to flow passing the fish from anterior to posterior and opposite, i.e. from posterior to anterior. If brainstem units indeed determine flow

velocity and flow direction by comparing inputs from two or more neuromasts that are organized in series on the fish surface, then units should be found that respond preferentially to particular flow velocities and flow directions. The spike activity of brainstem units in response to different constant flow velocities and continuously rising flow was systematically investigated. The data show that different MON units can exhibit quite variable responses to water flow. Moreover, most responses were different from those described for primary afferent fibres. Units were found that responded with an increase in discharge rate to both flow directions, with a decrease in both directions and units that exhibit an increase and/or decrease depending on flow direction. Units with a clear preference for a distinct flow velocity, i.e., units that responded only to a particular flow velocity, were not found. A few units differed in their responses to the presented flow directions. However, MON units apparently do not encode water velocities and directions in the same way as primary lateral line afferent fibres.

ABBREVIATIONS

ALLN	Anterior Lateral Line Nerve
AP	Anterior - Posterior
CN	Canal Neuromast
CNS	Central Nervous System
DON	Descending Octaval Nucleus, Dorsal Octavolateral Nucleus
HMW	Half Maximum Width
IF	Instantaneous Frequency
MON	Medial Octavolateral Nucleus
PA	Posterior - Anterior
PLLN	Posterior Lateral Line Nerve
PSTH	Peri Stimulus Time Histogram
RMS	Root Mean Square
SDI	Signed Directivity Index
SN	Superficial Neuromast
VRF	Velocity Response Function

INDEX

1. INTRODUCTION

The mechanosensory lateral line of fishes and aquatic amphibians detects water motions generated by biotic and abiotic sources. It plays a dominant role in many behaviours including rheotaxis (e.g., Montgomery et al. 1997, Kanter and Coombs 2003, Simmons et al. 2004), schooling (e.g., Partridge and Pitcher 1980), object recognition (e.g., von Campenhausen et al. 1981), communication (e.g., Satou et al. 1994), prey capture (e.g., New et al. 2001, Kanter and Coombs 2003) and predator avoidance (e.g., Blaxter and Fuiman 1990).

The lateral line of fish is almost permanently subject to sensory stimulation because either the fish or the water surrounding the fish is moving. Water movements are produced by abiotic sources such as currents (rivers and streams), wind, tidal currents, obstacles (substrate heterogeneity, stones, wood), and on the water surface by fallen leaves, drops, twigs, seeds and insects (review: Bleckmann 1994). Biotic sources of water movement are predators, prey (fish, zooplankton, insects), and conspecifics (Bleckmann et al. 1991). In addition, fish produce flow fields around their bodies due to relative movement between the skin and the surrounding water.

The sensory units of the lateral line are neuromasts, which are spread across large portions of the body surface (Figure 1A). In fish, two types of neuromasts exist, superficial neuromasts (SN) that are freestanding on the surface of the skin, and canal neuromasts (CN) that are embedded in lateral line canals (Northcutt 1989, Figure 1B). Usually there is one CN between two adjacent canal pores (Disler 1977, Puzdrowski 1989; Webb 1989, Engelmann et al. 2002). Goldfish, *Carassius auratus*, have a continuous lateral line canal system. It consists of supraorbital, infraorbital, operculomandibular and supratemporal commissural canals on the head and a trunk canal extending the length of the trunk (Puzdrowski 1989). Goldfish possess up to 200 CNs and up to 3000 SNs distributed over their head, trunk and tail fin (Puzdrowski 1989, Schmitz et al. 2008, Figure 1A).

Each neuromast consists of supporting cells, mantle cells and sensory hair cells (Münz 1979). The sensory epithelium of lateral line neuromasts can contain up to several hundred hair cells. Each of them carries up to 150 stereovilli and one kinocilium on its apical surface. The stereovilli increase in length from one side of the hair bundle to the other with the kinocilium always occurring eccentrically at the very edge of the bundle next to the longest stereovillus (Figure 1B). Thus, all hair cells have a morphological polarization. Within each neuromast, two populations of hair cells occur with antagonistically oriented ciliary bundles (Flock and Wersäll 1962). Thus, neuromasts have a polarization axis that is determined by the hair cell's polarization axis. The ciliary bundles of the hair cells are embedded in a gelatinous cupula that extends into the canal fluid (CN) or into the surrounding water (SN) (Flock 1971, Jørgensen and Flock 1973). On the fish surface, the orientation of SNs is typically such that their morphological polarization is either parallel or orthogonal to the rostro-caudal body axis (Coombs et al. 1988, Engelmann et al. 2002, Schmitz et al. 2008). In contrast, CNs are oriented such that their morphological polarization is parallel to the long axis of the canal (Engelmann et al. 2002, Schmitz et al. 2008).

Neuromasts are innervated by afferent and efferent fibres (Puzdrowski 1989). Neuromasts on the trunk of the fish are innervated by fibres of the posterior lateral line nerve (PLLN) whereas neuromasts located on the head are innervated by fibres of the dorsal or ventral anterior lateral line nerve (ALLN, Puzdrowski 1989). Individual afferent fibres innervate either a single CN or a single SN, or more than one SN located close together (Münz 1985, Bleckmann 1986, Schellart et al. 1992). Within each neuromast, an afferent fibre innervates more than one hair cell but only hair cells of identical orientation (Görner 1963, Figure 1B).

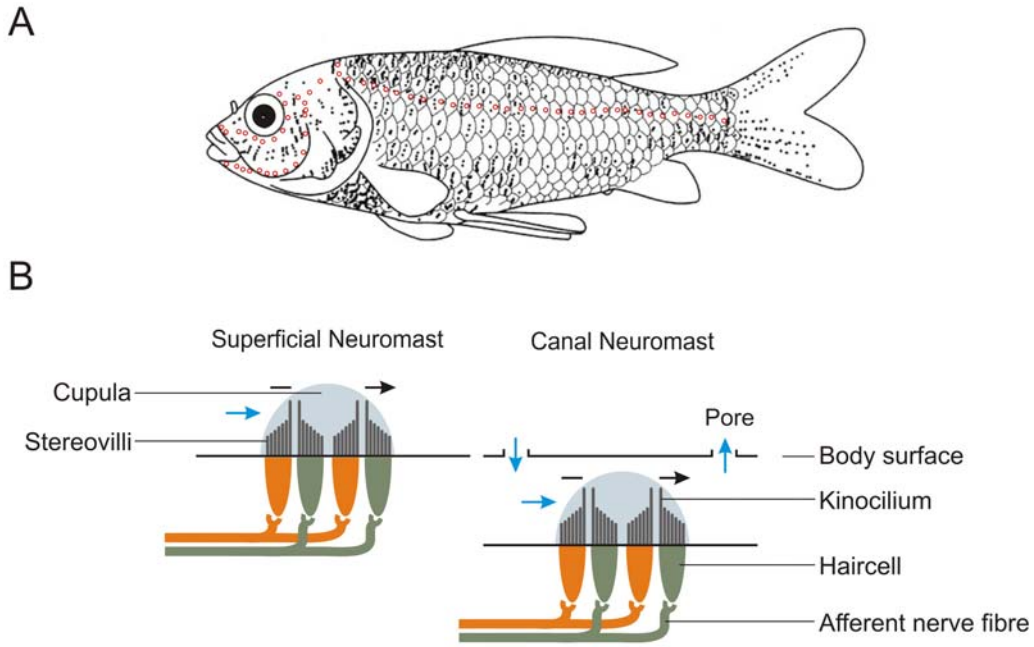

Figure 1: A: Distribution of neuromasts in the goldfish, *Carassius auratus*. Black dots indicate superficial neuromasts, red circles indicate lateral line canal pores. Modified after A. Grotefeld (Bleckmann 2004).
B: Schematic illustration of a superficial (left) and canal neuromast (right) and their afferent innervation. Different colours refer to different haircell orientations. Illustration is not drawn to scale. Arrows indicate fluid movement (blue) and cupula movement (black).

The adequate stimulus for lateral line neuromasts is fluid movement around the cupula. A displacement of the cupula induced by water movements causes shearing of the hair bundles (van Netten and Kroese 1987) leading to a change of the hair cells' resting potential. Movement of the ciliary bundle towards the kinocilium causes a depolarization, displacement in the opposite direction a hyperpolarisation of the hair cell (Kroese and van Netten 1989). Due to the antagonistic orientation of the hair cells within a neuromast, cupula motion in one direction causes a depolarization in one hair cell population and a hyperpolarisation in the other. Consequently, this leads to an increase in discharge rate of fibres innervating one population of hair cells and to a decrease in discharge rate of fibres innervating the hair cells aligned in the opposite direction.

SNs are typically smaller than CNs and function as velocity detectors, i.e., they respond proportional to the velocity of the water surrounding the cupula. In contrast, CNs function as acceleration detectors, i.e., they respond proportional to the acceleration of the water outside the canal (Coombs and Janssen 1990, Kroese and

Schellart 1992). Since water flow inside the canals is only produced by pressure differences between canal pores CNs can also be considered pressure gradient detectors (Denton and Gray 1988, Coombs et al. 1996). Lateral line canals act as high-pass filters (Denton and Gray 1988). Consequently, CNs should not be stimulated by laminar direct current (d.c.) water flow (Denton and Gray 1988, Voigt et al. 2000). However, CNs respond to the alternating current (a.c.) components of prey-generated water motions even in the presence of d.c. water flow (Engelmann et al. 2002). In terms of displacement, for SN the highest sensitivity is in the frequency range of 20 to 60 Hz, whereas for CN it is 60 to 120 Hz (Münz 1985, Montgomery et al. 1988, Kroese and Schellart 1992).

In the brainstem (Figure 2A), primary afferent fibres terminate in the medial octavolateral nucleus (MON, New et al. 1996), the first site of sensory processing in the central lateral line system of fishes (review: Montgomery et al. 1995). New et al. (1996) described four layers in the goldfish MON. The dorsalmost zone is the molecular layer, also called the cerebellar crest (Figure 2B). The transitional zone is the region where the ventral molecular layer merges into the deeper layers of the MON. Ventral to the transitional zone follows the so-called crest cell layer that contains the somata of the principal output neurons of the MON, the crest cells. The portion ventral to the crest cell layer comprises the deep neuropil of the MON. Within the deep layers of the MON, the basal dendrites of the crest cells receive ipsilateral input from lateral line afferent fibres either directly or via local interneurons (Montgomery et al. 1995, New et al. 1996). The termination fields of primary afferents extend across large parts of the rostro-caudal extent of the MON indicating that information is distributed widely in this nucleus (Northcutt 1989, Song and Northcutt 1991, Alexandre and Ghysen 1999). Crest cells also get synaptic input onto their apical dendrites that extend into the molecular layer and are contacted by small, unmyelinated parallel fibres descending from the eminentia granularis of the cerebellum. The crest cell axons project via the lateral lemniscus predominantly to neurons of the nucleus ventrolateralis of the contralateral midbrain torus semicircularis (McCormick and Bradford 1994, McCormick and Hernandez 1996).

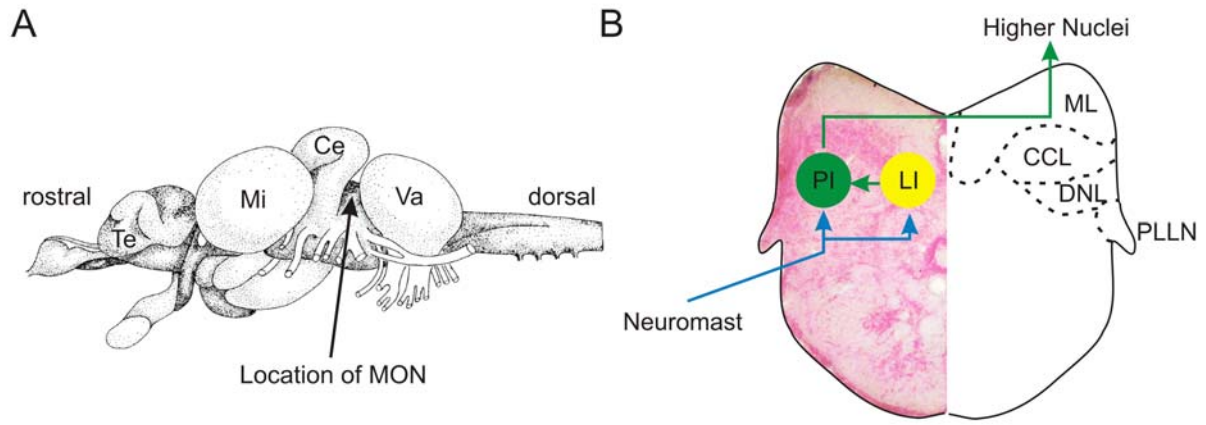

Figure 2: A: Drawing of a goldfish brain. Te = Telencephalon, Mi = Midbrain (tectum opticum), Ce = Cerebellum, Va = Vagus lobus. Modified after Wullimann and Northcutt 1989. **B:** Cross section through the goldfish brainstem and schematic representation of the processing pathway for lateral line information. The right part is a mirror-inverted drawing of the cross section on the left (cresyl-violet staining). ML = Molecular layer (cerebellar crest), CCL = Crest cell layer, DNL = Deep neuropil layer, PLLN = Posterior lateral line nerve, PI = Projection interneuron, LI = Local interneuron. Blue lines = Afferent nerve fibres, Green lines = Ascending fibres of interneurons

Various studies have described the responses of primary afferent nerve fibres and MON neurons to a dipole source, i.e., a stationary, sinusoidally vibrating sphere (primary afferents: e.g., Paul and Roberts 1977, Coombs and Janssen 1990, Kroese and Schellart 1992, Mogdans and Bleckmann 1999, Weeg and Bass 2002, MON: e.g., Caird 1978, Bleckmann et al. 1996, Montgomery et al. 1996, Wubbels et al. 1993, Mogdans et al. 1997, Mogdans and Goenechea 2000, Mogdans and Kröther 2001). These studies have revealed some fundamental differences between primary afferents and MON cells. Compared to primary afferents, MON neurons have lower spontaneous and evoked rates of activity, their responses to a vibrating sphere exhibit greater degrees of adaptation and heterogeneity (e.g., Coombs et al. 1998), and they appear to be less sensitive to vibrating sphere stimuli (e.g., Coombs et al. 1998, Mogdans and Goenechea 2000).

Despite the fact that naturally occurring oscillatory water movements rarely contain pure sine waves, in many studies sinusoidal water motions generated by a vibrating sphere have been used as stimulus to the lateral line (review: Bleckmann 1994). Sine wave stimuli are reproducible, can be accurately controlled and easily described mathematically. Moreover, the use of a vibrating sphere in lateral line experiments is

convenient since the hydrodynamic near-field produced by the sphere can be predicted (Curcic-Blake and van Netten 2006). Kalmijn (1989) has shown that several types of natural stimuli can be well approximated by the sinusoidal vibration of a sphere, i.e., a dipole source. The relevance of vibrating objects as lateral line stimuli has been documented in several experimental reports. Montgomery and Macdonald (1987) recorded the vibrations of water produced by swimming planktonic prey. They showed that these vibrations exhibited different frequencies that were detected by the lateral line. Bleckmann et al. (1991) measured sinusoidal water motion in the vicinity of hovering fish and crustaceans. They showed that hydrodynamic stimuli produced by different swimming animals contain frequencies between below 10 Hz and up to at least 100 Hz. Coombs and Janssen (1990) induced a feeding response in fish by the use of a vibrating sphere at 50 Hz. Satou et al. (1994) showed that a sphere vibrating at 21 Hz induces a spawning response in the himé salmon (*Oncorhynchus nerka*) demonstrating that the lateral line is involved in intersexual communication in this species.

Lateral line primary afferents respond to sinusoidal stimulation with phase-locked action potentials. Stimulus amplitude is encoded by the degree of phase-locking and by discharge rate and stimulus duration is encoded by the duration of the neuronal response (Bleckmann et al. 1989, Kroese and Schellart 1992, Wubbels et al. 1993, Coombs et al. 1998, Mogdans and Bleckmann 1999). While primary afferents are remarkably sensitive to sine wave stimuli (e.g., Mogdans and Bleckmann 1999, Coombs et al. 1996), MON neurons are less sensitive to pure sine waves, i.e., they require substantially higher stimulus amplitudes than primary afferents to increase discharge rates above ongoing levels (Coombs et al. 1988, Goenechea 1998). Primary afferents show linear frequency response properties, i.e., a linear increase in response amplitude with increasing stimulus frequency (Kroese and Schellart 1992, Mogdans and Bleckmann 1999). While the frequency response characteristics of primary lateral line afferent fibres have been described at least in some species (Kroese et al. 1978, Bleckmann and Topp 1981, Elepfandt and Wiedemer 1987, Coombs and Janssen 1990, Kroese and Schellart 1992, Montgomery and Coombs 1998, Weeg and Bass 2002), not much is known about the frequency response characteristics of brainstem lateral line neurons (Wubbels et al. 1993, Montgomery et al. 1996, Ali 2008). However, it is known that the frequency response characteristics

of brainstem lateral line units are much more diverse than those of primary afferents. Whereas lateral line afferents always increase discharge rate in response to sinusoidal stimulation, brainstem units may exhibit increases or decreases in discharge rate. In contrast to the linear response characteristic in primary afferents, central units (brainstem and midbrain) also show filter characteristics, including low-pass, band-pass, and high-pass (e.g., Plachta et al. 1999).

Theoretical data show that information about the position, vibration direction and distance of a vibrating dipole source is present in the pressure gradient pattern generated by the source (Coombs et al. 1996, Curcic-Blake and van Netten 2006, Goulet et al. 2008, Figure 3). This pressure gradient pattern results in a pattern of excitation across the array of neuromasts. Pressure gradient amplitude and direction at each neuromast are represented by the neuronal activity of the directionally sensitive hair cells and the innervating afferent nerve fibres. Changes in pressure gradient amplitude will lead to corresponding changes in discharge rate of the innervating fibre, and changes in pressure gradient direction will lead to corresponding shifts in the phase angle to which the neural response is locked. This latter effect originates from the bipolar flow field produced by the sinusoidal vibrating sphere and the fact that neuromasts are innervated by two populations of afferent fibres, each innervating hair cells of identical orientation. A change in source location and/or orientation can dramatically alter the pressure gradient field around the source and the subsequent spatial excitation pattern (e.g., Coombs and Patton 2008). When sphere vibration is parallel to a rostro-caudally oriented neuromast (Figure 3A, 0°), the pressure field is biphasic, resulting in a triphasic pressure gradient pattern consisting of a central peak bordered by two smaller negative side-peaks. The excitation pattern predicted for an afferent nerve fibre consists of a central peak of increased discharge rate bordered by two smaller side-peaks of increased discharge rate. In addition, the excitation pattern is characterized by two distinct changes in phase angle of 180° at the location between the excitation peaks. In contrast, when sphere vibration is orthogonal to a rostro-caudally oriented neuromast (Figure 3A, 180°), the pressure field is monophasic, resulting in a biphasic pressure gradient pattern consisting of a positive and a negative peak. The corresponding excitation pattern consists of two peaks of increased discharge rate of equal height and is characterized by a single 180° change in phase angle at the location between the

excitation peaks. Finally, when sphere vibration is intermediate between a parallel and orthogonal orientation (Figure 3A, 45° or 135°), the pressure field is monophasic and the resulting pressure gradient pattern is again biphasic. Depending on vibration angle, the pattern consists of a positive peak followed by a negative peak (45°) or vice versa (135°). The corresponding excitation pattern consists of two peaks of increased discharge rate that are of unequal height, i.e. a strong peak is followed by a smaller one (45°) or vice versa (135°). Between these peaks a single 180° change in phase angle occurs.

The theoretical predictions described above were confirmed by neurophysiological experiments performed on single fibres in the posterior lateral line nerve (PLLN) of different species (e.g., Sand 1981, Münz 1985, Montgomery et al. 1988, Wubbels 1991, Coombs et al. 1996, Coombs and Conley 1997a, Scholze et al. unpublished). Recently, Scholze et al. (unpublished) demonstrated for the first time that the spatial excitation patterns of primary afferent nerve fibres in goldfish exactly match the excitation patterns predicted for different axes of sphere vibration (Figure 3B). Scholze et al. (unpublished) also showed that the sequence of patterns shown in Figure 3A was obtained when the innervated neuromast was oriented with its polarization axis rostro-caudally but that the sequence was inversed (i.e., 0° and 90° patterns and 45° and 135° patterns were swapped) when the innervated neuromast was oriented with its polarization axis dorso-ventrally on the fish surface.

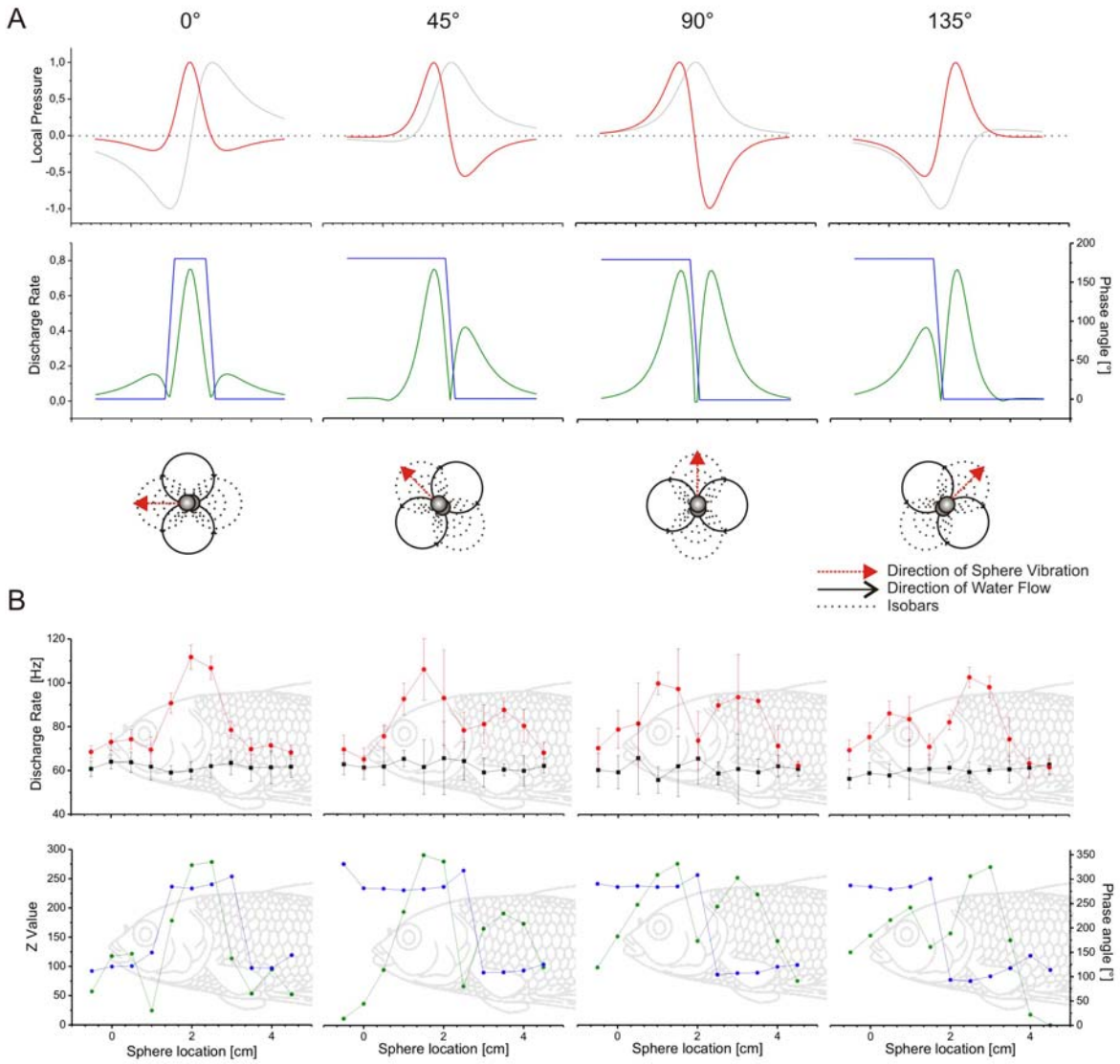

Figure 3: A: Calculated pressure and pressure gradient maps of a sinusoidally vibrating sphere oscillating at an angle of 0°, 45°, 90° or 135° relative to the fish (upper graphs) and the predicted evoked activity of a primary afferent nerve fibre (lower graphs). Grey: pressure, red: pressure gradient, green: predicted discharge rate, blue: predicted phase angle. The bottom-most drawings illustrate the direction of sphere vibration (red arrows), the associated water flow (solid lines), and isobars (dotted lines).
B: Excitation patterns of a primary afferent nerve fibre. Upper graphs: Ongoing discharge rates (black lines) and evoked discharge rates (red lines) averaged across eight stimulus presentations are plotted as function of sphere location along the side of the fish (stimulation 50 Hz, 500 ms, sphere displacement in the unit´s dynamic range). Vertical bars represent standard deviation. Lower graphs: Z-values indicating the degree of phase-locking (green lines, left Y-axis, Z-value criterion: $Z \geq 4.6$) and mean phase angles (blue lines, right Y-axis). The fish in the background is drawn to scale. Data from B. Scholze (unpublished).

Data from experiments in which source distance was increased show that response patterns extended across a greater area of space as source distance was increased, resulting in a broadening of response peaks and greater spatial separations of the 180° phase shifts (Coombs and Patton 2008). These results agree with earlier

modelling and physiological results from goldfish PLLN fibres, which showed that response patterns did not broaden in space when source distance was fixed and source amplitude was decreased (Coombs et al. 1996). This means that information about source distance contained by pressure gradient patterns cannot be confused with information about source amplitude.

Whereas these earlier theoretical and electrophysiological studies show, that pressure gradient patterns contain information about source location and orientation, there is still little knowledge on how these patterns are encoded centrally. Only few studies have described spatial excitation pattern of central neurons (Coombs et al. 1998, Mogdans and Kröther 2001, Meyer et al. unpublished). Coombs et al. (1998) and Mogdans and Kröther (2001) found primary-like MON excitation patterns comparable to those of primary afferent fibres, and excitation patterns that were unlike those of primary afferents. While primary-like excitation patterns in the MON could be modelled with excitatory-centre/inhibitory-surround and inhibitory-centre/excitatory-surround organizations (Coombs et al. 1998), the generation of non primary-like excitation patterns is not understood. In the current study it was investigated how central neurons encode for object location and orientation.

In their natural environment, fishes are exposed to flow conditions ranging from nearly still water in ponds to fast running rivers. The neuromasts of the mechanosensory lateral line detect flow over the surface of the body and have the anatomical distribution and physiological properties to detect the strength and the direction of flow or regional differences in flow over different parts of the body (Montgomery et al. 2000). As a consequence of the directional sensitivity of lateral line neuromasts, one would expect that about half of the flow sensitive afferent lateral line nerve fibres respond with an increase in ongoing activity to unidirectional water flow whereas the other half responds with a decrease in discharge rate. In contrast to this assumption, studies found that nearly all lateral line afferents increased their discharge rates if the fish was exposed to unidirectional water flow (Voigt et al. 2000, Carton and Montgomery 2002, Engelmann 2002, Chagnaud et al. 2008). This increase in discharge rate in running water was due to the fact that the fibres responded to flow fluctuations and not to the constant flow (Chagnaud et al. 2008).

Literature suggests that fluctuations within a water flow may be used to determine flow direction and flow velocity by comparing inputs from an array of peripheral receptors (Chagnaud et al. 2008). Performing double recordings, Chagnaud et al. (2008) showed that it is possible to extract flow velocity and flow direction from pairs of lateral line fibres. If brainstem neurons indeed determine flow velocity and flow direction by comparing inputs from two or more neuromasts that are organized in series on the fish surface, then neurons should be found that respond preferentially to particular flow velocities and flow directions.

Questions addressed in this thesis

The descriptions made above indicate that there is a fair amount of knowledge about the representation of hydrodynamic stimuli by primary lateral line nerve fibres but an obvious lack of similar knowledge for brainstem lateral line neurons. Therefore, in this thesis I studied the responses of single lateral line units in the medial octavolateralis nucleus (MON) of the goldfish to various hydrodynamic stimuli. First, I characterized the response behaviour of MON units to sine wave stimuli of different frequencies with respect to discharge rate, phase-locking and frequency preference. Second, I searched for MON units that encode location and vibration direction of a stationary dipole source. To do so, I characterized the spatial excitation patterns of MON neurons by recording neuronal activity in response to a sinusoidally vibrating sphere presented at various locations along the side of the fish and vibrating at different angles with respect to the surface of the fish. Finally, I assessed the responses of MON units in water flow. For this task, I recorded the activity from brainstem units in a constant-velocity water flow or in a flow of continuously rising velocity. Responses were analyzed with respect to directional sensitivity to flow passing the fish from anterior to posterior or opposite, i.e., from posterior to anterior, and with respect to a potential tuning to particular flow velocities.

2. MATERIAL AND METHODS

2.1 Animal handling

Data were collected from 88 goldfish, *Carassius auratus* (length 7.5 - 12.5 cm, weight 20 – 30 g). Animals were acquired from commercial dealers and were maintained in 200 l aquaria at 20 - 22 °C on a daily 10 - 14 h light-dark cycle. On the day of an experiment, a fish was anesthetized with tricaine methansulfonate (MS 222) in ice-cold water and immobilized by intramuscular injection of 100-150 µl Pancuroniumbromide (3.3 %, Organon Teknika) depending on fish weight. In addition, local anesthesia (a drop of Xylocain, 2 %, AstraZeneca) was applied to the surface of the head. During surgery, fish were artificially respirated by a water flow (approximately 120 ml*minute^{-1}) through a flexible tube inserted into the fish's mouth. A small opening (5*5 mm) was drilled into the fish's skull with a dental drill (Micromot 50/E, Proxxon) and fatty tissue was removed to visualize the surface of the brain (Figure 4A). The caudal part of the cerebellum was exposed and carefully moved rostral to visualize the underlying brainstem surface (Figure 4B). During these procedures the brain was kept moist with a physiological salt solution (Oakley and Schafer 1978) that was applied repetitively. A plastic cylinder (diameter 12 mm, height 15 mm) was glued around the scull opening (Vetbond, 3M Animal Care Products) to allow submersion of the fish below the water surface without water entering the brain case (Figure 4C). After surgery, the fish was transferred into a flow tank (dimensions 90x60 cm, canal width 15 cm, height 13 cm) that was positioned on a vibration-isolated table (TMC) (Figure 4D, 5). The fish was mounted to a stainless steel fish holder that consisted of a mouthpiece connected to a water supply for artificial respiration (flow rate approximately 100 ml*minute^{-1}) and two screws to secure the head in a stable position. A thread was attached to the fish's tail and fixed with its other end to the rear wall of the experimental tank to prevent lateral movements of the fish's trunk and tail (Figure 4C).

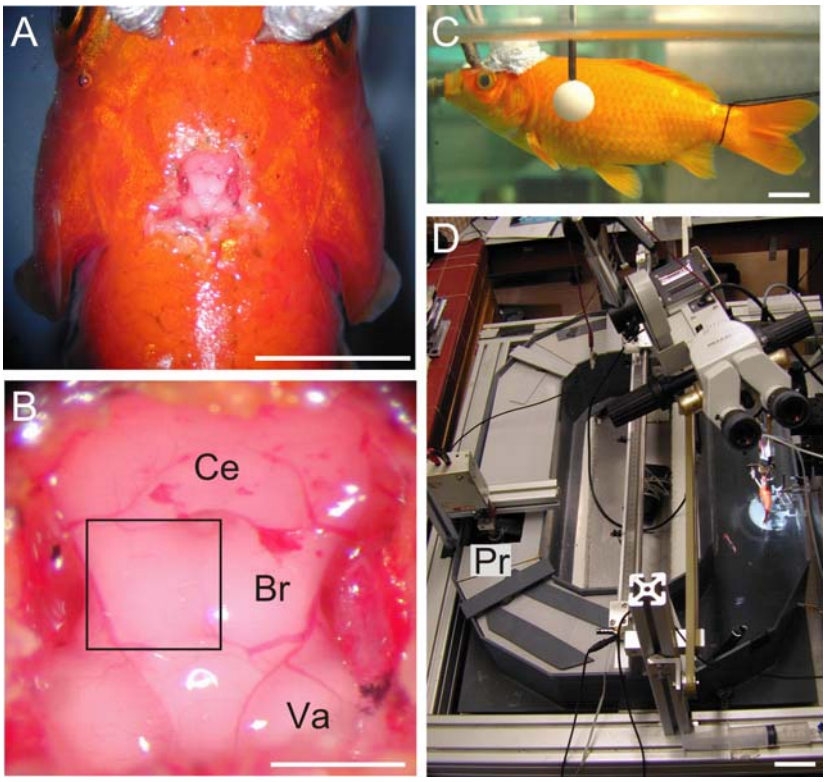

Figure 4: Illustration of experimental setup and animal. **A:** Surgery opening in the goldfish's skull. Scale bar corresponds to 1 cm. **B:** Magnification of skull opening. The square refers to the recording area (ipsilateral Medulla). Scale bar corresponds to 0.25 cm. Ce = Cerebellum, Br = Brainstem (Medulla), Va = Vagus lobus. **C:** Goldfish with plastic cylinder glued on the head in experimental position. Vibrating sphere is next to the fish. Scale bar corresponds to 1 cm. **D:** Photograph of the flow tank. Pr = Propeller. Scale bar corresponds to 5 cm.

For experiments in which the spatial excitation patterns of neurons were determined, the fish was adjusted in the flow tank such that its left side was aligned parallel to the long axis of the tank. This ensured that the distance between fish body and stimulus source (vibrating sphere, see below) was constant across most of the body surface except for the rostral-most (head) and caudal-most (tail) locations (trunk: 1.0 cm, head/tail: 1.4 cm). For experiments in which neuron responses to water flow were recorded, the fish was positioned such that its body midline was parallel to the long axis of the tank, i.e., such that the fish was facing the impinging flow. The fish was positioned with its dorsal surface at least 0.5 cm below the water surface (Figure 4C). To avoid inactivation of the lateral line receptors by MS 222 (Hensel et al. 1975, Spath and Schweikert 1977), recordings were not begun until 30 minutes after surgery.

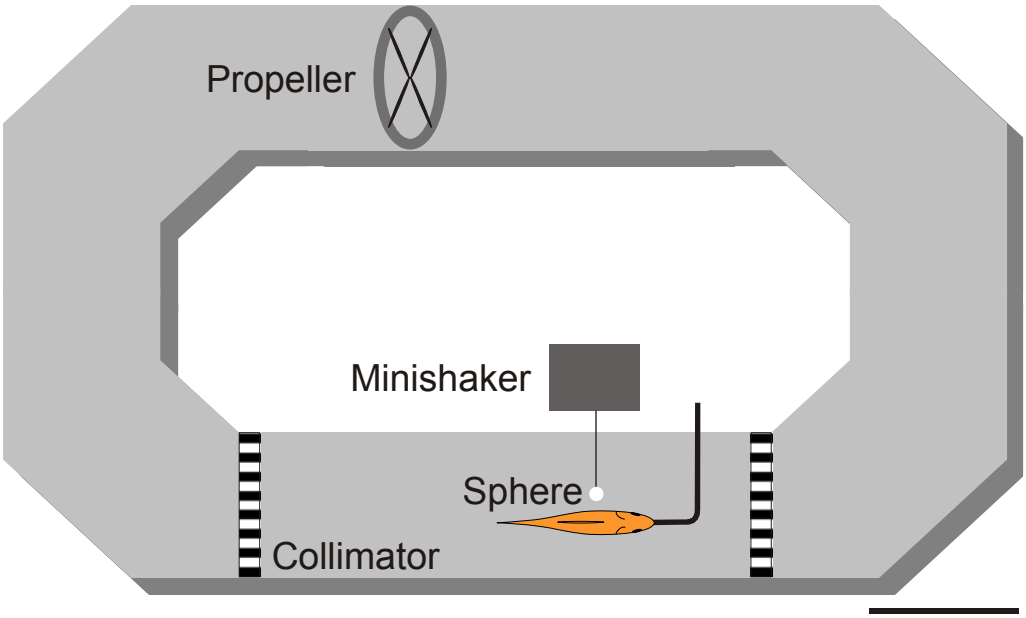

Figure 5: Schematic illustration of the flow tank. Scale bar corresponds to 10 cm.

2.2 Stimulation

Two types of hydrodynamic stimuli were used for the characterization of brainstem lateral line neurons, sinusoidal water motions generated by a stationary vibrating sphere (dipole source) and, water flow over the fish's body.

2.2.1 Vibrating Sphere

Sinusoidal water motions were generated by a vibrating sphere (8 mm diameter, see Figures 5, 6 and 7) that was attached to a mini-shaker (Ling, Model V101, Figure 6) by a stainless steel rod (2 mm diameter, 12 cm length). The mini-shaker was driven by computer-generated sinusoidal signals (see chapter 2.2.3). The signals were generated with the software Spike 2 (CED), read through a D/A converter (Power 1401, CED, 14-bit resolution, 3 kHz sampling rate), attenuated in steps of 5 dB (350D Attenuator Set, Hewlett Packard) and power-amplified (PA 25E, LDS) before getting to the mini-shaker. The mini-shaker was mounted to a sliding bar assembly that was mounted to a frame around the table with the experimental tank, i.e., it was vibration-

isolated from the experimental tank. The sliding bar allowed to manually move the sphere to any position along the side of the fish. In addition, the sphere was pivot-mounted around its centre axis such that the direction of sphere vibration could be adjusted in the horizontal plane in steps of 5° to various angles relative to the longitudinal axis of the fish (Figure 6). This mounting allowed to change vibration direction without changing the sphere position, i.e., the sphere's centre remained in its particular position. Stimulus frequency was 20, 50 or 100 Hz and direction of sphere vibration (vibration angle) was 0° (parallel to the fish), 90° (perpendicular to, i.e., towards the fish), or intermediate, i.e., 45° or 135° (see Figure 6).

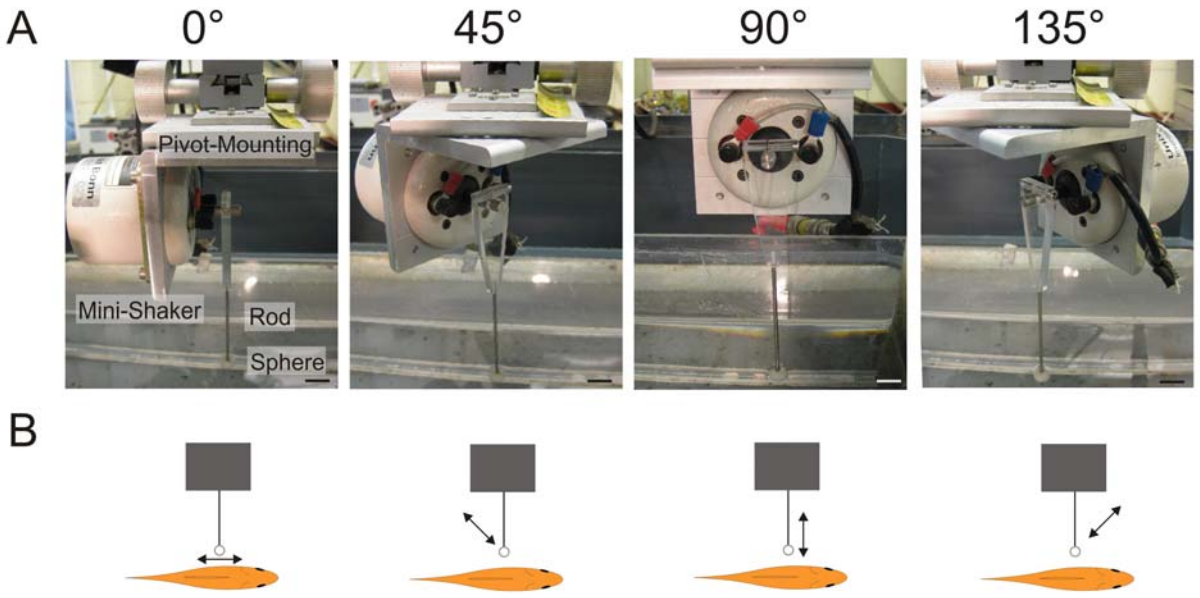

Figure 6: A: Photographs of the mini-shaker and pivot-mounting of the sphere. The sphere was adjusted to one of four vibration angles (0, 45, 90, or 135 °). Scale bar corresponds to 1 cm. **B**: Schematic drawing of the sphere and its motion relative to the fish. The arrows refer to the vibration direction.

2.2.2 Water flow

Water flow was generated with a propeller (diameter 8 cm, Aeronaut, Figure 1D) coupled to a d.c. motor (Conrad Electronic) that was driven by a power supply (6827A Bipolar Power Supply/Amplifier, Hewlett Packard). The output of the power supply was controlled by a signal voltage generated by the computer-controlled CED (Power 1401, see chapter 2.2.3). The propeller was suspended from a holder that was mounted onto the frame around the table with the experimental tank. It could be lowered into the arm of the flow tank opposite to the arm in which the fish was placed. To reduce turbulences created by the propeller the experimental tank was equipped with one upstream and one downstream collimator (first version: glued straws: tube diameter 4 mm, width 1 cm. second version: plastic custom build collimator: tube diameter 3 mm, width 2 cm) through which the water was passed before reaching the fish.

2.2.3 Stimulus characterization

Vibrating sphere

The displacement amplitude of the vibrating sphere depended on the type of experiment (see below, chapter 2.4.1) and was calibrated with a capacitive displacement transducer (Model 4810, LOT Oriel Group Europe, Figure 7A). For this purpose a brass disc (diameter 5 mm, Figure 4A) was glued to the rod holding the sphere and connected with the shielding of sensor of the displacement transducer with a silver wire (diameter 50µm). The movement of the rod was then measured as a change in capacitance between sensor and disc. The output signal was read into the PC and analysed (Power CED, Figure 7B). A signal amplitude of 1 V refers to a displacement amplitude of 25 µm (see calibration curve Appendix Figure 49).

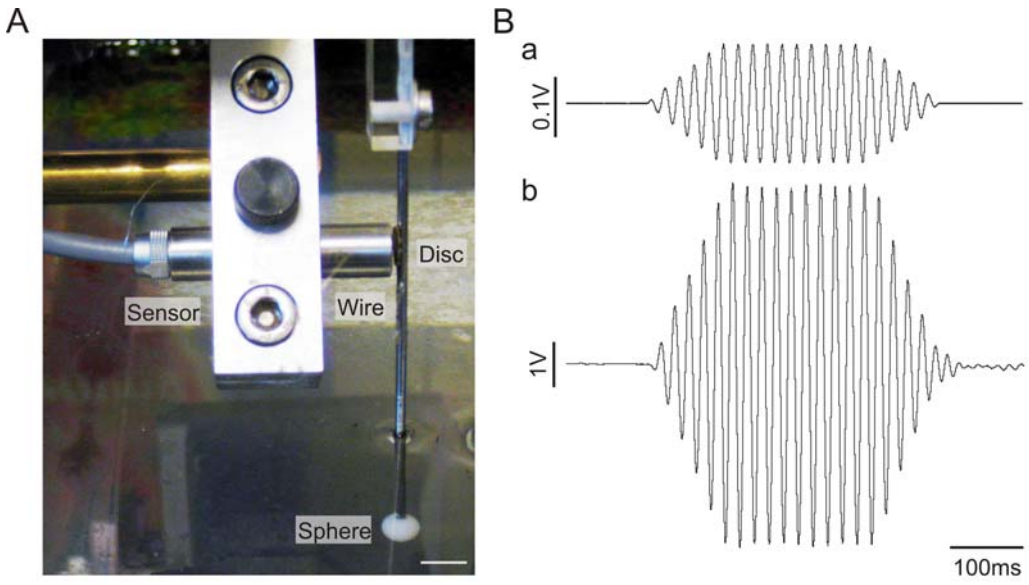

Figure 7: A: Photograph of the vibrating sphere and supporting rod and the sensor of the capacitive displacement transducer. Scale bar corresponds to 1 cm. **B:** Vibrating sphere stimulus trace (50 Hz).**a:** Computer generated signal (100 ms rising and falling ramp).**b:** Signal measured with the capacitive displacement transducer (1 V output refers to 25 µm peak to peak sphere displacement amplitude).

Water Flow

The water flow in the experimental tank was characterized using Negative Temperature Coefficient (NTC) Anemometry and Particle Image Velocimetry (PIV). Flow velocity was calibrated using Particle Image Velocimetry (PIV). For this purpose neutrally buoyant particles (Vestosint 1101, Hüls, Berlin, Germany) were illuminated with a green laser light layer (L-10-A3 laser, 10 mW, HB-Laserkomponenten GmbH) and videotaped (CCD video camera, Panasonic, WVBL200). The distance (in pixels) that the recorded particles moved at each applied water velocity was measured over approximately twenty to fifty video frames (frame rate 25 fps, Video Spot Tracker V05.25, Figure 8). This procedure was repeated for ten different particles. A distance of 76.2 pixels corresponds to 1 cm (see calibration curve Appendix Figure 50).

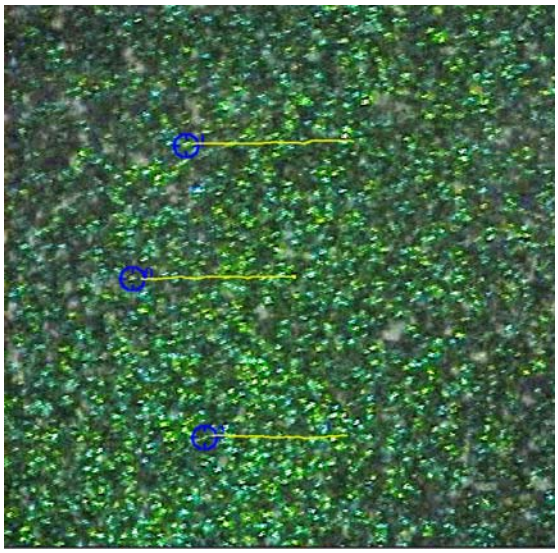

Figure 8: Single frame from analysis of the particle imaging velocimetry (PIV) video recording during water flow (posterior – anterior, i.e., right to left in this figure). Blue circles mark analysed illuminated particles, yellow lines refer to logging traces of particle movement (video spot tracker).

Flow profiles (see Voigt et al. 2000) were measured with a NTC-Anemometer (customized bridge amplifier, electronic laboratory, Institute of Zoology, University of Bielefeld). The temperature of the NTC-sensor correlates with the water velocity. A change in temperature is measured as a change in voltage and stored on the computer. Three flow profile traces of each measured velocity were averaged (Spike 2, Figure 9, see Appendix Figure. 50B-D, see equation of exponential regression in Figure 50D).

2.3 Data Acquisition

Neuronal activity from single units in the medial octavolateral nucleus (MON) was recorded extracellulary. Glass micropipettes were pulled from borosilicate glass (GB120F-8P, Science Products) on a Flaming/Brown puller (P-97, Sutter Instrument) and were filled with 1M LiCl-Solution. The electrodes had tip diameters of 1 - 2 µm and impedances between 5 and 50 MΩ. Electrodes were attached to a Plexiglas holder (precision mechanics laboratory, Institute of Zoology, University of Bonn) that was connected to a micromanipulator (Micos, Helias) and a motor-driven micro stepper (Nanostepper Micro Processor Control, Science Products Trading). For

recording, the electrode tip was positioned on the surface of the brainstem under visual control through surgery binoculars (Wild 651, Leica) and moved through the brain tissue in defined steps (typically 20 µm).
Recorded signals were amplified (x 1000), filtered (DAM80, World Precision Instruments, 0.3 - 1 kHz), fed through a noise (50 Hz and harmonics) eliminator (Hum Bug, Quest Scientific) and monitored on an oscilloscope (DL 1300 A, Yokogawa) and an audiomonitor (custom-built, electronic laboratory, University of Bielefeld). Signals were digitized (Instrunet Model 100B, GW Instruments, 14-bit resolution, 8 kHz sampling rate or Power 1401, CED, 14-bit resolution, 8 kHz sampling rate) and stored on a computer (Power Macintosh 7300 running SuperScope II, GWI, or Dell Optiplex GX520 running Spike 2, CED).

2.4 Localisation of recording site

Advancing the electrode tip deep into the brain tissue prohibits direct visual control of reaching the targeted recording site. Nevertheless, the recording position was still fairly accurately determined by using the distinctly structured surface of the medulla for orientation. Additionally, recording depth was indirectly controlled by using a micro stepper (see Chapter 2.3), which measures electrode depth. At the beginning of each penetration zero depth was defined as the depth at which the electrode touches the surface of the brain. The location of the MON in the goldfish brain has already been known from literature and own data (New et al. 1996, Fest 2003). It is located in the dorso-lateral part of the medulla. The recorded MON units were located between the depth of 200 and 500 µm. Auditory units are closely associated with MON units but are located in a more medio-ventral position of the medulla (McCormick and Bradford 1994). Accordingly, specific care was taken not to place the electrode too medial or too deep (> 500 µm) within the medulla, in order to avoid recording from octaval units in the DON (McCormick and Bradford 1994, McCormick and Hernandez 1996).

2.5 Stimulation protocol

To search for responsive lateral line neurons continuous sinusoidal water motions (50 Hz, 400 µm peak to peak displacement) were generated while the electrode was advanced through the brain. The stimulus was interrupted from time to time to avoid adaptation. In addition, water movements generated by moving the non-vibrating sphere manually alongside the fish were used as a search stimulus. If a unit responded to one of these stimuli, it was tested whether it also responded to sound or vibration by shouting, clapping hands and/or tapping against the tank walls. Units responding to these stimuli were assumed to receive input from the auditory and/or vestibular system and were not further investigated. Units responding to water movements but not to sound or vibration were assumed to be lateral line units. If a lateral line unit was encountered, the sphere was positioned at the location from which it apparently elicited the strongest response. This was initially determined by listening to the audio monitor.

2.5.1 Frequency sensitivity

In a first set of experiments, the frequency sensitivity of MON units was studied. In these experiments, the sphere was placed at the position that elicited the strongest response. Axis of sphere vibration was parallel to the rostral-caudal axis of the fish. Stimulus frequency was 20 Hz, 50 Hz or 100 Hz, duration was 400 ms (up-ramp/down-ramp: 16 ms), and peak to peak displacement was 400 µm. A single recording trace had a duration of 5 s and consisted of 0.5 s pre-stimulus activity and 4.1 s post-stimulus activity, i.e., stimulus interval was 4.6 s. Stimuli were presented ten times.

2.5.2 Spatial excitation patterns

In another set of experiments, the spatial excitation patterns of MON units were investigated. In these experiments, stimulus frequency was 50 Hz and duration was 500 ms (up-ramp/down-ramp: 100 ms), resulting in inter-stimulus intervals of 4.5 s

(0.5 s pre-stimulus and 4.0 s post-stimulus activity). The sphere was initially placed at the location from which it elicited the strongest response. With the sphere at this location, a unit's dynamic range was determined by varying the displacement amplitude of the vibrating sphere. For further measurements, displacement was adjusted to a value that was within the unit's dynamic range. Typically, this resulted in displacements between 200 µm and 650 µm. The sphere was then moved alongside the fish in steps of 5 mm. At each location responses to eight presentations of the 50 Hz stimulus at four vibration angles were recorded: 0° (parallel to the fish), 90° (perpendicular to or towards the fish), or intermediate, i.e., 45° or 135° (see Figure 6).

2.5.3 Water Flow

In a third set of experiments, the lateral line was stimulated with unidirectional water flow from anterior to posterior (AP) or opposite, i.e., from posterior to anterior (PA). Two stimulus paradigms were used: pulse flow stimulation and ramp flow stimulation.

Pulse Flow Stimulation

Neuronal activity in a constant velocity water flow was recorded for thirty seconds preceded by a 10 second pre-stimulus period and followed by a ten second post-stimulus period (Figure 9A). Flow velocity was chosen at random from one of the following velocities: 0.7, 2.6, 4.4, 6.2, 8.8, 10.0 or 12.0 $cm*s^{-1}$. Thereafter, a three minute recovery period was introduced during which the water was allowed to calm down. Then, the recording was repeated using a novel water velocity. When recordings to all water velocities were completed, this stimulus protocol was repeated up to three times.

Ramp Flow Stimulation

In this paradigm, neuronal activity in response to continuously increasing flow velocity was recorded. The flow velocity was increased either from 0 to 10 $cm*s^{-1}$ or from 0 to 12.3 $cm*s^{-1}$ over a time period of thirty seconds (Figure 9B). The flow on-

ramp was followed by a down-ramp over a time period of five seconds to reduce turbulences and backflow in the experimental tank that could lead to mechanical instability and consequent loss of the recording.

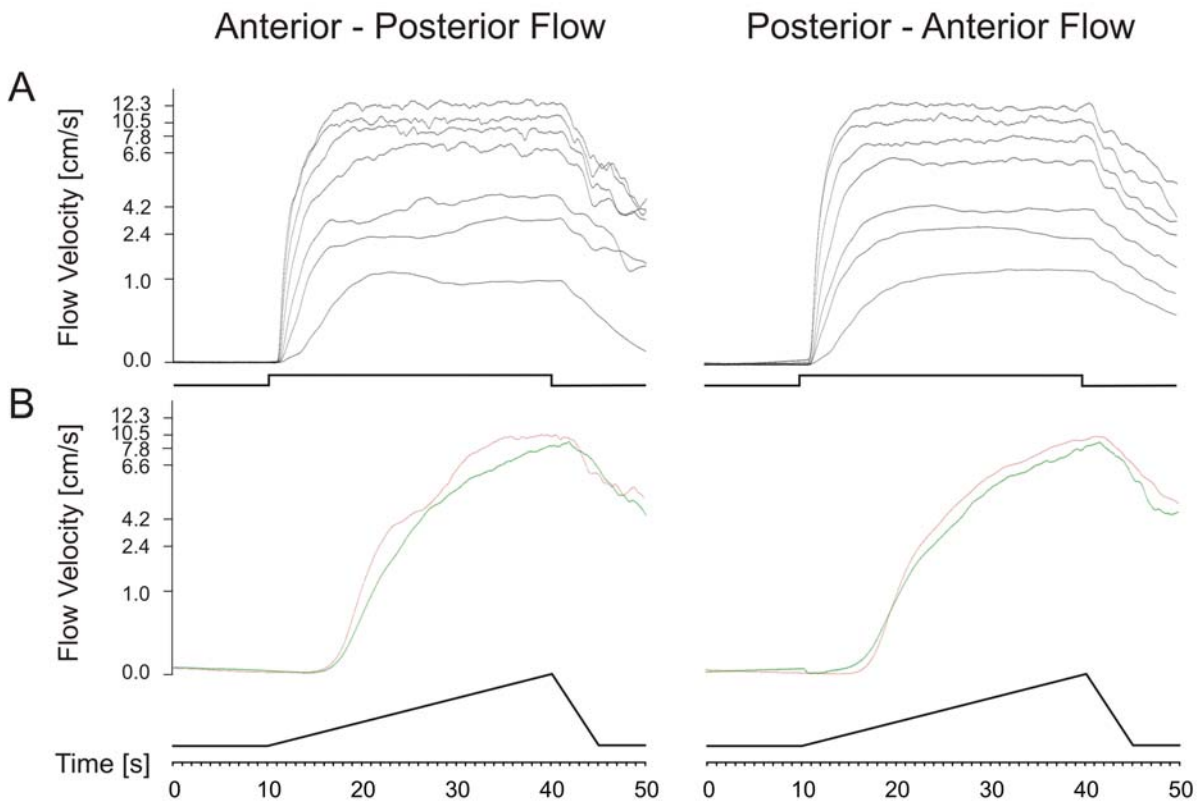

Figure 9: Flow profiles measured in the recording section of the flow tank by a NTC anemometer. Flow velocity is plotted as function of time. The bottom trace of each graph symbolizes the type of stimulation. Left plots: water flow direction in anterior to posterior direction. Right plots: reverse direction. **A:** Pulsed flow stimulation.
B: Ramped water flow. Green: 0 to 10 cm*s^{-1}. Red: 0 to 12.3 cm*s^{-1}.

2.6 Data analysis

2.6.1 Frequency sensitivity

Responses to the vibrating sphere were quantified by the average discharge rate (spikes*s^{-1}, evoked activity) during stimulation. Average firing rate was determined from the number of action potentials that occurred during ten stimulus presentations and compared with the average ongoing activity (spontaneous activity) during the

first 500 ms of each trace. Spike numbers were averaged across ten stimulus traces. The average phase angle (degree) of spikes with respect to the sinusoidal signal delivered to the mini-shaker and the synchronization coefficient R (vector strength after Goldberg and Brown 1969) were calculated. An R-value of 1 indicates that all spikes occurred at the same phase angle. The Rayleigh statistic Z was used to determine whether or not the degree of phase locking was statistically significant. Z-value was calculated as follows:

$$Z = R^2 * N,$$

where N = total number of spikes (Batschelet 1981). Z values above 4.6 indicate a probability of 0.01 or less that spikes were randomly distributed during one vibration cycle. Peri-stimulus-time histograms (PSTH, number of action potentials per bin), raster plots (each marker represents one action potential) and phase-histograms (number of action potentials per bin) were computed (Figure 10). A unit was defined as responsive to one of the applied frequencies if its discharge rate during stimulation was significantly different from its ongoing discharge rate during the pre-stimulus period (Mann-Whitney-U-Test, two-tailed, significance level $p \leq 0.05$) and/or if it exhibited a significant phase locking. The responses of the MON units to the applied frequencies in terms of discharge rate and phase locking were compared.

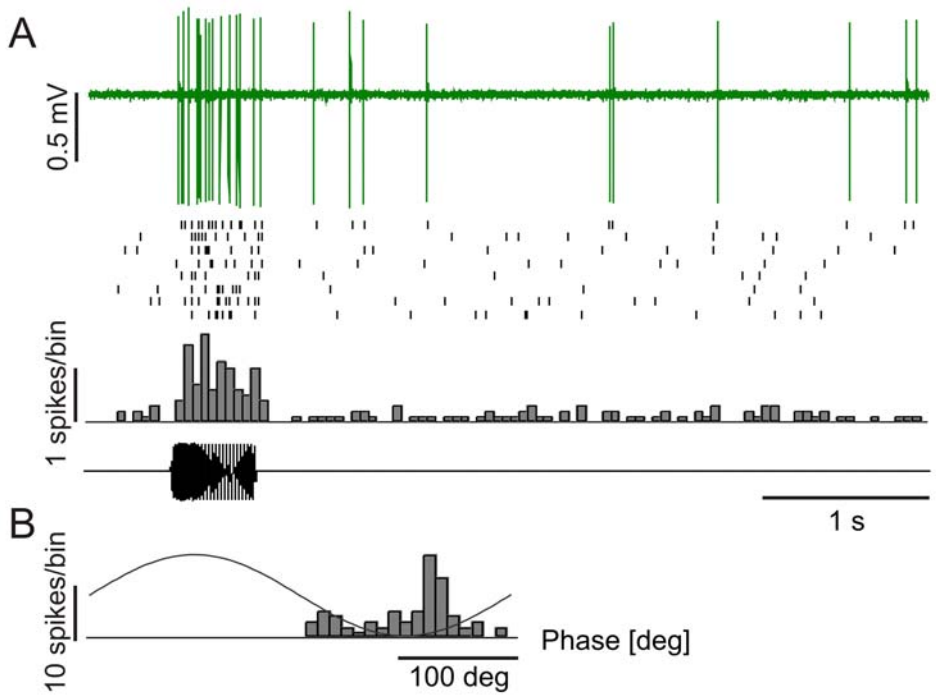

Figure 10: Example of a brainstem neuron's response to a 50 Hz sinusoidally vibrating sphere. **A:** Green: Original recording, black: Raster plot, grey: Peri-Stimulus-Time-Histogram (PSTH, bin width 50 ms). The bottom trace is the stimulus trace. **B:** Phase-histogram (bin width: 10 degrees).

2.6.2 Spatial excitation patterns

Responses to the vibrating sphere were quantified as described above (chapter 2.5.1) by the average discharge rate (spikes*s^{-1}) during the 50 Hz pulse, the average phase angle (degree) and the degree of phase-locking (synchronization coefficient R). These measures were plotted as function of sphere location alongside the fish to obtain spatial excitation patterns (Figure 11).

To quantify the spatial extent of excitation patterns, the half maximum width (HMW) was determined. This is a common parameter used to describe the extent of a function and is defined by the distance between points on a curve at which the function reaches half of its maximum or minimum value, respectively (e.g., Weisstein 1998). To determine HMWs, ongoing rates were subtracted from the evoked rates. If excitation patterns consisted of a single area of increased or decreased discharge rate, HMWs were readily determined. In those cases in which excitation patterns consisted of more than one area of increased or decreased activity, HMW was

defined as the distance between the rostral-most and caudal-most points at which discharge rate was at 50% of the maximum and/or minimum value, respectively. Those cases in which neuronal activity did not drop to below 50% of maximum across the range of stimulus locations tested were excluded from this analysis. To compare data across fish, HMWs were normalized to fish body length (measured from the tip of the snout to the caudal peduncle).

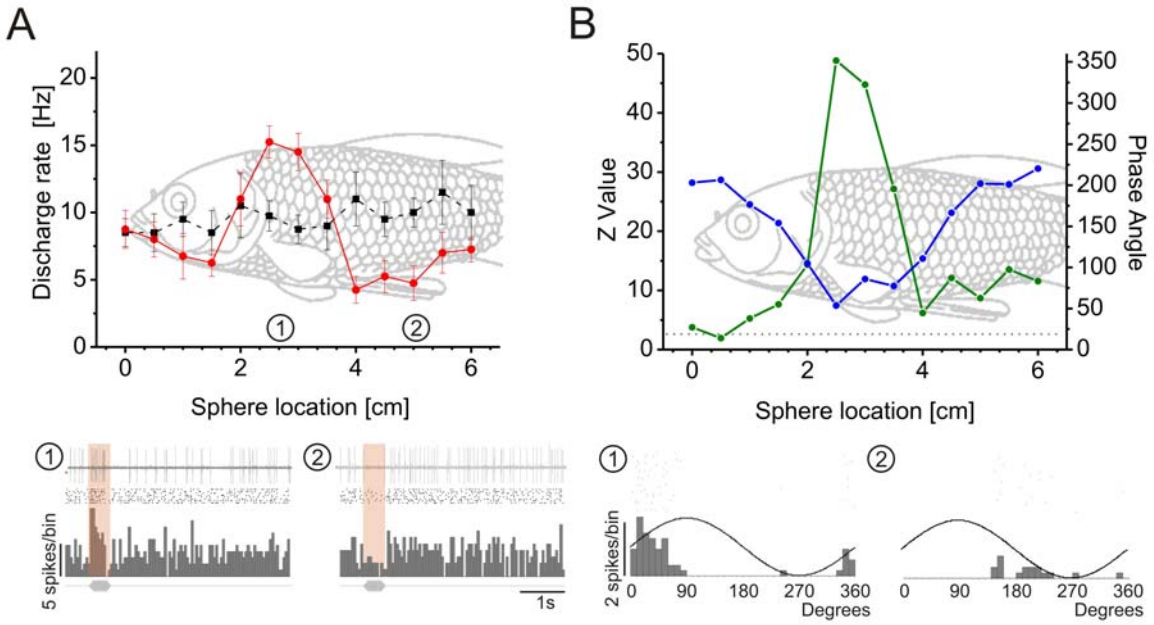

Figure 11: Spatial excitation pattern of a brainstem neuron. **A:** Upper graph: Discharge rate as function of sphere location along the side of the fish (fish drawing to scale). Black line: Ongoing discharge rate, red line: Evoked discharge rate (frequency 50 Hz, displacement 350 µm, 1 cm distance between sphere and fish). Vertical bars represent one standard deviation. Numbers (1) and (2) refer to the figures shown below. Lower graphs: Responses of the neuron at sphere locations (1) and (2). From top to bottom: Original recording traces, raster plots, Peri-Stimulus-Time-Histograms (bin width 50 ms) and stimulus trace **B:** Upper graph: Z-value (green lines, left Y-axis) and mean phase angle (blue lines, right Y-axis) as function of sphere location (fish drawing to scale). The horizontal grey dashed line indicates the Z-value criterion ($Z \geq 4.6$). Lower Graphs: Phase-histogram (bin width 10 degree) obtained at sphere locations (1) and (2).

2.5.3 Water Flow

Responses to running water were quantified by the average discharge rate during the stimulation period (Figure 12, bottom trace). Peri-stimulus-time histograms (PSTH), raster plots (spikes presented as vertical lines), instantaneous frequency (IF) and inter spike intervals were computed for the stimulation period and the pre-stimulus period (Figure 12). For each neuron the average ongoing rate (still water and running water conditions) was determined in absolute values and as the difference between the rates obtained at the different flow velocities (0-12.3 cm*s^{-1}, constant and continuously increasing flow).

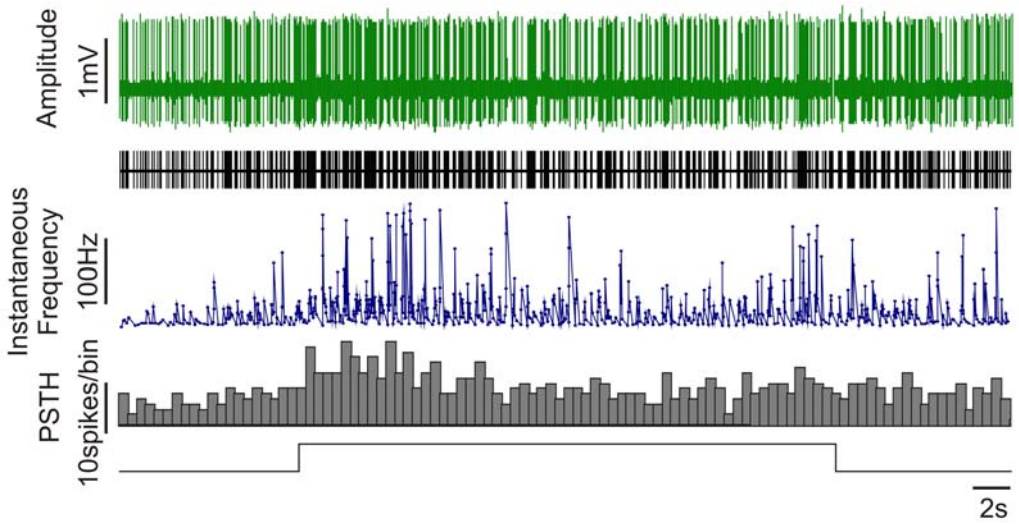

Figure 12: Response of a brainstem neuron to a pulsed flow stimulus. Green: Original recording, black: Raster plot, blue: Instantaneous frequency (IF), grey: Peri-Stimulus-Time-Histogram (bin width 500 ms). The bottom trace represents the stimulus. Flow velocity was 3.7 cm*s^{-1}, flow direction was from anterior to posterior.

Velocity response functions (VRFs) were constructed for those units that were stimulated with at least three different flow velocities by plotting the change in discharge rate in response to water flow as function of flow velocity. The threshold was defined as the minimal velocity causing a significant change in discharge rate. To compare the variability of discharges between different neurons, the average ongoing rate was subtracted from the instantaneous frequencies (IF) measured in

water flow. To determine the variability of firing, the root mean square (RMS) of the instantaneous frequencies (IF) was calculated. The RMS was calculated as follows:

$$\text{RMS} = \sqrt{\frac{1}{N}\sum_{i=1}^{N} x_i^2}$$

where N = total number of IFs and x = IF_i. A neuron was defined as flow sensitive if its discharge rate measured under still water conditions was significantly different from its discharge rate measured under running water conditions (Wilcoxon test, two-tailed, significance level $p \leq 0.05$).

To compare the responses to flow in the anterior – posterior and posterior – anterior direction a signed directionality index (SDI, Wagner and Takahashi 1992) was calculated which was defined as

$$\text{SDI} = 100 \left[1 - \frac{\text{discharge rate in PA direction}}{\text{discharge rate in AP direction}} \right]$$

if responses were greater in the anterior-posterior flow direction than in the posterior-anterior flow direction, and as

$$\text{SDI} = 100 \left[\frac{\text{discharge rate in AP direction}}{\text{discharge rate in PA direction}} - 1 \right]$$

if responses were greater in the posterior – anterior direction than in the anterior-posterior direction. Units with an SDI of zero exhibit identical discharge rates to both AP and PA flow direction, an SDI of 50 means that the response in discharge rate in one direction was twice that in the other direction, and units with an SDI of 100 respond only to one of the presented flow directions.

3. RESULTS

3.1 Frequency selectivity of MON units

A total of ninety-four single MON unit were recorded in thirty-four goldfish and their frequency selectivity was determined. To do so, these units were stimulated with sinusoidal wave stimuli of 20, 50 and 100 Hz (400 µm peak-to-peak displacement). Average ongoing activity was 16.4 ± 14.7 spikes*s^{-1} (mean ± SD; median: 10.4 spikes*s^{-1}, Table 1). Eighty-five units responded to at least one of the three stimulus frequencies with a change in discharge rate and/or with phase-locked action potentials (Figure 13A - C). Nine units did not respond to any of the applied stimuli (Figure 13D). Responses were highly idiosyncratic in that rate increases, rate decreases and phase-locked discharges were not consistent from one unit to the next or across frequencies. Based on whether units responded to one, two or three stimulus frequencies, they were assigned to one of three groups.

	Mean	SD	Median	Range
Spontaneous Discharge Rate [spikes*s^{-1}]	16.4	14.7	10.4	0.73 - 55.7
Maximal Evoked DischargeRate [spikes*s^{-1}]	20.5	17.6	15.6	0.0 - 76.2
Maximal Change in Discharge Rate [%]	98.3	283.9	18.6	-100 - 2383.9
Maximum Synchronization Coefficient (R)	0.4	0.3	0.3	0.01 – 1.0
Maximum Rayleigh Statistics (Z)	29.5	56.9	7.5	0.02 – 439.0

Table 1: Mean, standard deviation, median and range of various response properties of MON units.

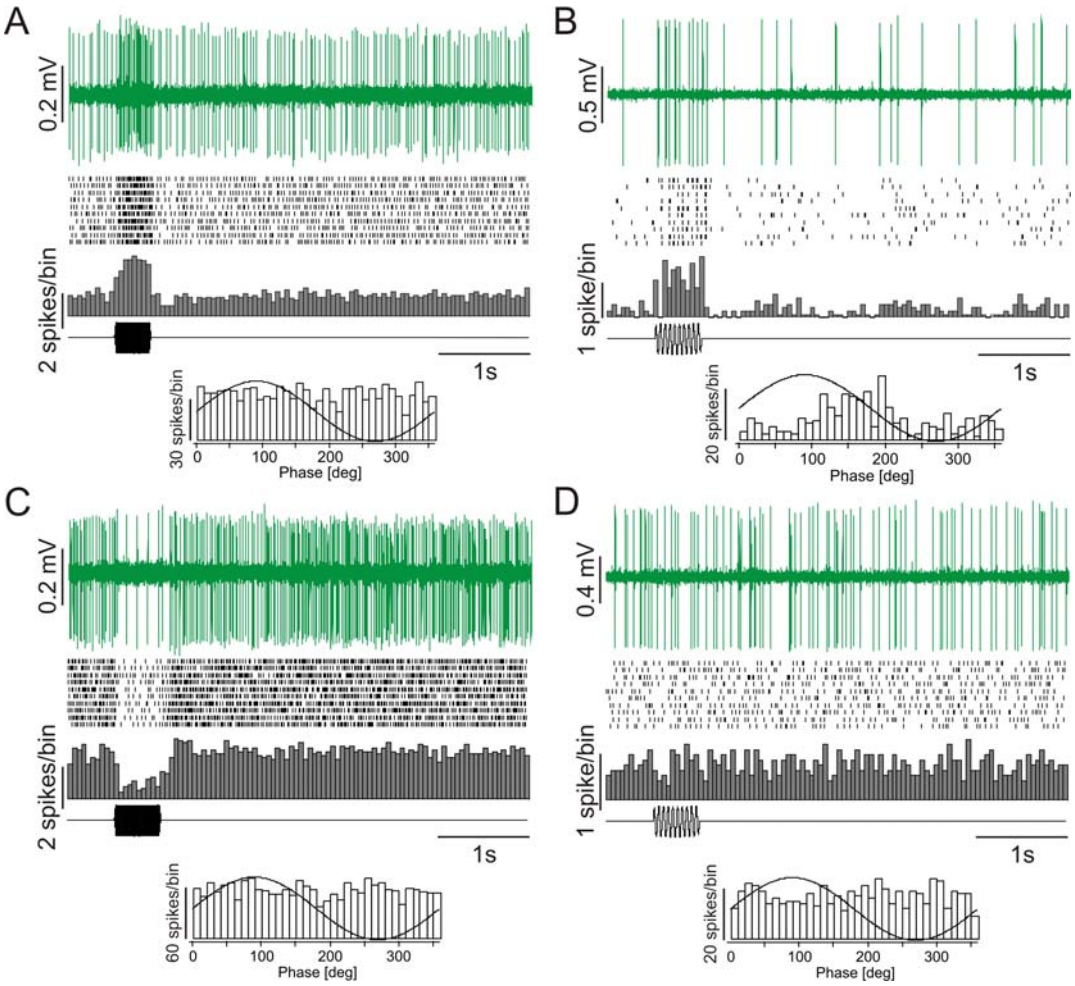

Figure 13: Responses of MON units to a sinusoidally vibrating sphere. Each graph shows from top to bottom an original recording trace (green), a raster plot of the responses to 10 stimulation repetitions (black), the corresponding Peri-Stimulus-Time-Histogram (PSTH, bin width 20 ms, grey), the stimulus trace and a period histogram (bin width 10 degree). **A:** Unit that responded with an increase in discharge rate to 100 Hz. **B:** Unit that responded with a phase-locked increase in discharge rate to 20 Hz (r = 0.63, Z = 43.94). **C:** Unit that responded with a decrease in discharge rate to 100 Hz. **D:** Unit that did not respond the vibrating sphere (20 Hz, Mann-Whitney, p = 0.471).

Group 1 units (n = 9)

Units in this group exhibited a change in discharge rate and/or phase-locking in response to only one of the applied frequencies (for an overview see Table 2, Figure 14A and Figure 15). **One** unit exhibited a weakly phase-locked (Z = 5.45) increase in discharge rate in response to the 20 Hz stimulus (Figure 14A). **Six** units decreased their discharge rate in response to either a 50 Hz (n=3) or a 100 Hz (n=3) stimulus but none of these units exhibited phase-locking. Finally, **two** units responded with phase-locking to a 50 Hz stimulus (Z = 5.37 and 19.97) but without a change in discharge rate.

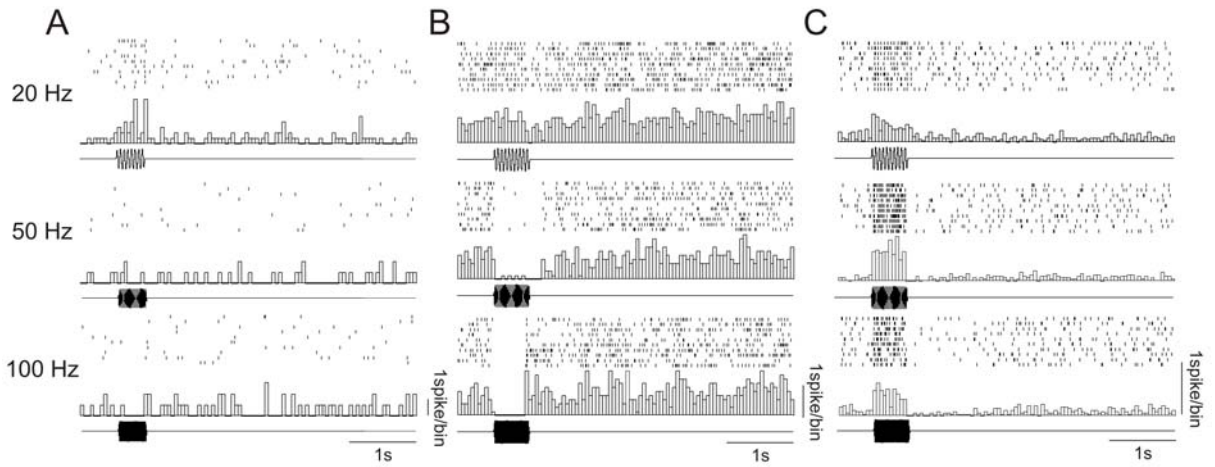

Figure 14: Examples of MON unit responses to different stimulus frequencies. **A:** Increase in discharge rate in response to 20Hz, no response to 50Hz and 100Hz (Group 1). **B:** Decrease in discharge rate in response to 50Hz and 100Hz, no response to 20Hz (Group 2). **C:** Increase in discharge rate in response to all three stimulus frequencies (Group 3).

	20 Hz	50 Hz	100 Hz	Total
Rate increase	-	-	-	0
Rate increase and phase-locking	1	-	-	1
Rate decrease	-	3	3	6
Rate decrease and phase-locking	-	-	-	0
No rate change but phase-locking	-	2	-	2

Table 2: Types of responses of MON units assigned to Group 1.

Changes in discharge rate and phase-locking of Group 1 units are shown in Figure 15. This figure shows that most of the units showed greatest change in discharge rate in response to 50 Hz (56 %, Figure 16 left). 56 % of the units exhibited their maximal Z-Value in response to 50 Hz stimulation and 22 % increased Z-Value with increasing stimulation frequency (Figure 16 right).

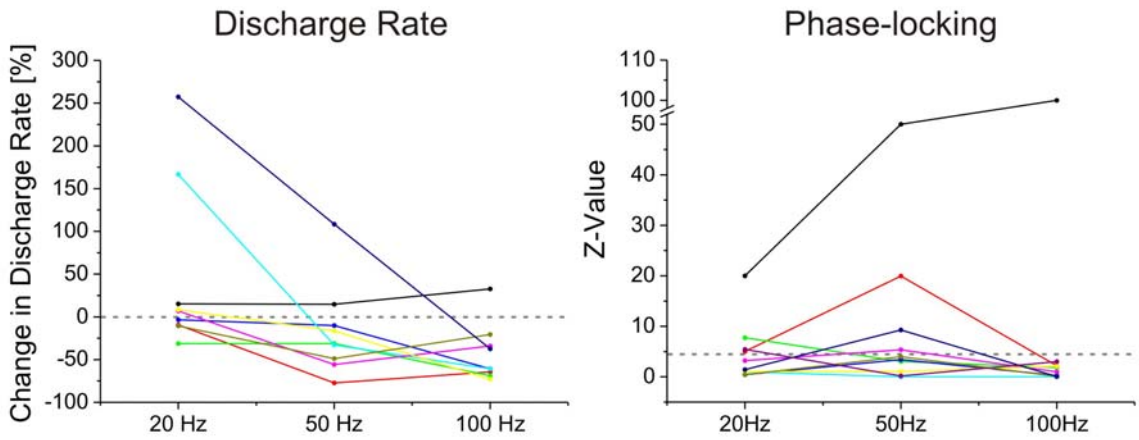

Figure 15: Rate changes and phase-locking in units assigned to Group 1. Different colours refer to different units. **Left:** Percent change in discharge rate as a function of stimulus frequency. The horizontal dashed line indicates no change in discharge rate. **Right:** Z-Value as function of stimulus frequency. The horizontal dashed line represents the Z-Value criterion (Z = 4.6).

Group 2 units (n = 24)

Units in this group exhibited a change in discharge rate and/or phase-locking in response to two of the three stimulus frequencies (for an overview see Table 3 and Figure 16).

An increase in discharge rate was observed in **thirteen** units. *Eleven* units increased discharge rate and showed phase-locking in response to distinct but different pairs of stimulus frequencies (20 and 50 HZ: n = 2, 20 and 100 Hz: n = 1, 50 and 100 Hz: n = 8, see Table 3, Figure 14B). The remaining *two* units increased discharge rate (50 and 100 Hz) without phase-locking.

A decrease in discharge rate was observed in **four** units. *Two* units decreased discharge rate in response to 50 and 100 Hz stimuli, and one of these units in addition exhibited phase-locking (Figure 14B). The other *two* units decreased discharge rate in response to 20 and 50 Hz but nonetheless exhibited phase-locked responses.

Six units did not change their discharge rates in response to any of the three stimulus frequencies but instead responded with phase-locked action potentials. *One* of those units exhibited phase-locking in response to 20 and 50 Hz and *five* units in response to 50 and 100 Hz.

One of the units of group 2 exhibited a response behaviour that was different from that of all other units in this group. It did not respond to 20 Hz, increased discharge

rate in response to 50 Hz and decreased discharge rate in response to the 100 Hz stimulus. Phase-locking was observed only in response to the 50 Hz stimulus (Z = 20.1).

	20 + 50 Hz	20 + 100 Hz	50 + 100 Hz	Total
Rate increase	-	-	2	2
Rate increase and phase-locking	2	1	8	11
Rate decrease	-	-	1	1
Rate decrease and phase-locking	2	-	1	3
No rate change and phase-locking	1	-	5	6
Rate increase and rate decrease			1	1

Table 3: Types of responses of MON units assigned to Group 2.

Figure 16 shows changes in discharge rate and phase-locking of Group 2 units. The majority of the units showed greatest change in discharge rate in response to 50 Hz (46 %) and 100 Hz (42 %, Figure 16 left). Most of the units exhibited their maximal Z-Value in response to 50 Hz stimulation (67 %). Only 13 % increased Z-Value with increasing stimulation frequency (Figure 16 right).

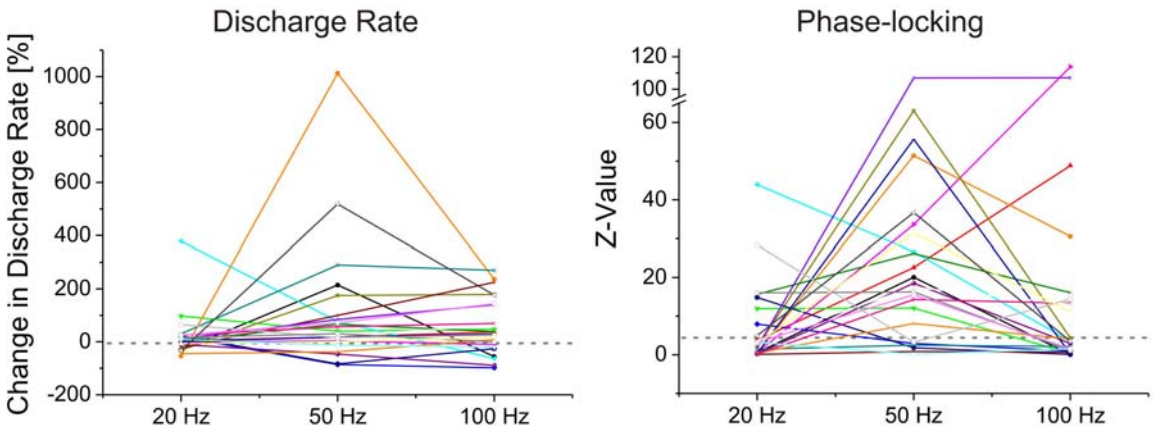

Figure 16: Rate changes and phase-locking in units assigned to Group 2. Different colours refer to different units. **Left:** Percent change in discharge rate as a function of stimulus frequency. The horizontal dashed line indicates no change in discharge rate. **Right:** Z-Value as function of stimulus frequency. The horizontal dashed line represents the Z-Value criterion (Z = 4.6).

Group 3 units (n = 52)

Units of this group comprised more than half of the units recorded. They responded with a change in discharge rate and/or phase-locking in response to all three stimulus frequencies (for an overview see Table 4 and Figure 17).

Thirty-three of these units exhibited increased discharge rates and/or phase-locking in response to the vibrating sphere. *Twenty-three* of these units showed an increase in discharge rate in response to all three applied frequencies. Nine of these units exhibited phase-locking in response to all three frequencies (e.g., Figure 14C), and the other fourteen exhibited phase-locking in response to only one or two of the presented frequencies (see Table 4A). *Eight* units showed an increase in discharge rate in response to two of the stimulus frequencies (20 and 100 Hz: n = 1; 50 and 100 Hz: n = 7). However, all but one of these eight units showed phase-locking in response to all three stimulus frequencies. This one unit had increased discharge rates to 20 and 100 Hz, and exhibited phase-locking in response to the 50 Hz stimulus. Finally, *two* units were recorded that increased discharge rate in response to one of the three stimulus frequencies (50 Hz) but exhibited phase-locking in response to all three stimulus frequencies.

Nine group 3 units decreased discharge rate in response to the sine wave stimuli. *Five* of these units decreased discharge rate in response to all three stimulus frequencies and the responses of three of these units in addition were phase-locked to one (20 Hz: n = 1; 50 Hz: n = 1) or all three frequencies (n = 1). In another *four* units, discharge rate were decreased in response to one or two stimulus frequencies but the discharges were phase-locked to the other (20 and 50 Hz: n = 1; 20 Hz: n = 1; 50 Hz: n = 1) or even to all three stimulus frequencies (n = 1). With one exception, in which phase-locking was observed in response to all three frequencies, the nine units described here exhibited phase-locked discharges in response to those frequencies to which they did not show a change in discharge rate.

Three group 3 units did not change discharge rate to any if the three stimulus frequencies but always exhibited phase-locking.

Seven units were recorded in which the type of response depended on stimulus frequency, i.e., these units responded with an increase or decrease in discharge rate and/or with phase-locking depending on stimulus frequency (Table 4B). *Two* units increased their discharge rate in response to the 20 Hz stimulus but decreased discharge rate in response to 50 and 100 Hz. One of them phase-locked in response

to 20 Hz, the other unit did not. *Three* units increased their discharge rate in response to 20 Hz (phase-locked: n = 2) but decreased discharge rate in response to 100 Hz. They did not show a change in discharge rate but phase-locked in response to 50 Hz. *One* of the seven units decreased discharge rate in response to stimulation with 20 and 100 Hz without phase-locking; the 50 Hz sine wave, however, did not evoke a change in discharge rate but the unit responded with phase-locking. Finally, *one unit* showed phase-locking without a change in discharge rate in response to 20 Hz stimulation, an increase in discharge rate with phase-locking in response to 50 Hz and a decreased discharge rate without phase-locking during stimulation with 100 Hz.

A

	Phase-locking (20, 50 and 100 Hz)	20 Hz	50 Hz	100 Hz	20 + 50 Hz	20 + 100 Hz	50 + 100 Hz	no Phase-locking	Total
Rate increase (all frequencies)	9	3	3	1	-	1	5	1	23
Rate increase (two frequencies)	7	-	1	-	-	-	-	-	8
Rate increase (one frequency)	2	-	-	-	-	-	-	-	2
Rate decrease (all frequencies)	1	1	1	-	-	-	-	2	5
Rate decrease (two frequencies)	1	1	1	-	-	-	-	-	3
Rate decrease (one frequency)	-	-	-	-	1	-	-	-	1
No Rate change but Phase-locking	3	-	-	-	-	-	-	-	3

B

20 Hz	50 Hz	100 Hz	Total
Rate increase	Rate decrease	Rate decrease	1
Rate increase	Rate decrease	Rate decrease	1
Rate increase	Phase-locking	Rate decrease	2
Rate increase	Phase-locking	Rate decrease	1
Rate decrease	Rate increase	Rate decrease	1
Phase-locking	Rate increase	Rate decrease	1

Table 4: Types of responses of MON units assigned to Group 3. Phase-locking refers to phase-locked responses without a change in discharge rate. **A:** Units which responded with an increase or decrease in discharge rate independent of stimulus frequency. **B:** Units which responded with an increase or a decrease in discharge rate depending on stimulus frequency. Red text denotes units that exhibited phase-locked responses.

Changes in discharge rate and phase-locking of Group 3 units are shown in Figure 17. This figure shows that most of the units showed greatest change in discharge rate in response either to 50 Hz (43 %) or 100 Hz (44 %, Figure 17 left). The majority of Group 3 units exhibited their maximal Z-Value in response to 50 Hz stimulation (63 %). Only 10 % increased Z-Value with increasing stimulation frequency (Figure 17 right).

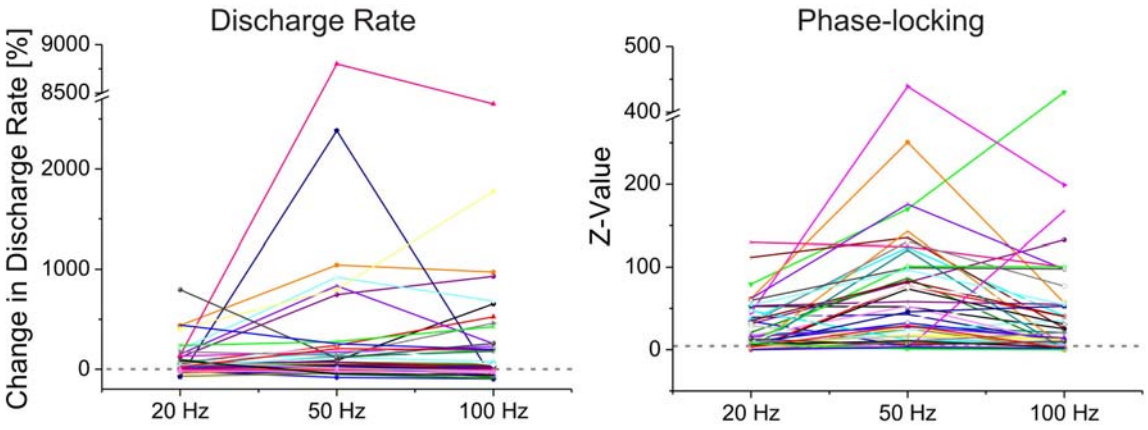

Figure 17: Rate changes and phase-locking in units assigned to Group 3. Different colours refer to different units **Left:** Percent change in discharge rate as a function of stimulus frequency. The horizontal dashed line indicates no change in discharge rate. **Right:** Z-Value as function of stimulus frequency. The horizontal dashed line represents Z-Value criterion (Z = 4.6).

Figure 18 illustrates that different MON units exhibited different frequency selectivities. The figure shows normalized frequency response functions (change in discharge rate as function of stimulation frequency) of MON units that were obtained as follows: First, for each unit the change in discharge rate relative to the ongoing rate was calculated. Then, the rate changes were normalized to the greatest change measured in response one of the three stimulus frequencies. Finally, units were grouped according to the frequency at which they exhibited the greatest change in discharge rate. This analysis was performed independent of the grouping of units described above and revealed that 15% of the recorded MON units exhibited low-pass characteristics, i.e., they exhibited the greatest change in discharge rate to a 20Hz stimulus, 40% exhibited band-pass characteristics, i.e., they responded best to 50Hz, and 45% exhibited high-pass characteristics, i.e., they showed the greatest change in discharge rate to a 100Hz stimulus.

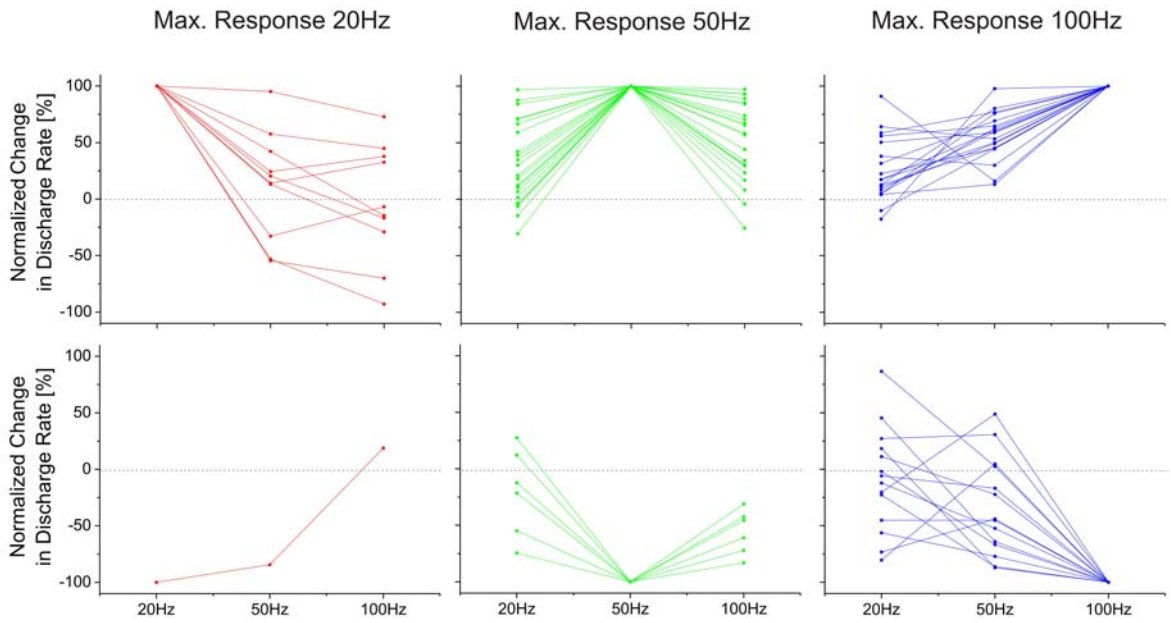

Figure 18: Normalized frequency response functions of MON units. Normalized changes in discharge rate (for explanation see text) are plotted as function of stimulus frequency. In terms of displacement MON units exhibited low-pass (**left**), band-pass (**middle**), or high-pass characteristics (**right**). Upper graphs: Units that responded with an increase in discharge rate. Lower graphs: Units that responded with a decrease in discharge rate.

Phase-locking

A large number of the responses of MON units to sine wave stimuli was characterized by statistically significant phase-locking. In about two thirds (63%) of the responses Z-values (Rayleigh statistic) were greater than 4.6 and for about one third of the responses R-values were greater than 0.5. This is evident from the data shown in Figure 19 in which Z value are plotted as function of synchronisation coefficients R for different stimulation frequencies (units that responded with decreased discharge rates to sine wave stimulation were not considered for this analysis). This analysis revealed that in about two thirds of the responses of MON units (63 %) the Z-value was greater than 4.6 and that in about one third of the responses (30 %) R-values were greater than 0.5 (Figure 19).

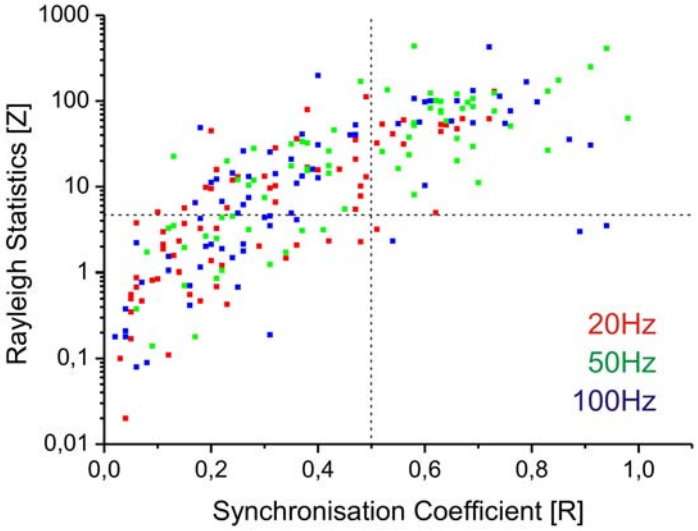

Figure 19: Scatter plot of Z-values as a function of synchronisation coefficients R. The horizontal dashed line indicates the critical value of the Rayleigh test (Z = 4.6), separating units without significant phase-locking (below) and with significant phase-locking (above). The vertical line at R = 0.5 is an arbitrary measure to distinguish weakly phase-locked (left) and strongly phase-locked (right) units. Note that the Y – axis has a logarithmic scale. Colours refer to different stimulation frequencies (red: 20 Hz, green: 50 Hz, blue: 100 Hz).

On average, responses to 50 Hz stimulation exhibited the greatest R-values and the greatest Z-values (Figure 20). Statistical comparison revealed that the distribution of both R-values and Z-values for the three stimulation frequencies were significantly different from each other (Figure 20, Wilcoxon test, $p \leq 0.05$).

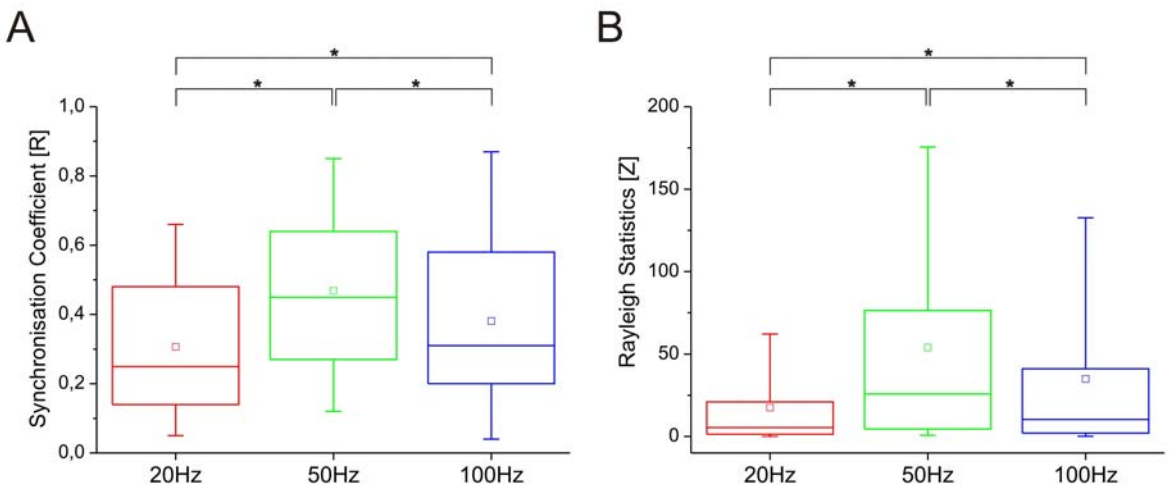

Figure 20: Box-Whisker-Plot of synchronisation coefficients R (**A**) and Rayleigh statistics Z (**B**) representing 25 % and 75 % percentiles, medians, means (squares), smallest and greatest observation. Colours refer to different stimulation frequencies. Asterisks indicate a significant difference between datasets (Wilcoxon test, $p \leq 0.05$).

3.2 Spatial Excitation Patterns

3.2.1 Classification of spatial excitation patterns

The spatial excitation patterns of 102 single MON units in 48 fish were determined by recording responses to a vibrating sphere that was positioned at various locations alongside the fish (distance 1 cm). Axis of sphere vibration was parallel to the longitudinal axis of the fish (0°, see Materials and Methods). Average ongoing activity of the recorded units was 13.8 ± 11.0 spikes*s^{-1} (mean ± SD; median: 11.9 spikes*s^{-1}, see Table 5).

The number of spatial excitation patterns measured was quite large. Moreover, spatial excitation patterns were highly variable between units. Therefore, in this part of the thesis only selected excitation patterns will be shown and described. A more complete overview of spatial excitation patterns will be given in the Appendix (pages 118-138).

	Mean	SD	Median	Range
Spontaneous Discharge Rate [spikes*s^{-1}]	13.8	11.0	11.9	0.1 – 57.0
Evoked Discharge Rate [spikes*s^{-1}]	18.5	13.1	13.7	1.6 - 65.6
Change in Discharge Rate [%]	132.9	401.7	42.6	-79.8 - 3300.0
Synchronization Coefficient (R)	0.5	0.2	0.5	0.1 - 0.9
Maximum Rayleigh Statistics (Z)	25.4	24.0	17.4	1.0 - 99.2
Maximum HMW [% body length]	45.8	27.0	38.7	4.6 - 105.0
Centre of HMW [% body length]	37.1	21.1	41.0	-12.1 - 87.4

Table 5: Ongoing rates and various measures of the evoked rates of MON units.

Based on the shape of the excitation patterns, they were assigned to one of three groups.

Group 1: Excitation patterns consisting of one or more excitatory areas (n = 78), from which stimulation with the vibrating sphere caused an increase in discharge rate (Figure 21A-C).

Group 2: Excitation patterns consisting of one or more inhibitory areas (n = 13), from which stimulation with the vibrating sphere caused a decrease in discharge rate (Figure 22A-C).

Group 3: Excitation patterns consisting of adjacent excitatory and inhibitory areas (n = 11, Figure 23A-C).

Excitation patterns with one or more excitatory areas (Group 1, n = 78)

The excitation patterns of 78 units consisted of one or more areas from which stimulation with the vibrating sphere elicited an increase in discharge rate (Figure 21A-C). Twenty-four of these units had excitation patterns consisting of a

single small area (Figure 21A), and in twenty-three units patterns consisted of at least two areas of increased discharge rate (Figure 21B). Thirty-one units had excitation patterns that were broad and extended along the entire length of the fish (Figure 21C).

The majority of the units in this group (n = 63, 84 %) exhibited responses that were phase-locked to the stimulus at one or more of the locations where the dipole caused a rate increase. In fact, in terms of phase-locking the spatial response patterns most often (n = 50) matched the spatial pattern of spike activity (Figure 21A-C). In the remaining cases (n = 13) the spatial phase-locking patterns matched at least partially the spatial discharge patterns, i.e., units exhibited phase-locking across a restricted range of locations from which the dipole caused an increase in spike activity (e.g., Figure 27).

A number of units (n = 26, 41%) exhibited distinct changes in phase angle from one stimulation location to the next with magnitudes of approximately 180° (range 119°-270°). In nineteen units a single change in phase angle (Figure 21C), and in seven units two changes in phase angle with opposite sign were observed within the spatial excitation pattern (Figure 27, Figure 28, 0° vibration direction). Single phase angle changes typically occurred at locations intermediate between two excitation peaks (n = 13). In contrast, two phase angle changes with opposite sign typically occurred at locations bordering an excitation maximum (n = 5). In the remaining cases, there was no apparent correlation between the locations of the phase angles changes and the location of excitation maxima. In about an equal number of units (n = 27, 43 %) no distinct changes in phase angles occurred within the spatial excitation pattern (Figure 21A/B). Finally, in a small number of units (n = 10, 16 %) phase angles changed systematically in small steps from either high or low values at the rostral-most and caudal-most sphere location to reach a minimum or maximum value, respectively, within a unit's excitation pattern (Figure 21A).

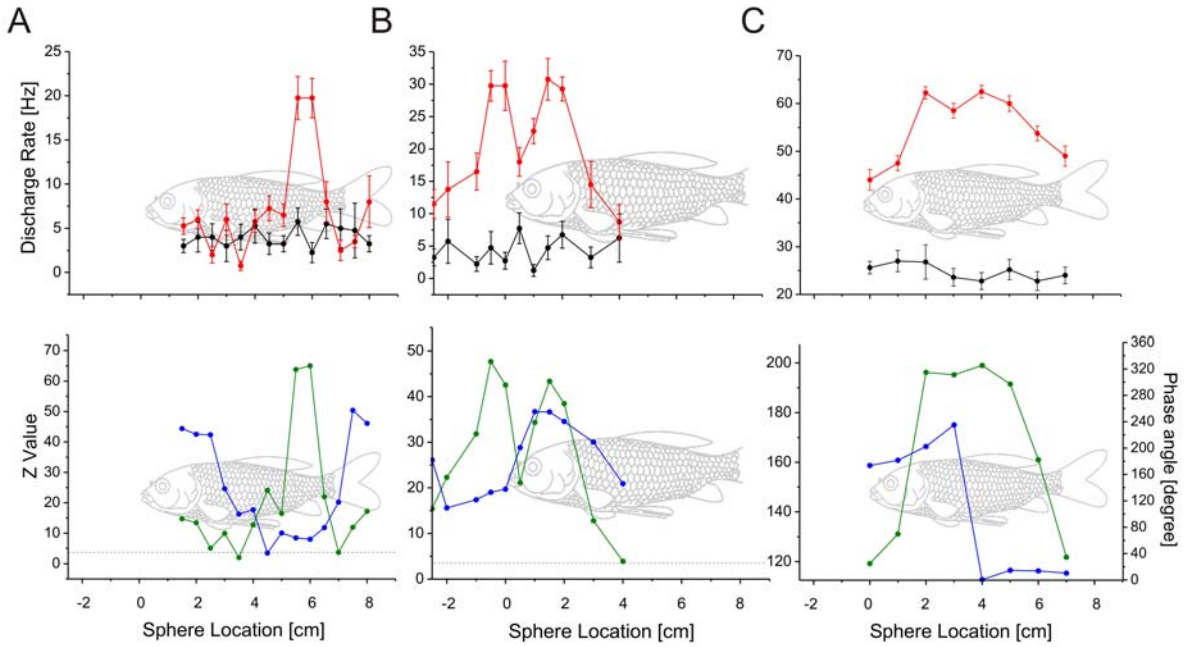

Figure 21: Spatial excitation patterns of MON units from Group 1 obtained by stimulating the lateral line with a sphere creating sinusoidal vibrations parallel to the fish (angle of vibration 0°). **A:** A spatial excitation pattern characterized by a single spatially restricted peak of increased discharge rate. **B:** Two adjacent peaks of increased discharge rate. **C:** A broad area of increased discharge rate that extends across most of the fish length. Upper graphs: Ongoing discharge rates (black lines) and evoked rates (red lines) as a function of sphere location along the side of the fish (sphere radius 8 mm, frequency 50 Hz, vibration displacements in A: 650 µm, B: 200 µm, C: 250 µm, 1 cm distance between sphere and fish). Vertical bars represent standard deviation. Lower graphs: Z-values (green lines, left Y-axis) and mean phase angles (blue lines, right Y-axis) as a function of sphere location along the side of the fish. The horizontal grey dashed line indicates the Z-value criterion ($Z \geq 4.6$). The fish in the background is drawn to scale.

Excitation patterns with one or more inhibitory areas (Group 2, n = 13)

The excitation patterns of thirteen units consisted of one or more areas from which stimulation caused a decrease in discharge rate. In five units the pattern consisted of a single small area (Figure 22A), in six units it consisted of a broad area that extended along the entire length of the fish (Figure 22C) and in two units it exhibited two or more such areas (Figure 22B, Figure 30, 0° vibration direction). Units within this group did not exhibit phase-locked responses (Figure 22A - C). Therefore, systematic changes in phase angle did not occur.

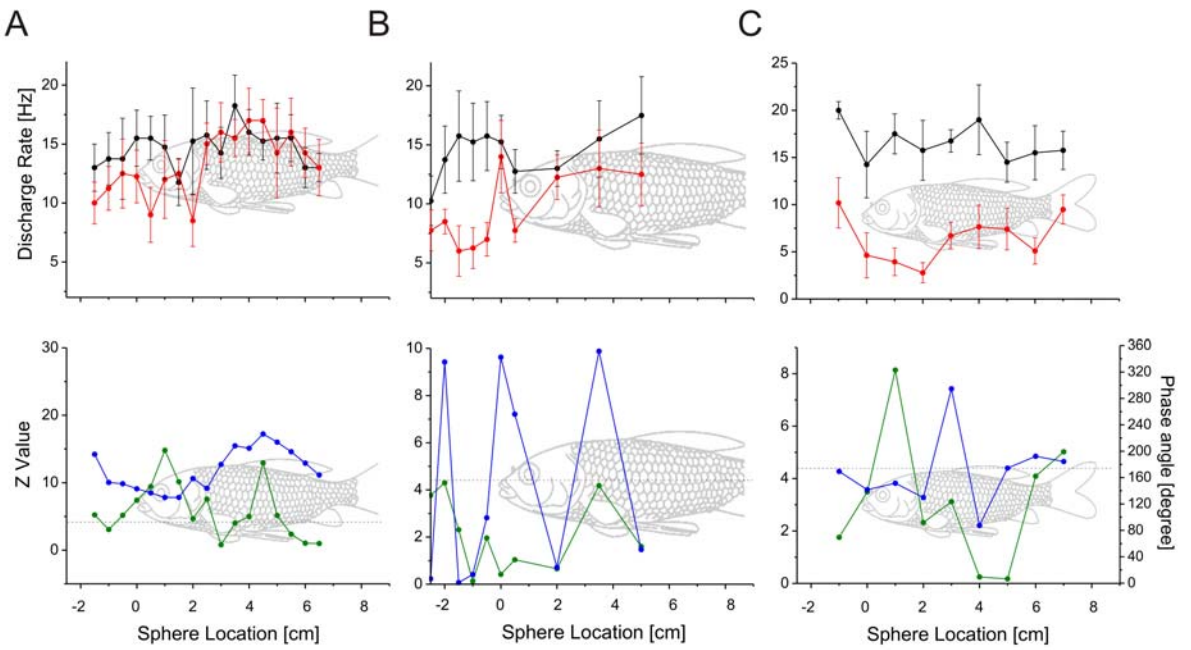

Figure 22: Spatial excitation patterns of MON units from Group 2 obtained by stimulating the lateral line with a sphere creating sinusoidal vibrations parallel to the fish (angle of vibration 0°). **A:** A spatial excitation pattern characterized by a single spatially restricted area of decreased discharge rate. **B:** Two adjacent areas of decreased discharge rate. **C:** A single broad area of decreased discharge rate that extends across most of the fish length. Upper graphs: Ongoing discharge rates (black lines) and evoked rates (red lines) as a function of sphere location along the side of the fish (sphere radius 8 mm, frequency 50 Hz, vibration displacements in A: 350 µm, B: 200 µm, C: 250 µm, 1 cm distance between sphere and fish). Vertical bars represent standard deviation. Lower graphs: Z-values (green lines, left Y-axis) and mean phase angles (blue lines, right Y-axis) as a function of sphere location along the side of the fish. The horizontal grey dashed line indicates the Z-value criterion ($Z \geq 4.6$). The fish in the background is drawn to scale.

Excitation patterns with excitatory and inhibitory areas (Group 3, n = 11)

The excitation patterns of eleven units consisted of one or more areas from which stimulation with the vibrating sphere caused an increase in discharge rate and one or more adjacent areas from which stimulation caused a decrease of ongoing discharge rate. Number and relative locations of excitatory and inhibitory areas differed across units. Five units had excitation patterns consisting of a single excitatory and a single adjacent inhibitory area; in two of these units the excitatory area was located caudally to the inhibitory area (Figure 23A) while in three units the excitatory area was located rostral to the inhibitory area (Figure 23B). In four units excitation patterns consisted of three adjacent areas: in two units an excitatory area was bordered rostrally and caudally by an inhibitory areas (Figure 23C) and in two other units an inhibitory area was bordered rostrally and caudally by excitatory areas. The final two units had

excitation patterns that were characterized by four areas from which the vibrating sphere caused increases or decreases in discharge rate.

Nine of the eleven units of this group exhibited phase-locked responses at one or more locations within the excitation pattern. In each case, the spatial pattern in terms of phase-locking (Z-value) matched the spatial pattern in terms of spike activity (Figure 23C). In five of these units phase angles increased and decreased independent on sphere location (Figure 23C) while in the remaining four units a continuous increase and/or decrease of phase angles without steep shifts occurred (Figure 23A).

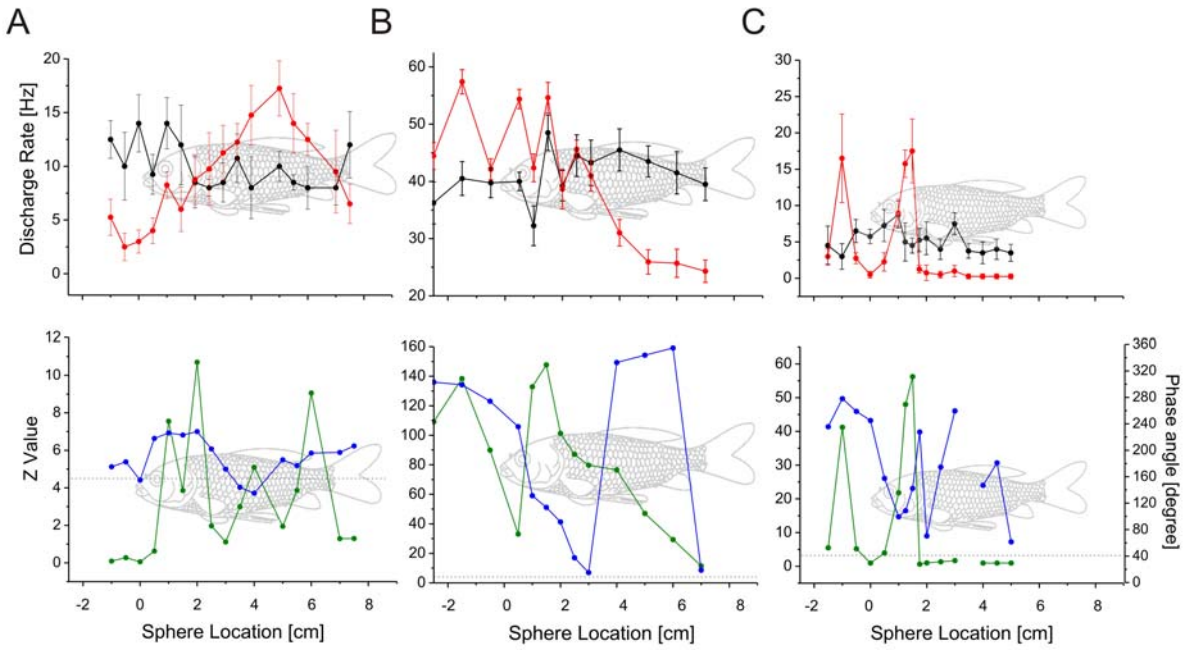

Figure 23: Spatial excitation patterns of MON units from Group 3 obtained by stimulating the lateral line with a sphere creating sinusoidal vibrations parallel to the fish (angle of vibration 0°). **A:** A spatial excitation pattern consisting of a rostral area of decreased and a caudal area of increased discharge rate. **B:** A spatial excitation pattern consisting of a rostral area of increased and a caudal area of decreased discharge rate. **C:** A central area of increased discharge rate bordered rostrally and caudally by areas of decreased discharge rate. Upper graphs: Ongoing discharge rates (black lines) and evoked rates (red lines) as a function of sphere location along the side of the fish (sphere radius 8 mm, frequency 50 Hz, vibration displacements in A: 650 µm, B: 200 µm, C: 250 µm, 1 cm distance between sphere and fish). Vertical bars represent standard deviation. Lower graphs: Z-values (green lines, left Y-axis) and mean phase angles (blue lines, right Y-axis) as a function of sphere location along the side of the fish. The horizontal grey dashed line indicates the Z-value criterion ($Z \geq 4.6$). The fish in the background is drawn to scale.

Size and location of excitation patterns

The sizes of the spatial excitation patterns were quantified by their half-maximum widths (HMW, n = 68). Across all groups of units, HMWs ranged between 10 and 105% of the fish's body length (mean: 43 %, median: 40%, Figure 24A). Among units with excitation patterns consisting of one or more excitatory areas HMWs ranged between 10% and 89 % of body length (mean: 41 %, median: 39%). These values were comparable to those obtained for units with excitation patterns consisting of one or more inhibitory areas (Mann-Whitney-U-Test, p = 0.721) for which HMWs ranged between 10 % and 105 % of body length (mean: 47 %, median: 30%). Units with excitation patterns consisting of adjacent excitatory and inhibitory areas had HMWs that were, on average, also comparable to those of units in the other groups (Mann-Whitney-U-Test, comparison with group 1: p = 1.00; comparison with group 2: p = 0.144,). HMWs of units from group 3 ranged between 39 % and 79 % of body length (mean: 61 %, median: 64%).
Most (83%) of the centre locations of the excitation patterns (midpoint between 50% values) were located between about 20% and 60% of the fish's body length. Excitation patterns with centre locations located more rostrally or caudally had HMWs that appeared to be smaller. However, there was no significant difference between the excitation patterns in terms of centre location and HMW (Figure 24B).

In many units (n = 34), HMWs could not be determined because discharge rates did not drop to below 50% of the maximum evoked rate across the range of sphere locations from which the units were stimulated. Typically, this happened in those units in which the excitation pattern extended beyond the length of the fish (e.g., Figure 21C). In twenty-seven of the incomplete measured excitation patterns discharge rates dropped to values between 54 % and 96 % of the maximum discharge rate. In seven neurons discharge rates were at maximum within the stimulated area. The distribution of the centre locations from incomplete excitation patterns differed from those obtained from completely measured excitation patterns (p = 0.049, Mann-Whitney-U-Test). Most of the centre locations from incomplete patterns (88%) were located more between about 10 and 50% of the fish's body length (Figure 24B), i.e., slightly more rostral than those from complete patterns.

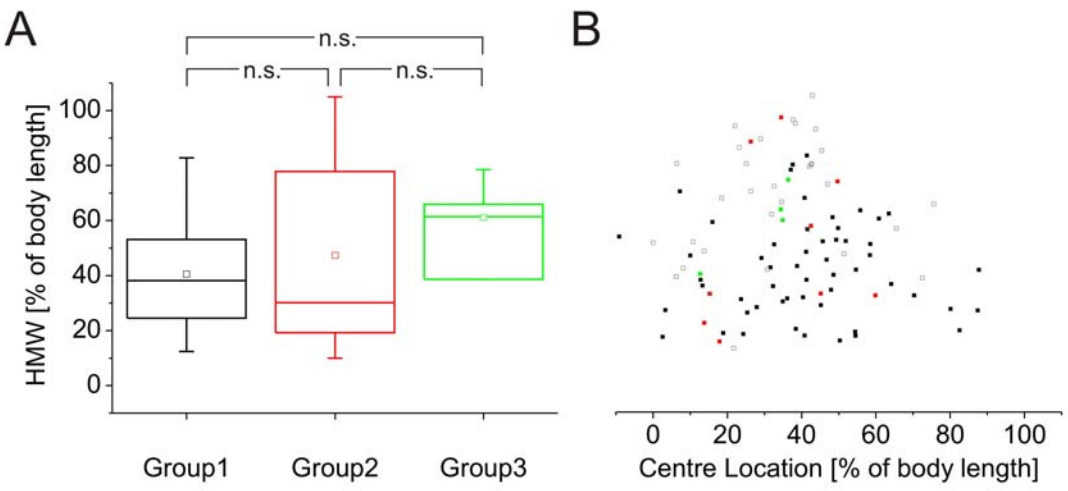

Figure 24: A: Half-maximum widths (HMW) of the excitation patterns from the three groups of units. Box-Whisker-Plot of HMWs with 25 % and 75 % percentiles, medians, means (squares), smallest and greatest observation.
B: HMWs as function of the centre locations of the excitation areas along the side of the fish (in percent of the fishes' body length). Differently coloured symbols represent the type of excitation pattern. Black squares: Excitation patterns where stimulation caused an increase in discharge rate. Red squares: Excitation patterns where stimulation caused a decrease in discharge rate. Green squares: Excitation patterns with increases and decreases in discharge rate. Grey squares: incomplete measured excitation patterns.

3.2.2 Effects of sphere vibration direction on spatial excitation patterns

The effects of sphere vibration direction on spatial excitation patterns were investigated in thirty-eight units. Due to the long stimulation protocol, many units were lost before the entire protocol was completed. Complete data sets, i.e., excitation patterns for all four vibration angles (0°, 45°, 90° and 135°) were obtained from 18 units, data sets for three vibration angles (0°, 90° and 45° or 135°) from five units, and for two vibration angles (0° and 90°) from fifteen units. In most units (n = 27, 71 %) at least subtle changes were observed in the excitation patterns in terms of shape, size, discharge rates and/or phase-locking when the direction of sphere vibration was altered. In eleven units (29%), spatial excitation patterns were apparently independent of sphere vibration angle.

A few units exhibited changes in excitation patterns with changing sphere vibration direction that were comparable to the changes observed among primary afferent fibres in terms of both, discharge rate and/or phase-locking (n = 3). In most units,

however, changes in excitation pattern size and/or shape with changing sphere vibration direction were not comparable to those described for primary afferents (n = 24). Depending on vibration angle, the excitation patterns of these units differed in terms of number of response areas, location of excitation pattern maxima/minima, half-maximum width, discharge rate, and/or phase-locking. In most cases, more than one of these parameters was changed concurrently. A detailed description of all effects observed is given below.

Effects on spatial discharge patterns

Changing the vibration angle affected the spatial excitation patterns of twenty-seven MON units in terms of their discharge rates. Three units were recorded in which spatial excitation patterns depended on sphere vibration direction in a manner that is characteristic for primary afferents. When sphere vibration direction was parallel to the fish (0°), these units exhibited spatial excitation patterns that consisted of a single peak of excitation which, in some cases, appeared to be bordered by one or two smaller side peaks (e.g., Figure 25). When sphere vibration direction was altered from parallel to orthogonal (90°), the excitation pattern changed in a predictable manner. The single excitation peak was replaced by a discharge rate trough separating two excitation peaks located rostrally and caudally to it (Figure 25). The effects of changing sphere vibration direction on phase-locking and phase-angles in these units were also as primary-like. This will be described in the following subchapter.

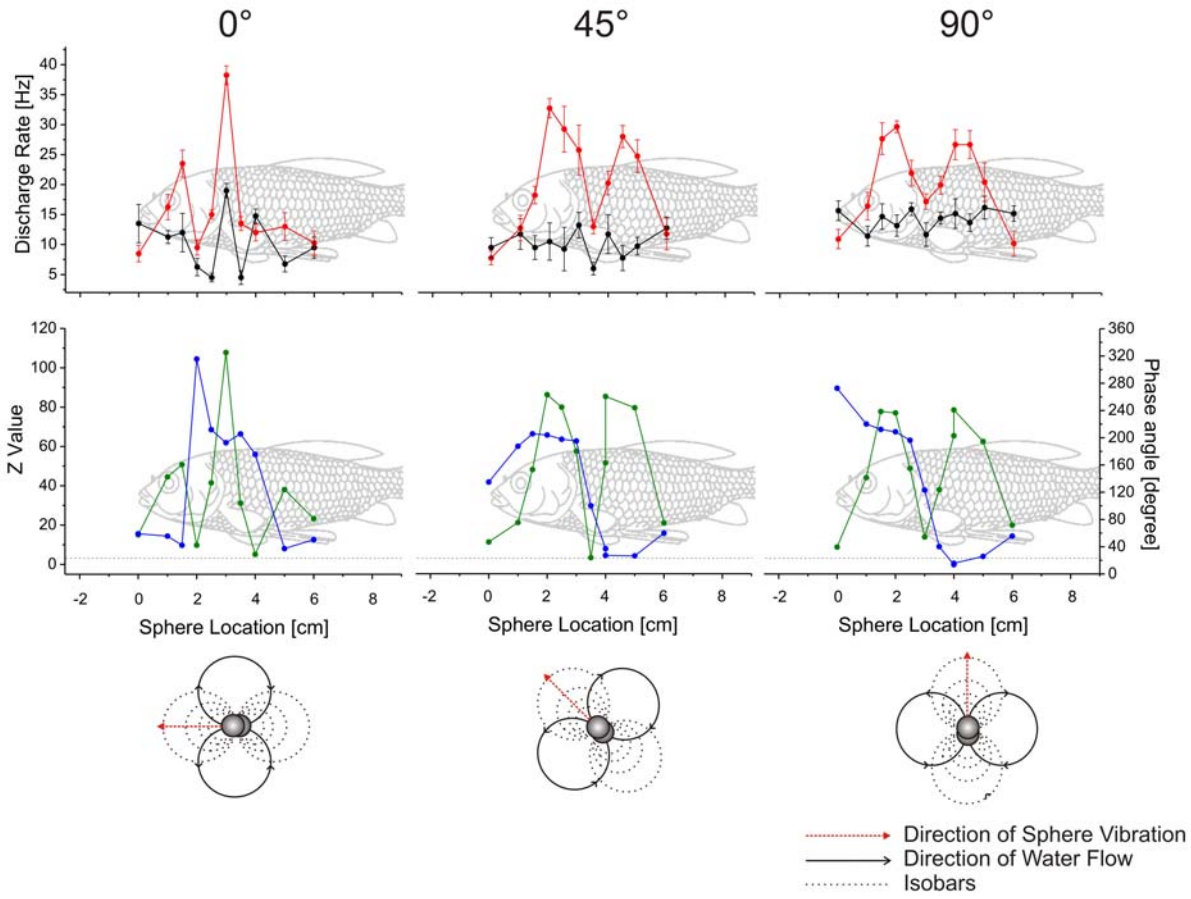

Figure 25: Spatial excitation patterns of a MON unit obtained with different vibration directions (0. 45 and 90°) of a vibrating sphere. **Upper graphs:** Ongoing discharge rates (black lines) and evoked discharge rates (red lines) averaged across eight stimulus presentations are plotted as function of sphere location along the side of the fish (sphere radius 8 mm, frequency 50 Hz, vibration displacement 200 µm, 1 cm distance between sphere and fish). Vertical bars represent standard deviation. The fish in the background is drawn to scale. **Lower graphs:** Z-values (green lines, left Y-axis) and mean phase angles (blue lines, right Y-axis). The horizontal grey dashed line indicates the Z-value criterion ($Z \geq 4.6$).The bottom-most drawings illustrate the direction of sphere vibration (red arrows), the associated water flow (solid lines), and isobars (dotted lines).

Twenty-four units were recorded in which spatial excitation patterns depended on sphere vibration direction in a manner that was not characteristic for primary afferents. Two of these units, when stimulated at 0° vibration direction, had spatial excitation patterns that consisted of adjacent areas of increased and decreased discharge rate. When vibration direction was 90°, these areas were swapped, i.e., the area of increased rate was now characterized by a decreased rate and the area of decreased rate was now characterized by an increased rate (Figure 26).

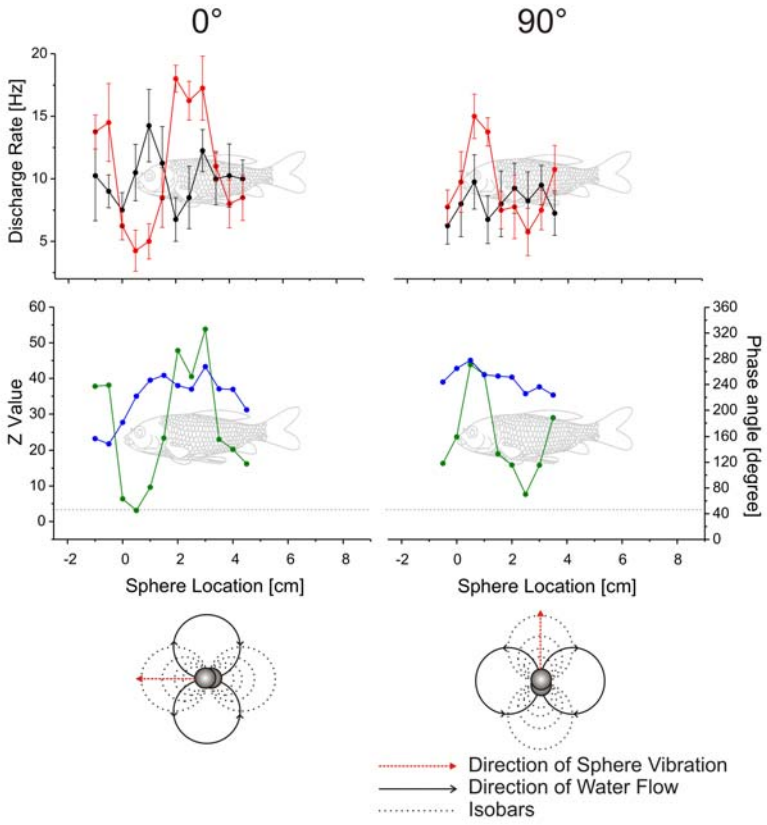

Figure 26: Spatial excitation patterns of a MON unit obtained with different vibration directions (0. 45 and 90°) of a vibrating sphere. **Upper graphs:** Ongoing discharge rates (black lines) and evoked discharge rates (red lines) averaged across eight stimulus presentations are plotted as function of sphere location along the side of the fish (sphere radius 8 mm, frequency 50 Hz, vibration displacement 500 µm, 1 cm distance between sphere and fish). Vertical bars represent standard deviation. The fish in the background is drawn to scale. **Lower graphs:** Z-values (green lines, left Y-axis) and mean phase angles (blue lines, right Y-axis). The horizontal grey dashed line indicates the Z-value criterion ($Z \geq 4.6$).The bottom-most drawings illustrate the direction of sphere vibration (red arrows), the associated water flow (solid lines), and isobars (dotted lines).

In three units, the overall shape of the rather broad excitation patterns at first glance appeared to be independent of sphere vibration direction. However, the edges of the excitation patterns moved to different locations along the fish's body axis when sphere vibration direction was altered. This was particularly evident in one unit, in which the rostral border of the excitation pattern shifted caudally in a systematic manner with increasing vibration angle (Figure 27).

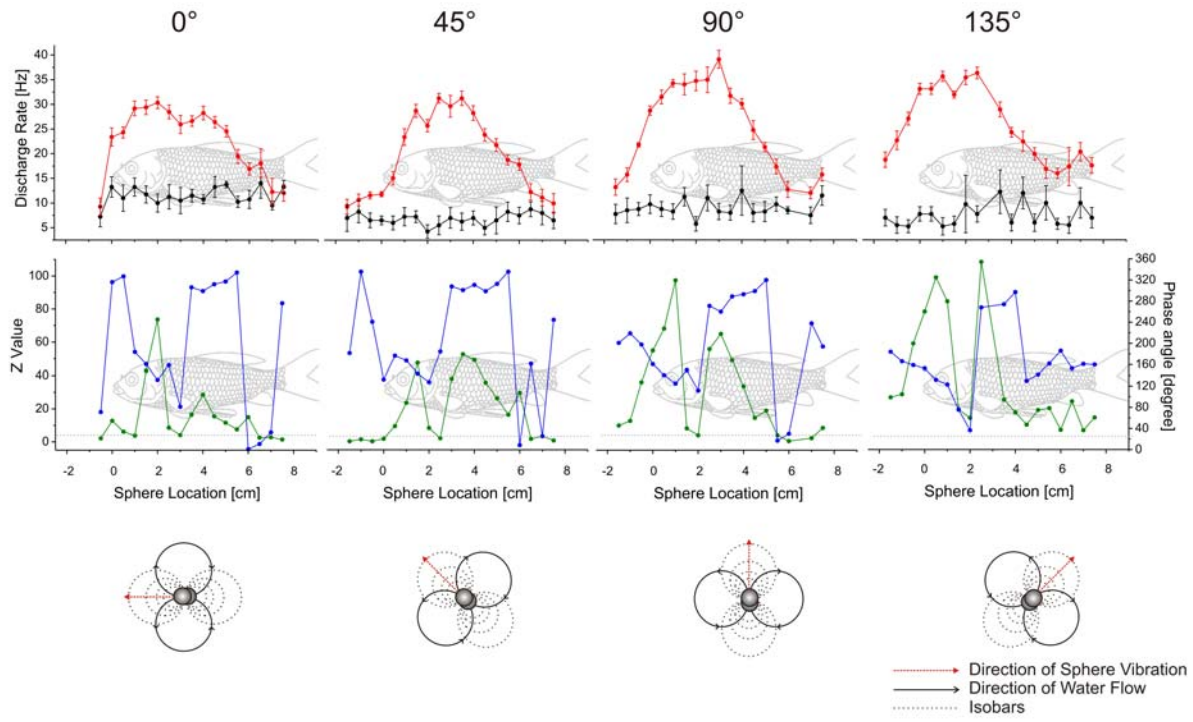

Figure 27: Spatial excitation patterns of a MON unit obtained with different vibration directions (0. 45, 90 and 135°) of a vibrating sphere. **Upper graphs:** Ongoing discharge rates (black lines) and evoked discharge rates (red lines) averaged across eight stimulus presentations are plotted as function of sphere location along the side of the fish (sphere radius 8 mm, frequency 50 Hz, vibration displacement 250 µm, 1 cm distance between sphere and fish). Vertical bars represent standard deviation. The fish in the background is drawn to scale.
Lower graphs: Z-values (green lines, left Y-axis) and mean phase angles (blue lines, right Y-axis). The horizontal grey dashed line indicates the Z-value criterion ($Z \geq 4.6$).The bottom-most drawings illustrate the direction of sphere vibration (red arrows), the associated water flow (solid lines), and isobars (dotted lines).

In the remaining nineteen units, the effects of changing sphere vibration angle of spatial excitation patterns were variable and affected number, size, and/or location of response areas. An example of one of these units is shown in Figure 28. This unit had broad spatial excitation patterns at all vibration angles but the exact shape differed from one angle to the next. For instance, at 0° vibration angle, the pattern consisted of a strong excitatory peak located rostrally and a weaker excitatory response area across the trunk region. In contrast, at 90° vibration angle two strong excitatory peaks extended across the fish, whereas at 45° and 135° vibration angle multiple excitatory areas with lower discharge rate appeared.

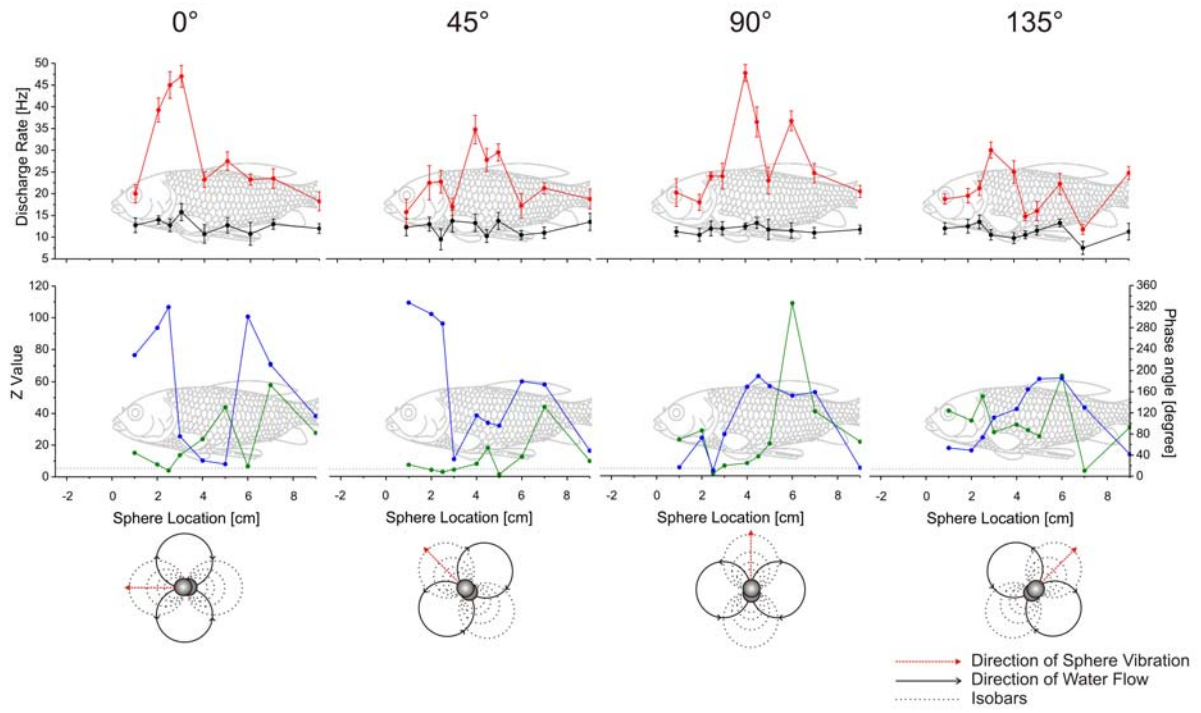

Figure 28: Spatial excitation patterns of a MON unit obtained with different vibration directions (0. 45 and 90°) of a vibrating sphere. **Upper graphs:** Ongoing discharge rates (black lines) and evoked discharge rates (red lines) averaged across eight stimulus presentations are plotted as function of sphere location along the side of the fish (sphere radius 8 mm, frequency 50 Hz, vibration displacement 350 µm, 1 cm distance between sphere and fish). Vertical bars represent standard deviation. The fish in the background is drawn to scale. **Lower graphs:** Z-values (green lines, left Y-axis) and mean phase angles (blue lines, right Y-axis). The horizontal grey dashed line indicates the Z-value criterion ($Z \geq 4.6$).The bottom-most drawings illustrate the direction of sphere vibration (red arrows), the associated water flow (solid lines), and isobars (dotted lines).

Effects on half-maximum widths

To investigate whether changes in sphere vibration angle had systematic effects on the width of spatial excitation patterns, HMWs of seventeen units (four vibration angles $n = 14$, three vibration angles $n = 3$) and the location of the maximum response peak were determined (Figure 29). HMWs from units with excitation patterns consisting of adjacent excitatory and inhibitory areas and from units that were stimulated with less than three different angles were excluded from this analysis. Overall, HMWs ranged between 8.7 and 95.8 % of body length (mean 47.2 %). In twelve units the location of the response maximum varied by 15% or more of fish body length with changing sphere vibration angle (Figure 29A). In five units the location of the response maximum varied by less than 15 % of body length, i.e., the location of maximum response was fairly independent of stimulation angle (Figure 29B).

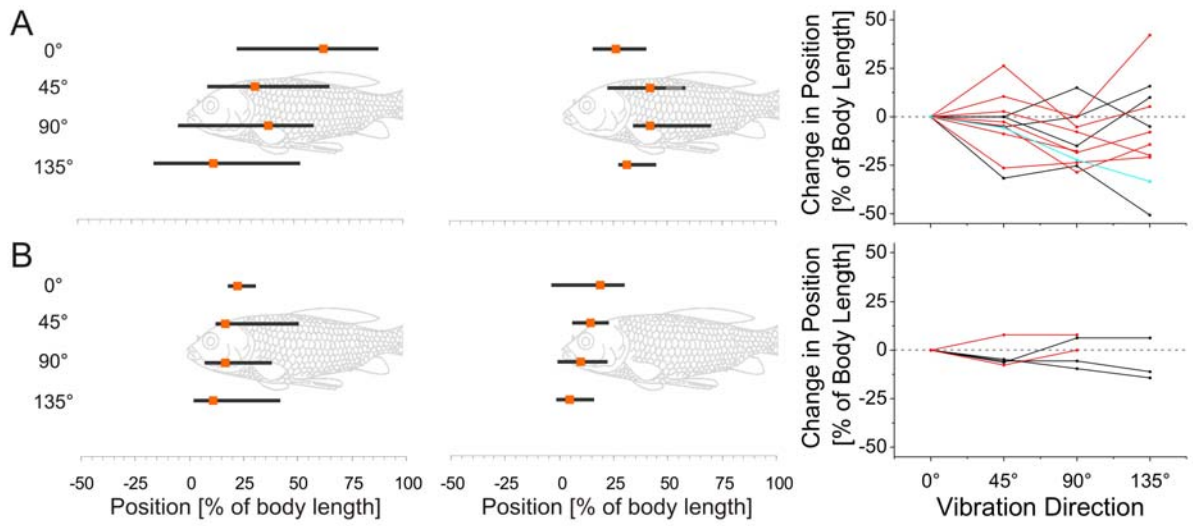

Figure 29: Position and extent of half maximum widths (horizontal black bars) and position of maximum response (orange squares) for different sphere vibration angles (0°, 45°, 90° and 135°). **A: Left:** Examples of HMWs of MON units in which the position of maximum response varied with sphere vibration angle by 15% of body length or more. **Right:** Normalized spatial location of the position of maximum response as function of vibration angle. 0 indicates the position of the response maximum (increase or decrease) for 0° vibration angle. Negative values indicate more caudal and positive values more rostral locations. Black: Excitation patterns with one excitatory area. Red: Excitation Patterns with two excitatory areas. Blue: Excitation Patterns with one inhibitory area. **B: Left:** Examples of HMWs of MON units in which the position of maximum response varied with sphere vibration angle by less than 15% of body length. **Right:** Normalized spatial location of the response maxima as function of vibration angle. The fish in the background is drawn to scale.

Effects on spatial phase-locking and phase angle patterns

In the following, the effects of changing sphere vibration direction on the phase angle patterns of MON units will be described. Note that extremely large changes in phase angle changes (270°- 360°) were not considered here. Such large changes in phase angle most likely were due to the fact that phase angles within a distinct area of space were distributed around 0° (= 360°), thereby increasing the possibility of abrupt shifts from small to large values or vice versa (see e.g., Figure 27). Moreover, to make sure that phase shifts were due to neuronal processing they were only included into the analysis if phase-locking was significant ($Z \geq 4.6$).

In twenty-one units, different vibration angles resulted in different spatial patterns of phase-locking and/or phase angles. For the three units that had primary-like excitation patterns in terms of discharge rate (see above), the effects of sphere vibration direction on phase-locking and phase-angles were also as predicted from primary afferents. In particular, the spatial pattern of Z-values followed the spatial

discharge patterns for all vibration angles and thus changed accordingly with changing sphere vibration direction (Figure 25). Moreover, when sphere vibration direction was 0°, at least in one unit two distinct 180° changes in phase angle with opposite sign bordering the central response peak were observed. When vibration direction was 90° a single 180° change in phase angle occurred just between the two response maxima (Figure 25).

In one unit a phase angle pattern similar to a pattern predicted for primary afferents was obtained (Figure 27). When sphere vibration direction was 0°, two distinct 180° changes in phase angle with opposite sign bordering the central response peak were observed. Again, when vibration direction was 90° a single 180° change in phase angle occurred just between the two phase-locking maxima (Figure 27). The same was true for the two intermediate vibration directions (45° and 135°). However, in terms of discharge rate, this neuron did not show a primary-like excitation pattern but exhibited a broad excitatory area that extended across most of the fish length.

In fourteen units the spatial pattern of Z-values followed the spatial discharge patterns for all vibration angles, i.e., at each stimulation angle Z-values were correlated with the excitatory (inhibitory) response peaks (troughs) (Figure 30, Figure 31). Among these units different phase angles patterns were observed. The phase angle patterns of seven units exhibited no systematic or predictable changes with changing sphere vibration direction (e.g., Figure 26). In another three units phase angles changed systematically in small steps from either high or low values at the rostral-most and caudal-most stimulation location to reach a minimum or maximum value, respectively, within the centre of unit's excitation pattern (Figure 30).

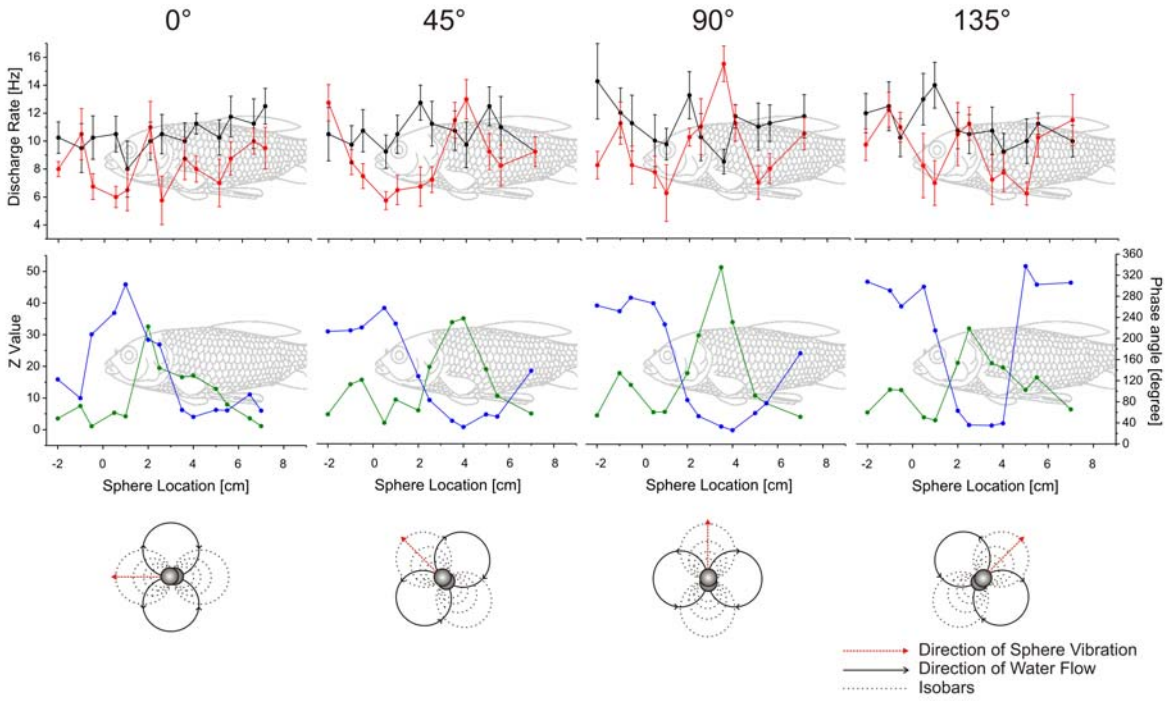

Figure 30: Spatial excitation patterns of a MON unit obtained with different vibration directions (0. 45 and 90°) of a vibrating sphere. **Upper graphs:** Ongoing discharge rates (black lines) and evoked discharge rates (red lines) averaged across eight stimulus presentations are plotted as function of sphere location along the side of the fish (sphere radius 8 mm, frequency 50 Hz, vibration displacement 350 µm, 1 cm distance between sphere and fish). Vertical bars represent standard deviation. The fish in the background is drawn to scale. **Lower graphs:** Z-values (green lines, left Y-axis) and mean phase angles (blue lines, right Y-axis). The horizontal grey dashed line indicates the Z-value criterion ($Z \geq 4.6$).The bottom-most drawings illustrate the direction of sphere vibration (red arrows), the associated water flow (solid lines), and isobars (dotted lines).

In the remaining four of these fourteen units differences in phase angle pattern were observed when stimulation direction was altered. Either distinct 180° changes in phase angle, systematic changes in small steps or no distinct changes occurred depending on vibration direction. Figure 31, for instance, shows excitation patterns from one unit that contain abrupt change in phase angle when vibration angle was 0° and 135° (0°: between 2 and 3 cm, 135°: between 4.5 and 5 cm), but a more gradual change in phase angle from high to low and back to high values when vibration angle was 45° and 90°. To illustrate these phase angle changes period histograms are presented in Figure 31B.

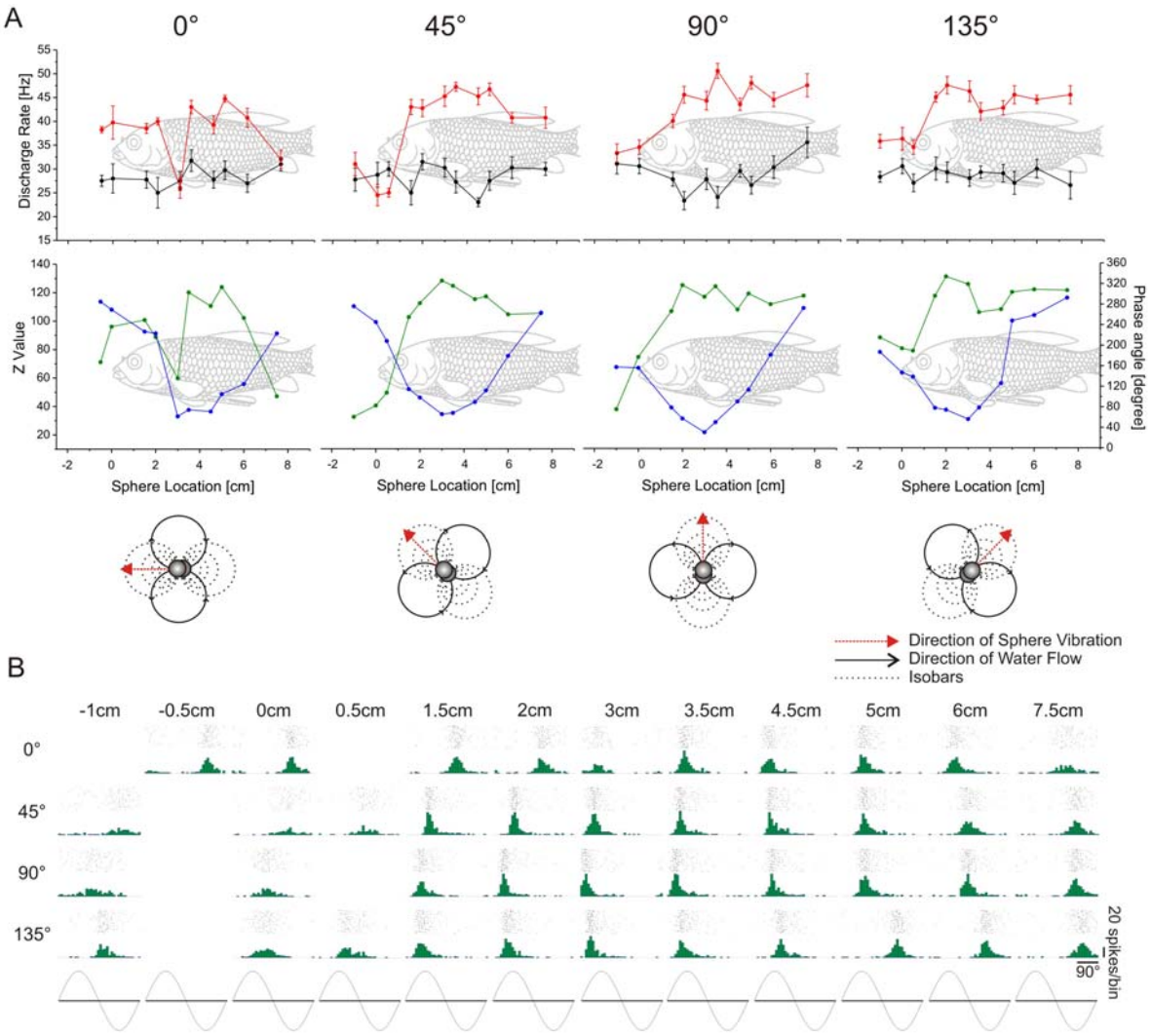

Figure 31: A: Spatial excitation patterns of a MON unit obtained with different vibration directions (0, 45 and 90°) of a vibrating sphere. **Upper graphs:** Ongoing discharge rates (black lines) and evoked discharge rates (red lines) averaged across eight stimulus presentations are plotted as function of sphere location along the side of the fish (sphere radius 8 mm, frequency 50 Hz, vibration displacement 350 µm, 1 cm distance between sphere and fish). Vertical bars represent standard deviation. The fish in the background is drawn to scale. **Lower graphs:** Z-values (green lines, left Y-axis) and mean phase angles (blue lines, right Y-axis). The horizontal grey dashed line indicates the Z-value criterion ($Z \geq 4.6$).The bottom-most drawings illustrate the direction of sphere vibration (red arrows), the associated water flow (solid lines), and isobars (dotted lines). **B:** Phase-locking histograms (bin width 10°). Sinus stimulus is shown below.

Three units showed the spatial response patterns which, in terms of phase-locking did not match the spatial pattern of spike activity patterns. Among these units various phase angle patterns occurred. One unit exhibited an unpredictable and unsystematic change of phase angles within its spatial excitation pattern when sphere vibration direction was parallel (0°) to the fish (Figure 31). When sphere vibration direction was 45°, 90° or 135°, phase angles changed systematically in

small steps from high values at the rostral-most and caudal-most stimulation location to low values at central stimulus locations (Figure 31). Another unit exhibited a similar behaviour, i.e., it did not show phase-locking in response to 0° stimulation but in response to 45°. 90° and 135° stimulation phase angles changed systematically in small steps from high values at the rostral-most and caudal-most stimulation location to low value directions at central stimulus locations. Finally, in the remaining unit single 180° changes in phase angle occurred in the phase angle patterns in response to all vibration directions independent from its discharge rate pattern.

3.2.3 Effect of changing sphere distance on excitation patterns

In ten units, the effects of different distances between vibrating sphere and fish on spatial excitation patterns were studied. To do so, excitation patterns were measured at 1 cm, 2 cm and 3 cm sphere distance. In all ten units the general shapes and the spatial locations of the excitation patterns were similar for different sphere distances in terms of both, discharge rate and phase-locking (Figure 32).

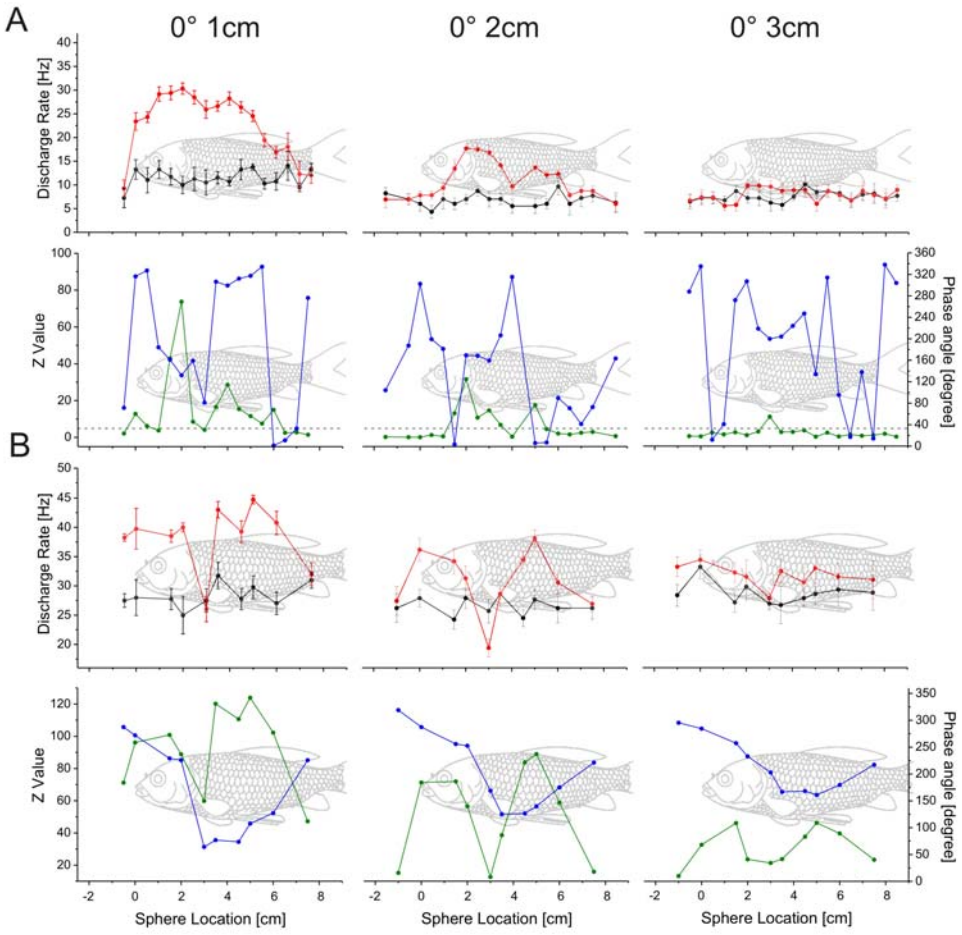

Figure 32: Responses Spatial excitation patterns of a MON unit obtained with different sphere distances (sphere radius 8 mm, frequency 50 Hz, 1, 2 and 3 cm distance between sphere and fish, parallel stimulation direction). Upper graphs: Ongoing discharge rates (black lines) and evoked rates (red lines) as a function of sphere location. Vertical bars represent standard deviation. The fish in the background is drawn to scale. Lower graphs: Z-values (green lines, left Y-axis) and mean phase angles (blue lines, right Y-axis) as function of sphere location along the side of the fish. The horizontal grey dashed line indicates the Z-value criterion ($Z \geq 4.6$). **A:** Unit with a broad area of increased discharge rate in response to stimulation (vibration displacement 250 µm). **B:** Unit with two areas of increased discharge rate in response to stimulation (vibration displacement 350 µm).

However, the strength of the responses (discharge rates) and the strength of phase-locking (Z-values) decreased with increasing distance in most of the units (n = 8) (Figure 33A/B). Similarly, HMWs decreased with increasing stimulation distance in seven of these units between 6% and 75 % of fish body length (Figure 33C). In one unit HMW increased by 30 % at 2 cm sphere distance.

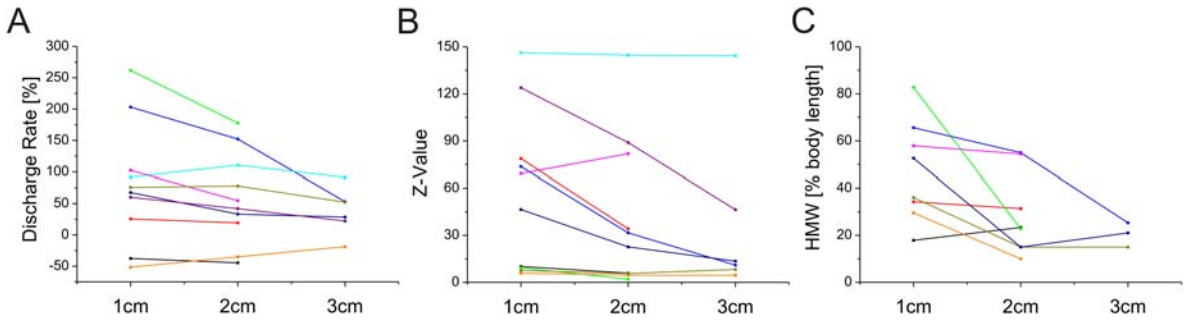

Figure 33: Response measures of MON units as function of distance between sphere and fish. Different colours represent different units. **A:** Discharge rate as a function of sphere distance. The orange and black lines represent units that decreased discharge rate in response to stimulation. **B:** Z-Value as a function of sphere distance. **C:** Half-maximum width (HMW) as a function of sphere distance. HMW of two units with two or more response areas are not shown here.

3.3 Responses of MON units to water flow

Single unit activity in water flow was recorded from 57 MON units in twenty-one goldfish. The average ongoing activity of these units under still water conditions was 17.2 ± 8.8 spikes*s^{-1} (mean ± SD; median: 12.9 spikes*s^{-1}, Table 6). Forty-one units were stimulated with a pulse flow stimulus in both AP and PA directions, i.e., they were stimulated with constant velocity water flow (see Material and Methods, chapter 2.4.3, Figure 9A, Figure 12). Velocity response functions (VRF) were constructed for those units that were stimulated with at least three different flow velocities (n=32). Twenty-nine units were stimulated with the ramp stimulus in both AP and PA direction, i.e., they were stimulated with water flow of increasing velocity (see Material and Methods 2.4.3, Figure 9B). In thirteen of 57 units both stimulation paradigms were used. The recorded units exhibited a large variability in terms of discharge rate, discharge pattern, velocity- and directional sensitivity.

	Mean	SD	Median	Range
Ongoing Discharge Rate [spikes*s^{-1}] (Still water)	17.2	8.8	12.9	0.8 - 36.1
Evoked Discharge Rate [spikes*s^{-1}] (Running water)	15.6	11.3	11.5	0 – 52.4
RMS Value	295.0	338.5	177.6	24.7 - 3249.4

Table 6: Ongoing rates of MON units in still water and various measures of the evoked rates in running water.

3.3.1 Responses to constant velocity water flow (Pulse flow stimulation)

Temporal response patterns

Of the forty-one units that were stimulated with constant velocity water flow in anterior-posterior direction, thirty-seven units (90 %) responded with a change in discharge rate and/or discharge pattern (Figure 34A-C) and were therefore classified as flow-sensitive. Consequently, the remaining four units were flow-insensitive (Figure 34D). Approximately two thirds of the thirty-seven flow-sensitive units (n = 28, 76 %) increased discharge rate in response to water flow (Figures 34A, 35A, C, D, 36, 38), whereas the other one third (n=9, 24 %) decreased discharge rate (Figures 34B, 35B, E, 39). In thirteen units responses to water flow depended on flow direction (Figure 34C). This will be described in more detail below (see pages 68-70, 75-76).

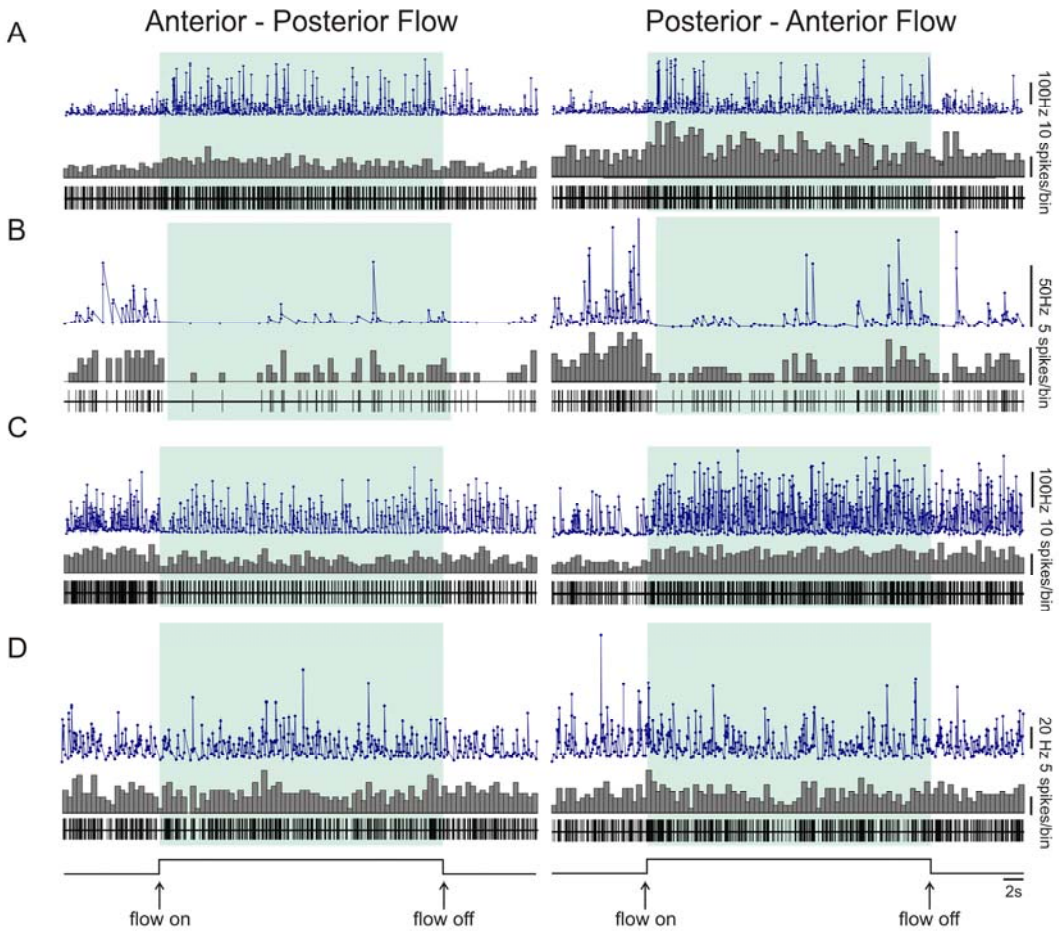

Figure 34: Flow-sensitive and flow-insensitive MON units. The figure shows responses of four units to running water (flow velocity 4.4 $cm*s^{-1}$). Left: Flow in anterior-posterior direction. Right: Flow in posterior-anterior direction. Each graph shows from top to bottom: instantaneous frequency (blue), peri-stimulus-time-histograms (grey, bin width 500 ms), and raster plot (black, each marker represents one action potential). The bottom black line is the stimulus trace. Areas highlighted in green indicate the time during which water flow was on. **A**: Unit with an increase in discharge rate in response to both flow directions. **B**: Unit with a decrease in discharge rate in response to both flow directions. **C**: Unit with a decrease in discharge rate in response to flow in anterior-posterior and an increase in response to flow in posterior-anterior direction. **D**: Flow-insensitive unit.

The temporal discharge patterns of the responses to flow were phasic, phasic-tonic or tonic. More than half of the units (54 %) had a tonic response, i.e., they responded with a change in discharge rate and/or firing pattern that persisted for the entire stimulation period (Figure 35C). Fourteen units (38%) had a phasic-tonic response to flow, i.e., they exhibited a change in discharge rate (increase or decrease) that was greatest immediately after stimulus onset, but continued to fire at a rate different from the ongoing activity throughout the remainder of the flow stimulation (Figure 34A/B, 35A). Three units (8%) had a phasic response, i.e., discharge rate increased (Figure 35D) or decreased (Figure 35E) shortly after stimulation onset, but returned

to spontaneous discharge levels while the flow was still on. In five of the thirty-seven units (14%) an additional increase in discharge rate was observed after the flow was turned off (Figures 35D, 36).

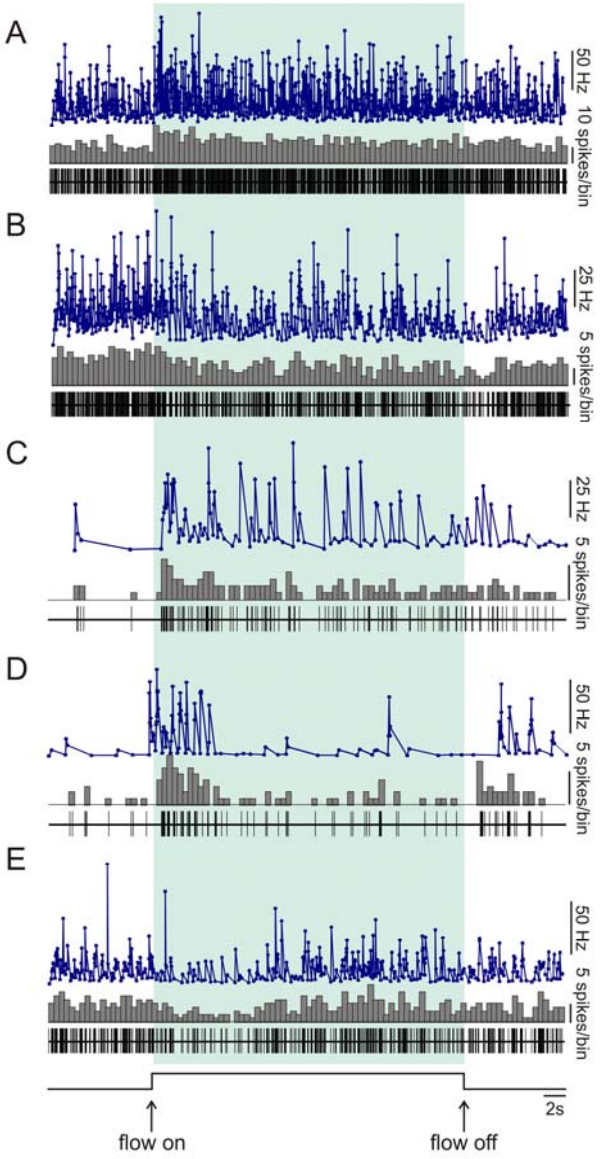

Figure 35: Temporal discharge patterns of MON units in a constant water flow. The figure shows the responses of five units to running water (AP-flow direction, flow velocity 4.4 cm*s^{-1}). Each graph shows from top to bottom: instantaneous frequency (blue), peri-stimulus-time-histograms (grey, bin width 500 ms), raster plot (black, each marker represents one action potential). The bottom black line is the stimulus trace. Areas highlighted in green indicate the time during which water flow was on. **A**: Unit with a tonic increase in discharge rate (flow velocity 9.0 cm*s^{-1}). **B**: Unit with a tonic decrease in discharge rate (flow velocity 3.7 cm*s^{-1}). **C**: Unit with a phasic-tonic increase in discharge rate (flow velocity 6.2 cm*s^{-1}). **D**: Unit with a phasic increase in discharge rate (flow velocity 10.0 cm*s^{-1}). **E:** Unit with a phasic decrease in discharge rate (flow velocity 2.6 cm*s^{-1}).

To verify the reproducibility of the observed response patterns, most of the stimulations were repeated at least once. Figure 36 shows responses of a MON unit to two successive stimulations. The phasic increase in discharge rate immediately after stimulus onset and the increase after stimulus end are clearly visible in both recordings.

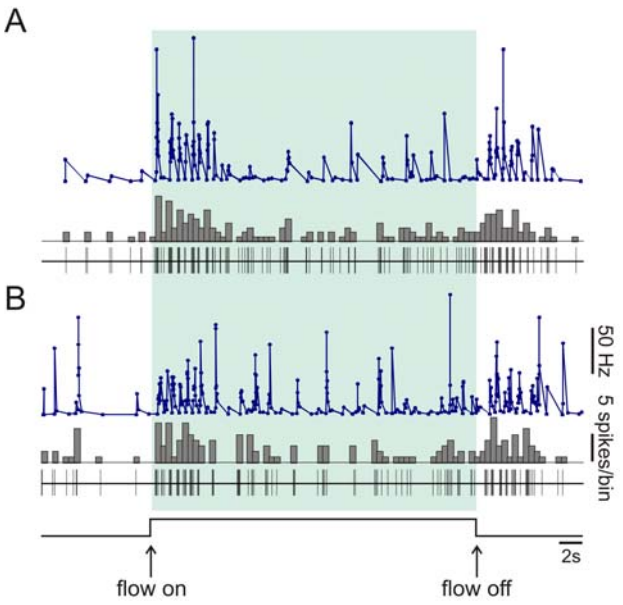

Figure 36: Reproducibility of responses. The figure shows the responses of a brainstem unit to two successive flow stimulations (AP-flow direction, flow velocity 4.4 cm*s^{-1}). Inter-stimulus-interval was 200 s. Each graph shows from top to bottom: instantaneous frequency (blue), peri-stimulus-time-histograms (grey, bin width 500 ms), and raster plot (black, each marker represents one action potential). The bottom black line is the stimulus trace. Areas highlighted in green indicate the time during which water flow was on. **A:** First presentation. **B:** Second presentation.

To quantify the temporal variability of firing, the root mean square (RMS) of the instantaneous frequencies (IF) was calculated (see Chapter 2.4.3). Figure 37 shows that RMS values increased with increasing changes in discharge rate, i.e., the greater the change in discharge rate - independent of whether it was an increase or decrease - the greater was the temporal variability of firing. For those units that increased discharge rate in flow, the average RMS value was 343 ± 713 % (mean ± SD, median 153 %, n = 29). As expected from their low discharge rates, those units that decreased rate in flow had lower firing variabilities than those that increased rate, with an average RMS value of 196 ± 147 % (mean ± SD, median 139 %, n = 8).

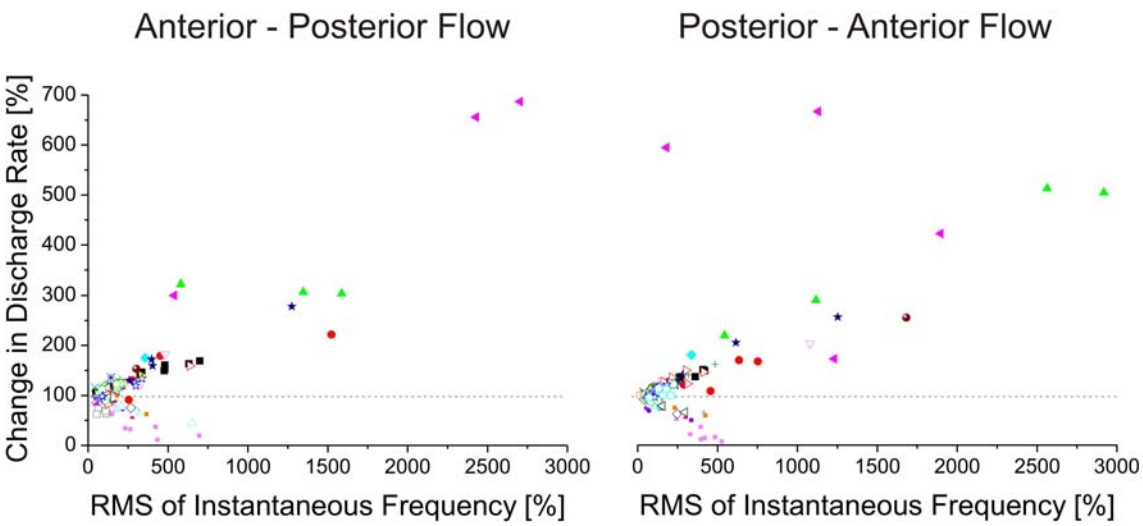

Figure 37: Temporal variability of firing. Change in discharge rate is plotted as function of the normalized RMS values of the Instantaneous Frequency (ongoing rate = 100%, grey dashed line). **Left**: Flow in anterior-posterior direction. **Right**: Flow in posterior-anterior direction. Different colours/symbols refer to different units.

Velocity response functions

Of the forty-one units that were stimulated with constant water velocity, twenty-six units were stimulated with more than three different water velocities which made it possible to construct velocity response functions (VRF). Figures 38 and 39 show exemplary responses of two MON units to different flow velocities and directions. The unit in Figure 38 increased its discharge rate in response to water flow. However, VRFs of this unit differed for AP and PA flow direction. In response to AP flow, discharge rate increased steadily with increasing flow velocity, was greatest at 6.2 $cm*s^{-1}$, and decreased again at 10.0 $cm*s^{-1}$. In contrast, in response to PA flow, discharge rate increased steadily up to the greatest flow velocity presented. Figure 39 shows data from a unit that decreased its discharge rate in response to water flow. In this case response strength decreased steadily with increasing velocity in both flow directions.

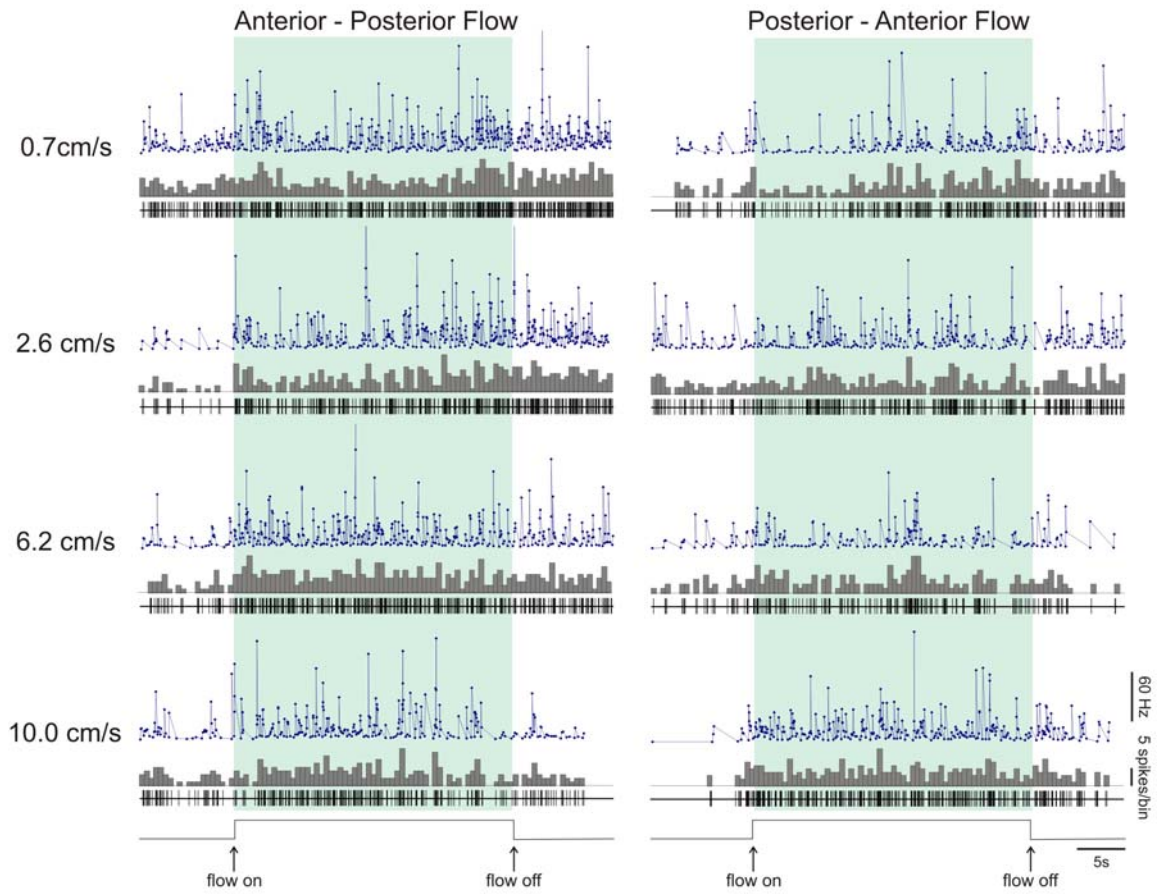

Figure 38: Discharge rate increases of a MON unit to running water with different velocities. Left: Flow in anterior-posterior direction. Right: Flow in posterior-anterior direction. Each graph shows from top to bottom: instantaneous frequency (blue), peri-stimulus-time-histograms (grey, bin width 500 ms), and raster plot (black, each marker represents one action potential). The bottom black line is the stimulus trace. Areas highlighted in green indicate the time during which water flow was on.

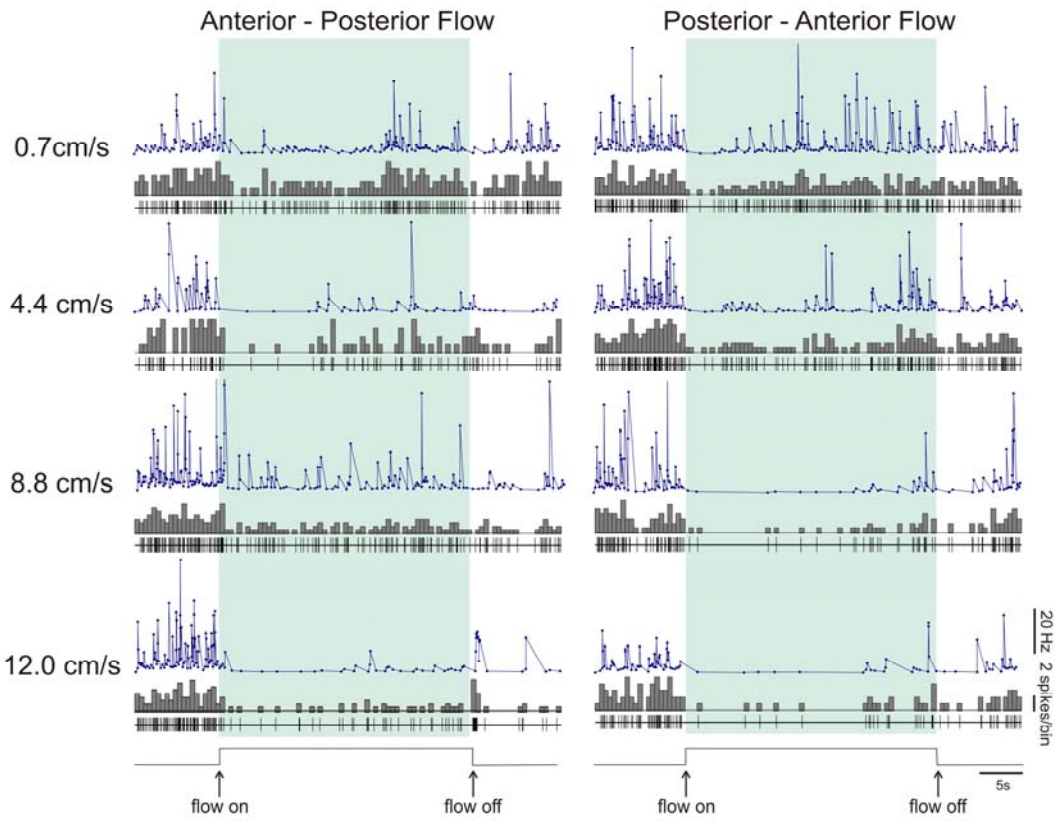

Figure 39: Discharge rate decreases of a MON unit to running water with different velocities. Left: Flow in anterior-posterior direction, right: Flow in posterior-anterior direction. Each graph shows from top to bottom: instantaneous frequency (blue), peri-stimulus-time-histograms (grey, bin width 500 ms), and raster plot (black, each marker represents one action potential). The bottom black line is the stimulus trace. Areas highlighted in green indicate the time during which water flow was on.

Figure 40 shows VRFs obtained from units stimulated with more than three flow velocities. For better visibility VRFs from different units were plotted in different graphs. Figure 40A shows data from units that increased their discharges by less than 75 % of their spontaneous discharge rate (n = 6), Figure 40B shows data from units that increased their rates to at least one of the velocities by more than 75 % (n = 6), and Figure 40C shows VRFs of units which decreased discharge rate in flow (n = 6). Finally, Figure 40D shows VRFs of units which increased discharge rate in one flow direction and decreased discharge rates in the opposite flow direction or were unresponsive to one of the two flow directions (n = 8).

As Figure 40 illustrates, VRFs were highly variable. Some units exhibited a systematic increase (n = 5, Figure 40A e.g., black and red line, Figure 40B red line) or decrease (n = 4, Figure 40C e.g., blue, green and black line) of discharge rate with increasing flow velocity. In other units, discharge rates increased (n = 4, Figure 40A

e.g., orange and turquoise line, Figure 40B pink and green line) or decreased (n = 1, Figure 40C red line) at low flow velocities but decreased (or increased) again at high flow velocities, i.e., they exhibited a maximum (or minimum) discharge rate at intermediate flow velocities. Finally, in some units (n = 4) discharge rate increased and/or decreased steeply from one flow velocity to the next independent of flow velocity (e.g., Figure 40A green and blue line, Figure 40B light blue line and Figure 40C pink line). In twelve units (46%) VRFs were comparable for AP and PA flow direction whereas in fourteen units (54%) VRFs depended on flow direction. Directional effects on VRFs and discharge rates will be described in the following subchapter.

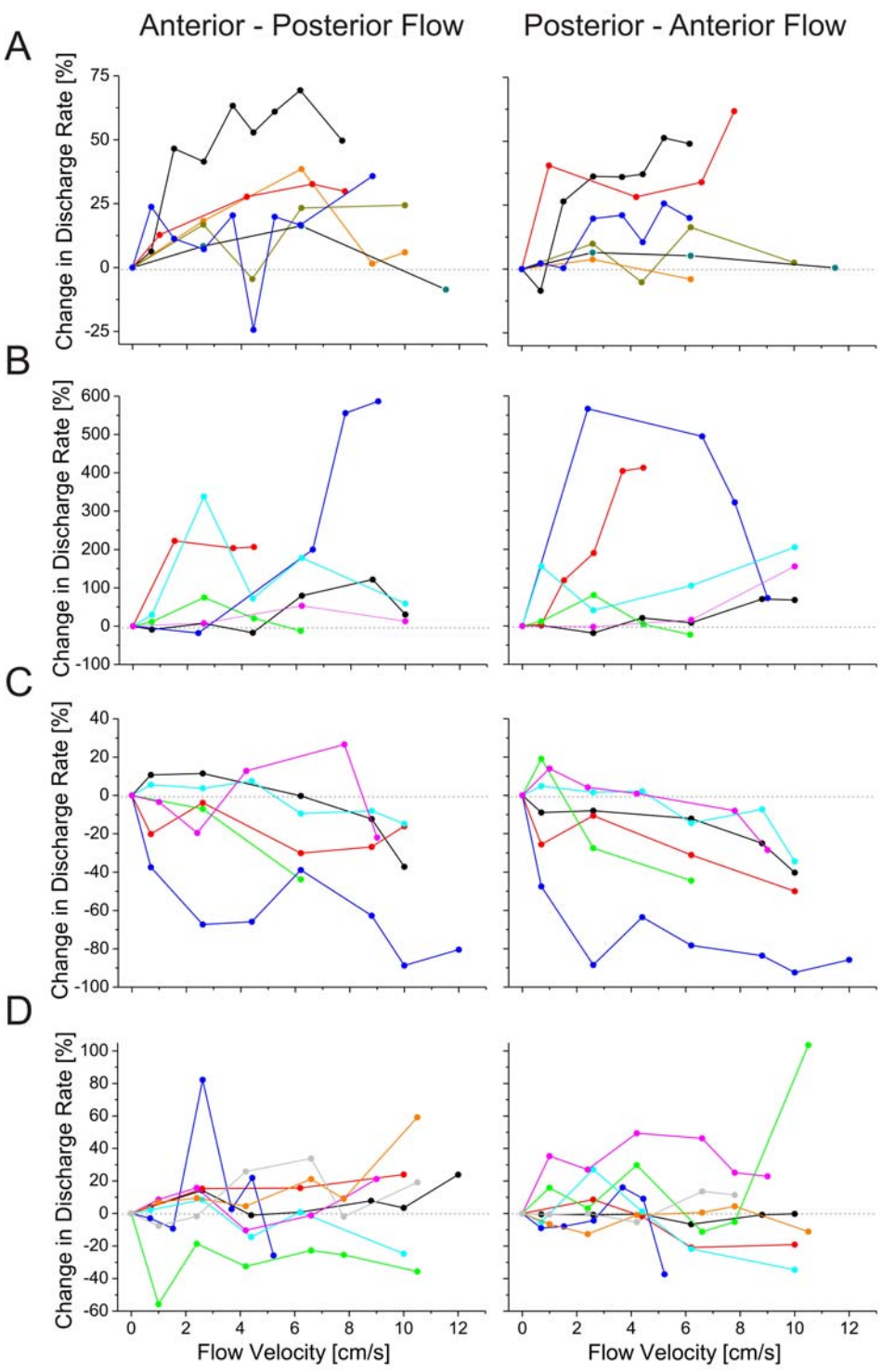

Figure 40: Velocity response functions of MON units. Percent change in discharge rate is plotted as function of flow velocity. **Left plots**: Flow in anterior-posterior direction. **Right plots**: Flow in posterior-anterior direction. Different colours refer to different units. The horizontal stippled line indicates no change in discharge rate. Note that the graphs have different scaling. **A, B**: Units with an increase in discharge rate to both flow directions. **C**: Units with a decrease in discharge rate to both flow directions. **D:** Units with a decrease and/or increase in discharge rate depending on flow direction.

Directional sensitivity

In fourteen units, velocity response functions (VRFs) depended on the direction of water flow. In eight of these units, the type of the response, i.e., whether the unit responded with an increase or a decrease in discharge rate, depended on flow direction (e.g., Figure 41). In five of these units responses were characterized by increased discharge rate in one flow direction and decreased discharge rates in the opposite flow direction (Figure 40D, red, black, blue, turquoise and green line), and in three units VRFs were characterized by an increase or by a decrease in discharge rate to one flow direction and no change in discharge rate to the opposite flow direction (Figure 40D, orange, grey and pink line). In the other six units, the type of response, namely an increase in discharge rate, was the same for both flow directions. However, in these six units and in the aforementioned eight units, the exact course of the VRF, i.e., whether discharge rate changed continuously or discontinuously with increasing flow velocity, differed for AP and PA flow. The VRFs of the fourteen direction-sensitive units were characterized, as described in the previous chapter (see Figure 40A-C), by either a systematic and continuous increase in discharge with increasing flow velocity (n=12), by unpredictable changes in discharge rate at different flow velocities (n=4), by sudden steep changes in discharge rate in response to a step increase in flow velocity (n=6), or by stronger responses to intermediate flow velocities than to lower and higher flow velocities (n=6). Various direction-dependent combinations of these patterns occurred in different units. The most frequent combination (n=12), however, consisted of a systematic and continuous increase in discharge rate with increasing flow velocity in response to one flow direction and a completely different VRF in response to the opposite flow direction (e.g., blue line in Figure 40B, red and green lines in Figure 40D).

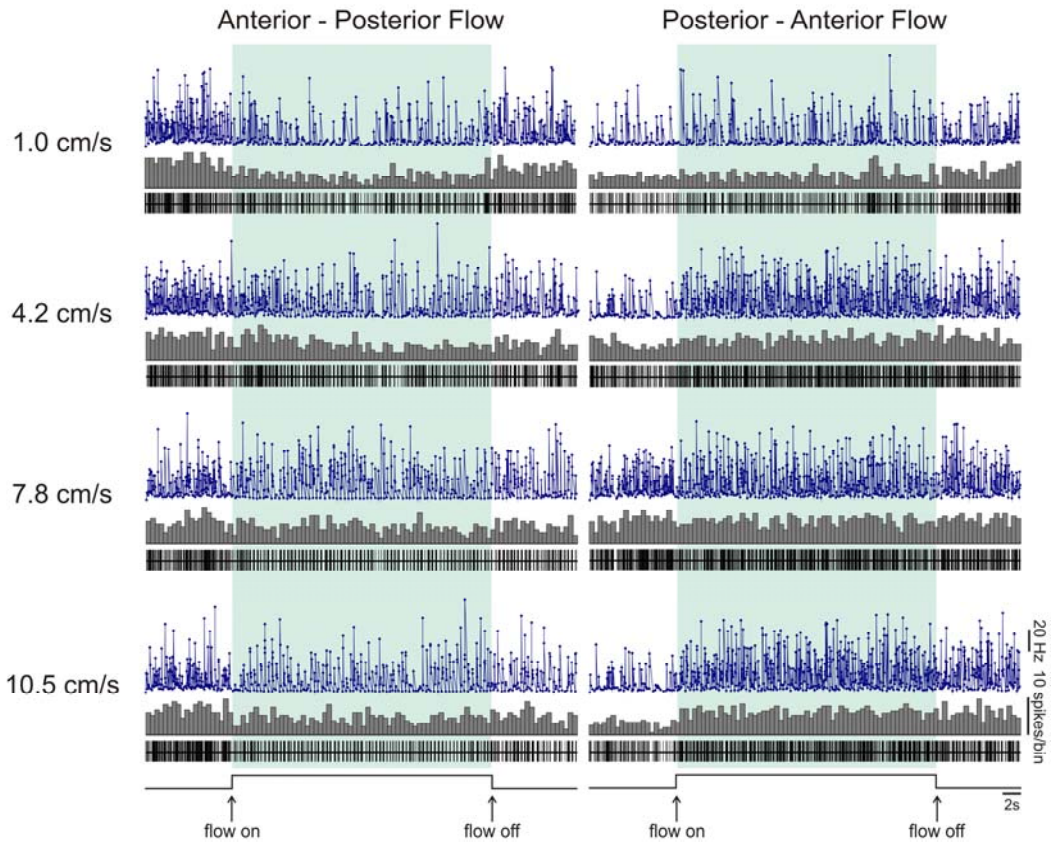

Figure 41: Direction sensitive responses of a MON unit to running water with different velocities. This unit decreased discharge rate in response to AP flow and increase discharge rate in response to PA flow. Left: Flow in anterior-posterior direction. Right: Flow in posterior-anterior direction. Each graph shows from top to bottom: instantaneous frequency (blue), peri-stimulus-time-histograms (grey, bin width 500 ms), and raster plot (black, each marker represents one action potential). The bottom black line is the stimulus trace. Areas highlighted in green indicate the time during which water flow was on.

To quantify directional sensitivity, signed directivity indices (SDI, see Chapter 2.5.3) were calculated for thirty-six units. SDI values ranged between -87.7 and 92.1 (median: -0.4, n = 36). Approximately half of the units exhibited negative SDI values (51 %) while the other half had positive SDI values (49 %, Figure 42). The majority of the units (n = 33, 92 %) had SDI values between -50 and 50, i.e., discharge rates to one flow direction were at best twice the discharge rates to the opposite flow direction. Only few units (n = 3, 8 %) had SDI values greater than 50 or smaller than -50, i.e., the units responded with more than twice the number of spike to one flow direction compared to the opposite flow direction.

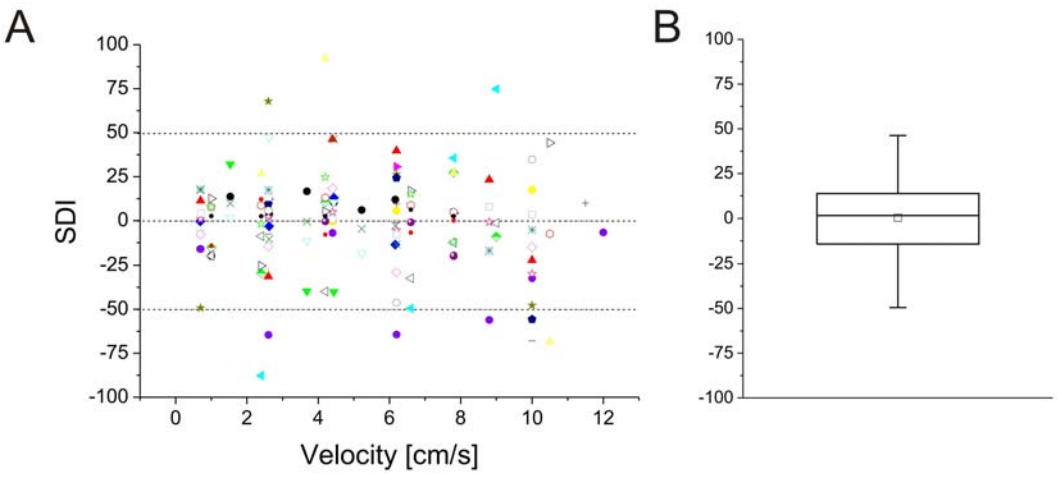

Figure 42: Signed Directivity Indices (SDI) of MON units stimulated with different constant water flow velocities (pulsed flow) in AP or PA direction. **A**: SDI as function of flow velocity. **B:** Box-Whisker-Plot of SDI - Values with 25 % and 75 % percentiles, median, mean (square), smallest and greatest observation.

3.3.2 Responses to Continuously Rising Flow Velocity (Ramp Flow Stimulation)

Temporal response patterns

Twenty nine units were stimulated with a ramp flow stimulus, i.e., flow velocity was steadily increased from 0 to 10 $cm*s^{-1}$ or from 0 to 12.3 $cm*s^{-1}$. Eighteen of these units (62%) changed their discharge rates or patterns at least within a distinct time window during stimulation (e.g., Figure 43A-C), i.e., they were flow-sensitive. Nine units (38%) showed no response to the ramp stimulus (e.g., Figure 43D), i.e., they were flow-insensitive.

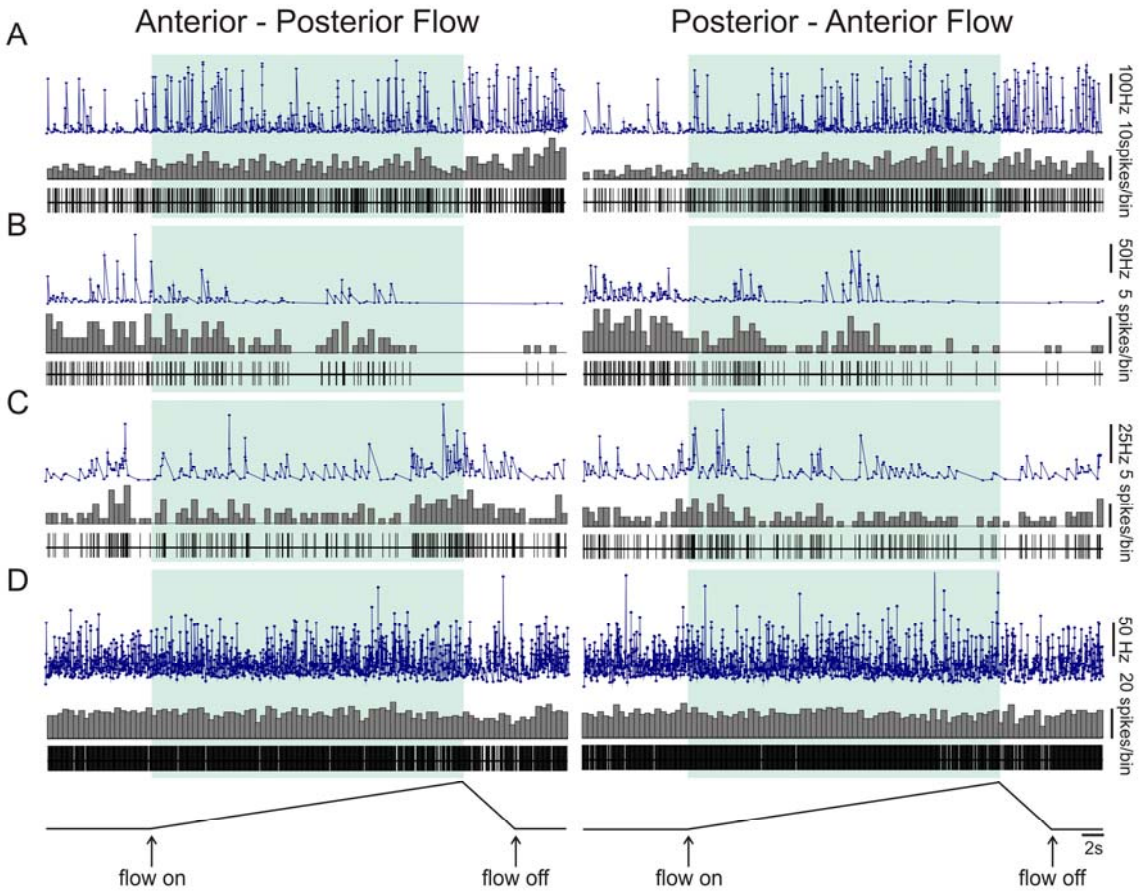

Figure 43: Flow-sensitive and flow-insensitive MON units. The figure shows responses of four brainstem units to running water with continuously increasing velocity (0 – 12.3 $cm*s^{-1}$). Left: Flow in anterior-posterior direction. Right: Flow in posterior-anterior direction. Each graph shows from top to bottom: instantaneous frequency (blue), peri-stimulus-time-histograms (grey, bin width 500 ms), and raster plot (black, each marker represents one action potential). The bottom black line is the stimulus trace. Areas highlighted in green indicate the time during which water flow was on. **A**: Unit with an increase in discharge rate in response to both flow directions. **B**: Unit with a decrease in discharge rate in response to both flow directions. **C**: Unit with an increase in discharge rate in response to flow in anterior-posterior and a decrease in response to flow in posterior-anterior direction at high flow velocities. **D**: Flow insensitive unit.

The temporal discharge patterns of the responses to ramped flow were similar to those obtained with pulsed flow, i.e., they were phasic, phasic-tonic or tonic. Of the eighteen flow sensitive units stimulated with ramped water flow, twelve (67%) responded with an increase in discharge rate in response to both flow directions (Figure 43A). Four of these units exhibited a tonic response, i.e., they responded with an increased discharge rate throughout the entire stimulation period, even at the lowest velocities within the ramp stimulus (e.g., Figure 43A). Five units increased their rates only at very high velocities, i.e., towards the end of the ramp stimulus (Figure 44A). Two units exhibited discharge rates that were particularly high during

the middle of the ramp stimulus but lower at the beginning and towards the end of the ramp stimulus (Figure 44C, 45). The remaining two units showed no distinct pattern of discharge rate increase over the duration of the ramp.

Two of the eighteen flow-sensitive units (11%) decreased discharge rate in response to water flow. In both units the decrease in discharge rate grew stronger with increasing duration of the ramp stimulus. In other words, suppression became more and more apparent the more the flow velocity increased (e.g. Figures 43B, 44B). The responses of the remaining four units (22 %) depended on flow direction and will be described in the following subchapter.

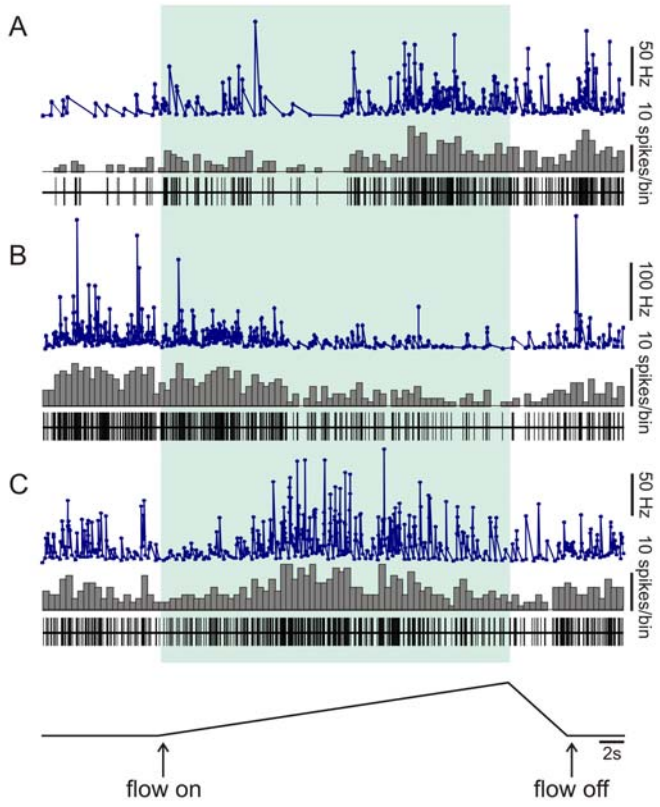

Figure 44: Types of responses to ramped flow. The figure shows responses of three MON units to running water with continuously increasing velocity (0 – 12.3 cm*s^{-1}). Each graph shows from top to bottom: instantaneous frequency (blue), peri-stimulus-time-histograms (grey, bin width 500 ms), and raster plot (black, each marker represents one action potential). The bottom black line indicates begin and end of stimulus. The green areas refer to the stimulation period. **A**: Unit with an increase in discharge rate in response to high flow velocities (AP flow direction). **B**: Unit with an increase in discharge rate in response to low flow velocities (AP flow direction). **C**: Unit with an increase in discharge rate in response to intermediate velocities (PA flow direction).

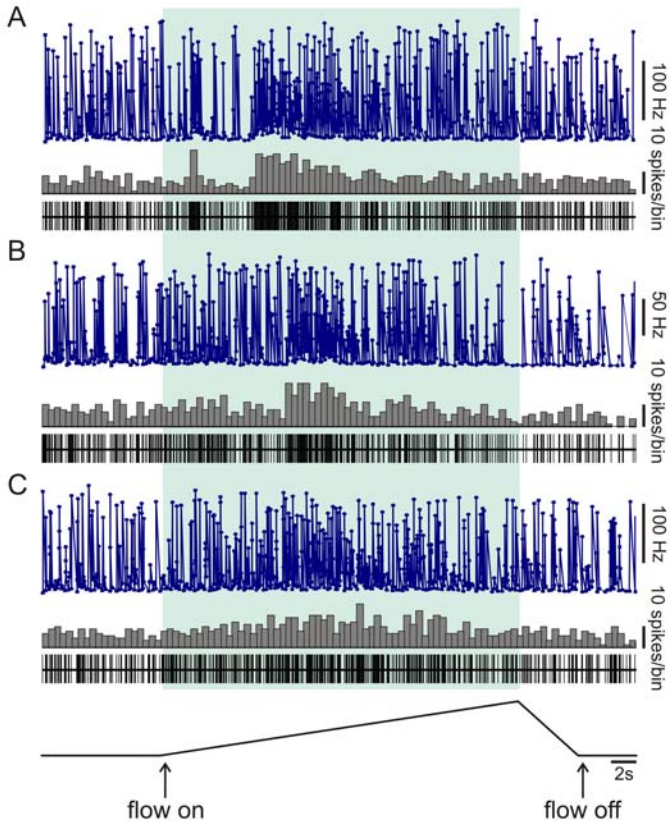

Figure 45: Responses of a MON unit to running water with continuously increasing velocity. The unit increased discharge rate during the middle of the ramp stimulus and decreased its rate towards the end of the ramp. Each graph shows from top to bottom: instantaneous frequency (blue), peri-stimulus-time-histograms (grey, bin width 500 ms), and raster plot (black, each marker represents one action potential). The bottom black line indicates begin and end of stimulus. The green areas refer to the stimulation period. **A**: Water flow in AP direction, 0 – 10.5 cm*s^{-1}. **B**: Water flow in AP direction, 0 – 12.3 cm*s^{-1}. **C**: Water flow in PA direction, 0 – 10.5 cm*s^{-1}.

To verify the reproducibility of the observed response patterns, most of the stimulations were repeated at least once. Figure 46 shows responses of a MON unit to two successive stimulations. The phasic increase in discharge rate immediately after stimulus onset and the increase after stimulus end are clearly visible in both recordings.

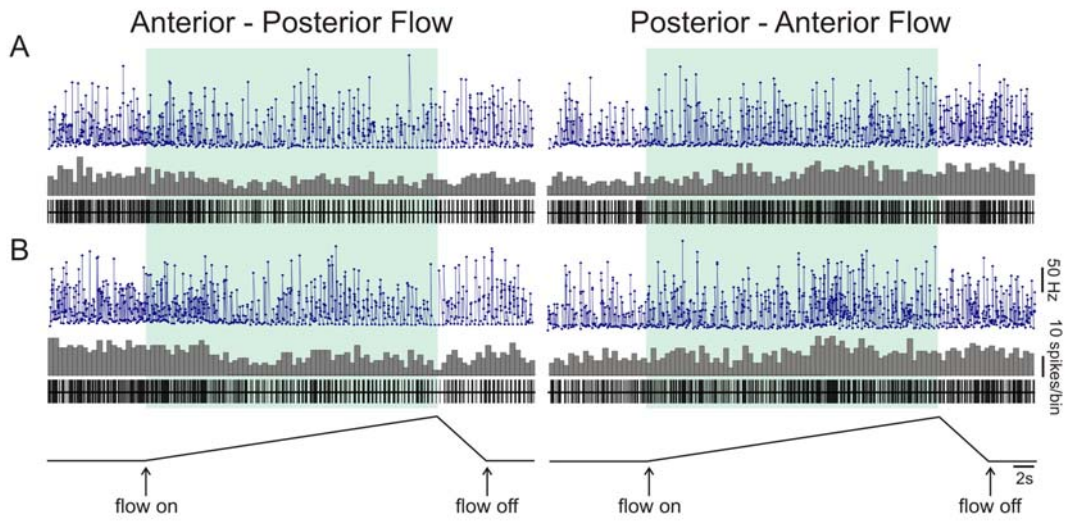

Figure 46: Reproducibility of responses. The figure shows the responses of a MON unit to two presentations of a ramped flow. i.e., running water with continuously rising velocity (0 - 12.3 $cm*s^{-1}$). Left: Flow in anterior-posterior direction. Right: Flow in posterior-anterior direction. Each graph shows from top to bottom: instantaneous frequency (blue), peri-stimulus-time-histograms (grey, bin width 500 ms), and raster plot (black, each marker represents one action potential). The bottom black line is the stimulus trace. Areas highlighted in green indicate the time during which water flow was on. **A:** First presentation. **B:** Second presentation.

In addition to increases or decreases in discharge rate, the recorded units exhibited changes in the firing variability as expressed by their RMS values. Figure 47 shows that RMS values of most units increased with increasing changes in discharge rate (72.5 %). The average RMS values for spikes elicited during stimulation was 442 ± 892 % (mean ± SD, median 162 %) for the AP direction and 298 ± 262 % (mean ± SD, median 191 %) for the PA direction. Units which increased discharge rate in response to water flow were excluded in this analysis since in these units discharge rates were as low as a few spikes per second.

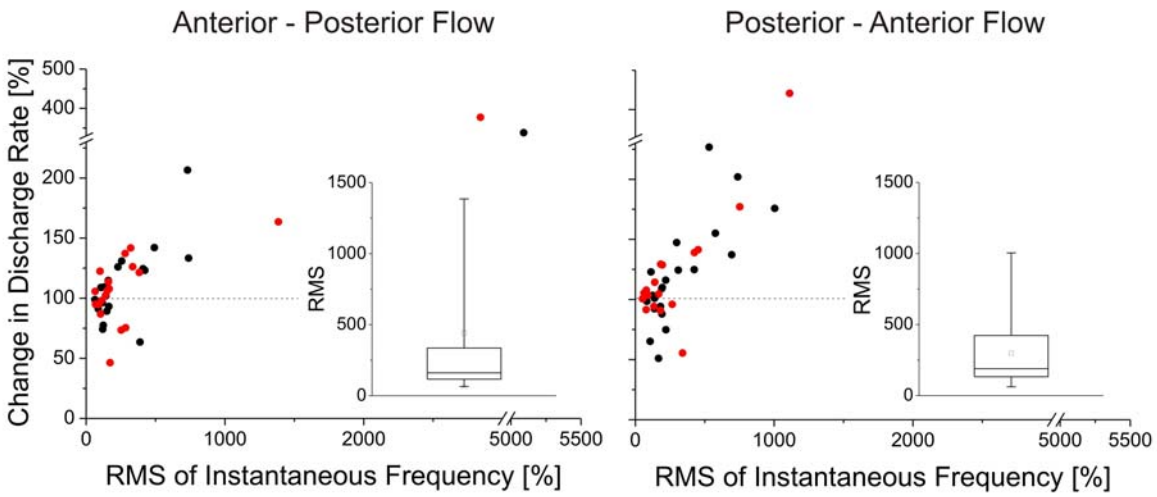

Figure 47: Temporal variability of firing. Change in discharge rate is plotted as function of the normalized RMS values of the Instantaneous Frequency (ongoing rate = 100%, dashed grey line). Insets: Box-Whisker-Plot of average RMS - Values with 25 % and 75 % percentiles, median, mean (square), smallest and greatest observation. Left inset: For reason of scaling maximum the RMS value (5090 %) is excluded from graph. Left: Flow in anterior-posterior direction, right: Flow in posterior-anterior direction. Different colours refer to different units. In units with stimulation repetitions values are averaged. Note that axes have different scaling.

Directional sensitivity

Of the eighteen flow sensitive units, fourteen units showed a response behaviour that was independent of stimulus direction. In contrast, in four units differences were found between the responses to AP and PA flow direction. One neuron showed a decrease in discharge rate to AP water flow and an increased rate to PA water flow (e.g., Figure 43C). This was particular evident at high flow velocities. Two units showed the opposite behaviour (Figure 46A/B). The remaining unit decreased its discharge rate to PA direction but did not change discharge rate in response to AP water flow.

To quantify directionality in terms of discharge rates, SDI values were calculated. Approximately half of the units that were stimulated with continuously rising flow in both directions exhibit a negative SDI (51.5 %), the other half a positive SDI value (48.5 %, Figure 48). SDI values ranged between -65.9 and 54.9 (median: -0.44). 45.5 % of the units had SDIs between -50 and zero and an equal percentage of units had SDI values between zero and 50. The remaining 9% of the units had SDI values smaller than -50 or greater than 50.

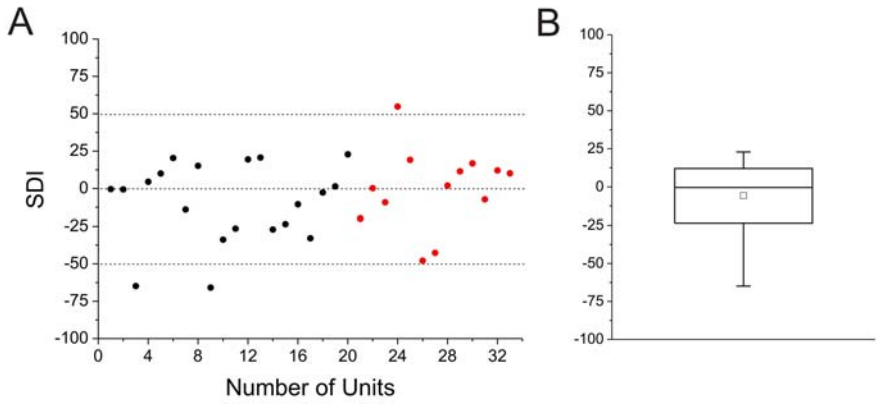

Figure 48: Signed Directivity Indices (SDI) of MON units stimulated with continuously rising water flow in AP or PA direction. **A**: SDI as a function of flow velocity. Black dots: Values of units stimulated with ramped flow from 0 to 11.5 cm*s^{-1}, red dots: Values of units stimulated with ramped flow from 0 to 12.3 cm*s^{-1}. The grey dotted lines refer to SDI values of 0, -50 and 50. **B:** Box-Whisker-Plot of SDI - Values with 25 % and 75 % percentiles, median, mean (square), smallest and greatest observation.

Analysis of units stimulated with both pulsed and ramped flow

Twelve units were stimulated with both constant velocity flow and continuously rising water flow (see Chapter 3.3.1 and 3.3.2). Seven of these units responded in a comparable fashion to both stimulation paradigms: an increase in discharge rate in response to both flow directions was observed in three units, a decrease in discharge rate in one unit, one unit decreased its discharge rate in the AP direction and increased rate in PA direction, and two units were flow insensitive regardless of flow direction. In the other five units the type of response depended on the stimulation paradigm, i.e., pulsed or ramped flow.

In five of the twelve units responses depended on stimulation paradigm. Three units did not show a change in discharge rate and/or patterns in response to the continuously rising flow, but responded to the pulsed flow. These units increased their discharge rate in response to either AP (n = 1, threshold: 4.2 cm*s^{-1}) or PA direction (n = 1, threshold: 1.0 cm*s^{-1}) or decreased discharge rate in response to both flow directions (n = 1, threshold AP: 2.4 cm*s^{-1} PA: 9.0 cm*s^{-1}). One of the five units increased discharge rate in response to continuously rising flow in both directions while it increased rate only in response to pulsed flow in AP direction (threshold: 6.6 cm*s^{-1}). The remaining unit increased discharge rate to the continuously rising flow in both directions. This unit showed a decrease in discharge rate in response to pulsed flow in AP direction and an increase in PA direction (threshold AP: 1.0 cm*s^{-1} PA: 4.2 cm*s^{-1}).

4. DISCUSSION

The present study describes the responses of lateral line units in the medial octavolateralis nucleus (MON) of the goldfish, *Carassius auratus*, to various hydrodynamic stimuli. In particular, it was investigated how MON units respond to different frequencies, locations and orientations of a sinusoidally vibrating sphere. Moreover, the spatial excitation patterns of the units were described and categorized. Finally the response behaviour of MON units to water flow in different directions and with different velocities was assessed.

Ongoing discharge rates

Ongoing discharge rates of MON units under still water conditions ranged between 0.1 and 66.0 spikes*s^{-1} (mean ± SD: 17.3 ± 15.5 spikes*s^{-1}; median: 12.5 spikes*s^{-1}, n = 253). These numbers are in fair agreement with those reported in previous studies (e.g., Müller et al. 1996, Coombs et al. 1998, Kröther et al. 2002). However, they were on average lower than those reported for primary afferent nerve fibres but still greater than those reported for units in the midbrain torus semicircularis. An overview of spontaneous rates of units recorded in various studies in the peripheral and central lateral line is given in Table 7. These data consistently demonstrate that ongoing rates decrease with increasing hierarchy in the ascending lateral line pathway.

	Mean ± SD [spikes*s^{-1}]	Median [spikes*s^{-1}]	Range [spikes*s^{-1}]
Lateral Line Afferents			
Mogdans and Bleckmann 1998	n.a.	21.5	1.4-63.0
Montgomery and Coombs 1998	35.0 ± 6.1	n.a.	n.a.
Chagnaud 2006	26.6 ± 21.0	23.3	n.a.
Chagnaud et al. 2008	19.1 ± 15.3	15.3	n.a.
Scholze et al. (unpublished)	41.1 ± 25.5	n.a.	0.4-89.1
Mogdans and Geisen 2009	30.3 ± 24.0	30.0	0.2-102.3
MON			
present study	17.3 ± 15.5	12.5	0.1-66.0
Wubbels et al. 1993	27.0 ± 20.0	n.a.	n.a.
Müller et al. 1996	15.0 ± 21.0	n.a.	0-86.0
Mogdans et al. 1997	n.a.	1.1	0-16.0
Coombs et al. 1998	5.5 ± 5.3	n.a.	n.a.
Mogdans and Goenechea 1999	n.a.	6.8	0.9-25.4
Kröther et al. 2002	11.4 ± 7.0	n.a.	0-24.0
Midbrain			
Müller et al. 1996	n.a.	n.a.	0-7.0
Wojtenek et al. 1998	n.a.	n.a.	1.3-3.9
Plachta et al. 1999	<1	n.a.	n.a.
Engelmann and Bleckmann 2004	0.5 ± 0.9	n.a.	0-4.0
Meyer et al. (unpublished)	4.4 ± 12.6	0.4	0-51.7
Hofmann et al. (unpublished)	0.9 ± 2.1	0	0-17.2

Table 7: Spontaneous discharge rates of lateral line afferents, MON and midbrain units obtained in various studies. n.a. = not available.

The high spontaneous activity of the peripheral lateral line fibres improves the neuronal representation of the hydrodynamic environment. This implies that a high range of frequencies, as well as changes in stimulation frequency can be suitably encoded. It is advantageous for units to have the potential not only to increase but also to decrease their discharge rates. This in turn leads to enlargement of the fibres' dynamic range. Another advantage of exhibiting high spontaneous activity is a better temporal resolution of stimulus coding. In contrast, low ongoing discharge rates of units in higher brain centres facilitate "feature" processing (Schellart and Wubbels 1998). These have narrower dynamic ranges and preferentially respond to very specific stimuli. Their responses are likely a result of processing of information by primary afferents.

4.1 Frequency selectivity of MON units

The present study describes the responses of lateral line units in the MON of goldfish to three vibration frequencies (20Hz, 50Hz and 100Hz) of identical displacement amplitude. Responses were highly idiosyncratic, i.e., rate increases, rate decreases and phase-locked discharges were not consistent from one unit to the next or across frequencies. The observed patterns of discharge were much more diverse than those of primary afferents. Primary lateral line afferents respond to a sine wave stimulus always with phase-locked action potentials and, depending on stimulus amplitude, an increase in discharge rate (Kroese et al. 1978, Bleckmann and Topp 1981, Elepfandt and Wiedemer 1987, Bleckmann et al. 1989, Coombs and Janssen 1990, Kroese und Schellart 1992, Wubbels et al. 1993, Coombs et al. 1998, Montgomery and Coombs 1998, Mogdans und Bleckmann 1999, Weeg and Bass 2002). Decreases in discharge rate in response to a vibrating sphere do not occur among primary afferents. At the level of the MON, such decreases may be caused by the action of inhibitory interneurons in the deep layers of the MON (New et al. 1996).

Comparing the responses to different frequencies revealed that most units responded preferentially to one particular stimulus frequency and weaker or not at all to other frequencies. Based on whether units responded to one, two or three stimulus frequencies, they were assigned to one of three groups (see Results 3.1). Thus, MON units exhibited either low-pass band-pass, or high-pass, characteristics (see Figure 18). This is again different from primary afferent nerve fibres. In terms of displacement, lateral line afferents are most sensitive to frequencies between 20 and 60 Hz (superficial neuromasts) and between 60 and 120 Hz (canal neuromasts, see review Bleckmann 1994). In addition, primary afferents show linear frequency response properties, i.e., a linear increase in response amplitude with increasing stimulus frequency (Kroese and Schellart 1992, Mogdans and Bleckmann 1999). The finding that MON unit can exhibit low–pass, band–pass, and high–pass characteristics is in agreement with data from another study on the frequency response characteristics of MON units (Ali 2008). However, the relative percentages of units preferring distinct frequencies were different between this and the present study. Ali (2008) found that 45 % of the recorded units responded maximally (in terms of highest spike count) to 100 Hz, 42 % to 200 Hz, 13 % to 50 Hz and 11 % to

33 Hz. In the present study, 45 % of the units responded best to the 50 Hz stimulus, 42 % preferred the 100 Hz, and 13 % preferred 20 Hz. Brainstem lateral line units in the dwarf scorpionfish, *Scopeana pappilosus*, on average, were most responsive to frequencies up to 50 Hz but less responsive to higher frequencies (Montgomery et al. 1996). As in the present study, individual units exhibited low-pass or band-pass properties (see Figure 4 in Montgomery et al. 1996). Midbrain units also showed preferences to different frequencies. In the study of Plachta et al. (1999) midbrain units were found which responded maximally to frequencies of 33 Hz (18 %), 50 Hz (16 %), 100 Hz (35 %) or 200 Hz (31 %), thus exhibiting low-pass, band-pass and high-pass characteristics. Decreases in discharge rate in response to sinusoidal stimulation did not occur (Plachta et al. 1999), as recorded units had ongoing rates of less than 1 spike*s^{-1}.

Another finding was that MON units did not respond with strong phase locking to the stationary vibrating sphere. This is again different from primary afferent fibres that always respond with phase-locked discharges to a sinusoidal stimulus (e.g., Mogdans and Bleckmann 1999). In the present study, 41 % of the recorded units either did not show phase-locking (15 %), or responded to only one of the applied stimulation frequencies with phase locked discharges (26 %). Averaged across all responses of MON units recorded, the mean synchronization coefficient R was 0.38 (see Chapter 2.5.1). However, considering the entirety of responses, two thirds (63%) were significantly phase-locked ($Z > 4.6$, Figure 19) and about one third (30.3%) of the responses was strongly phase-locked ($R > 0.5$). The strongest phase-locking both in terms of Z-values and R-values occurred in response to stimulation with 50 Hz (Figure 19). Responses to 20 Hz and 100 Hz were characterized by lower Z- and R-values (Figure 19). Similar to MON units, toral units in the goldfish midbrain barely phase lock to a vibrating sphere. In the study of Plachta et al. (1999) R-values were smaller than 0.5 and Z-values smaller than the criterion of 4.6. Phase locked discharge rates in this case occurred more often in response to amplitude modulated sine waves than in response to constant amplitude stimuli.

Phase-locking is a behaviour that is characteristic for primary afferent fibres in all hair-cell based sensory systems. It enables the fibres to encode temporal aspects of a stimulus, i.e., phase and frequency. As the present and previous studies show,

phase-locking in the lateral line system is still present to some degree at higher levels in the brain, but the number of units, which exhibit phase-locked discharge behaviour, decreases (e.g., MON: Mogdans and Goenechea 2000, Mogdans and Kröther 2001; Midbrain: Plachta et al. 1999, Meyer et al. unpublished). This could mean that different central lateral line units may have different functions. Units exhibiting phase-locking may be used by the system to encode the fine structure of a stimulus, i.e., its frequency content, whereas those units that do not show phase-locking may be used for the encoding of other aspects of a hydrodynamic stimulus, for instance its direction or velocity.

The assumption that frequency information is preserved in the central lateral line is supported by various behavioural studies that have shown that fish and other aquatic animals are able to distinguish between stimuli of different frequencies (Bleckmann et al. 1981, Frühbeis 1984, Elepfandt 1986, Vogel and Bleckmann 1997). For instance, the catfish, *Poecilia reticulata*, a nocturnal predator, was able to track a wake produced by piscine prey with the aid of its lateral line (Pohlmann et al. 2004). The animals possibly were able to analyse the frequency content of the wake to distinguish between relevant and irrelevant pattern. In this study the fish's ability to follow and catch prey decreased significantly with ablated lateral line. The clawed frog *Xenopus laevis* can analyse wave pattern and distinguish with its lateral line between 18Hz and 20 Hz, but not between 19Hz and 20 Hz (Elepfandt 1986). The surface feeding fish *Aplocheilus lineatus* was able to discriminate between single frequency surface waves with 15 % difference in their frequency (Vogel and Bleckmann 1997). Bleckmann et al. (1981) also showed that *Aplocheilus* detects frequency differences of 2.5 Hz at 20 Hz; 3.7 Hz at 40 Hz; 6.5 Hz at 80 Hz and 17.2 Hz at 100 Hz. Nauroth (2008) investigated behaviourally the frequency discrimination performance of oscars, *Astronotus ocellatus*. The approaching and turning behaviour towards a vibrating sphere was analysed. This study has shown, that oscars were able to discriminate between frequencies of 70 Hz and 100 Hz. It would be interesting to conduct comparable behavioural experiments with goldfish in order to determine their frequency discrimination ability.

There are two aspects of the present study that should be considered for future studies. First, the range of the presented frequencies was limited to three, due to technical problems with stimulation. Thus, in future experiments, a wider range of frequencies should be used. Second, in the present study the different frequencies were presented with constant displacement amplitudes. Since superficial and canal neuromasts function as velocity and acceleration detectors, respectively (e.g., Kroese and Schellart 1992), it would be interesting to know to what extent these properties are preserved in the central lateral line. Therefore, in future studies the frequency characteristics of MON units in response to sinusoidal stimuli of constant velocity and accelerations should be determined.

4.2 Spatial Excitation Patterns of MON units

Spatial excitation patterns of lateral line units in the goldfish MON were measured in response to a vibrating sphere presented at various locations along the side of the fish. Four vibration angles were applied, 0° (parallel to the fish), 90° (orthogonal to the fish), 45° and 135°. While stimulation parallel to the fish has been used previously (e.g., Coombs et al. 1998, Mogdans and Kröther 2001) the excitation patterns caused by stimulation with the other directions were examined here for the first time.

Theoretical data suggest that the spatial excitation patterns of the peripheral lateral line contain information about the location of the vibrating source (Curcic-Blake and van Netten 2006, Goulet et al. 2008). In short, source location alongside the fish and source distance can be derived from the location and separation of peaks and troughs within the spatial excitation pattern (see Introduction pages 7-10). The theoretical predictions were confirmed by measuring receptor potentials of the hair-cells within a neuromast (Curcic-Blake and van Netten 2006) and by recording neuronal activity of single fibres in the posterior lateral line nerve (PLLN) (Coombs et al. 1996, Coombs and Conley 1997, Goulet et al. 2008, Scholze et al. unpublished). However, it is not known in which way neurons in the fish brain use the information that is provided by afferent nerve fibres to encode source location. If a central neuron integrates across inputs from a series of peripheral receptors, such that it represents the spatial locations of excitation peaks and troughs, then this neuron has the

potential to directly code for object location, distance and vibration direction. Evidently, neurons in the MON receive inputs from widely distributed lateral line receptors (Northcutt 1989, Montgomery et al. 1995, Mogdans and Kröther 2001, own data). Therefore, in the present study, the MON was screened for neurons encoding source location by quantitatively describing spatial excitation patterns as a function of location and vibration angle of a dipole source.

The results show that spatial excitation patterns of MON neurons are highly variable, consisting of areas from which stimulation caused an increase and/or decrease in discharge rates (see e.g., Figures 21-23). In this respect, the data from the present study are comparable to those reported previously (Coombs et a. 1998, Mogdans and Kröther 2001). Depending on size and shape of the excitation pattern the units of this study were assigned to one of three groups. More than two thirds of the units were assigned to Group 1 (76%, Figure 21). In these units dipole stimulation caused an increase in discharge rate and/or phase-locking in one or more areas of different size. A smaller proportion of units (13 %) were assigned to Group 2. Units in this group showed a decrease in discharge rate in response to sine wave stimulation (Figure 22). Finally, 11 % of the units were assigned to Group 3. They were characterised by excitation patterns that consisted of adjacent excitatory and inhibitory response areas (see e.g. Figure 23).
Based on their responses to changing vibration angles, most MON units (n = 35, 92 %) had excitation patterns that differed from those of primary afferent nerve fibres, while only a few units showed primary-like excitation patterns (n = 3, 8 %).

Non primary-like excitation patterns in the MON

The majority of goldfish MON units had excitation patterns with properties that were unlike those of primary afferent fibres both in terms of discharge rate and, if units were phase-locking, in terms of phase angles. For instance, excitation patterns were found that were fairly broad, extending almost across the entire fish body (30 %, see e.g. Figure 21C, 27). These patterns are similar to those found in MON units by Coombs et al. (1998). In the present study, in addition to broad patterns characterized by discharge rate increases, broad patterns characterized by discharge rate decreases were found (6 % see e.g. Figure 22C). road excitation patterns most likely are produced by convergence of primary afferents that innervate neuromasts

distributed across large parts of the lateral line periphery. These inputs to the MON may be either purely excitatory or inhibitory. Units with broad spatial excitation patterns are possibly involved in the detection of object movement rather than in the encoding of object location. It would therefore be interesting to know whether these units are particularly sensitive to an object moving along the lateral line. Sensitivity to a moving object was not investigated in the present study. However, in previous studies MON units were found that responded exclusively to a sphere moving along the side of the fish but not to a stationary vibrating sphere (Mogdans and Goenochea 2000; Mogdans and Bleckmann 2001). An advantage of exhibiting broad spatial excitation patterns with decreased discharge rates could be to reinforce contrast through the combined processing of different spatial excitation patterns, i.e., if information from units with broad inhibitory excitation patterns were combined with information from units with small excitatory patterns this would lead to contrast enhancement. Approximately one third of the excitation patterns was found to consist of small areas where stimulation caused an increase (24 %) or decrease in discharge rate (5 %, Figure 21A, 22A). Other excitation patterns showed two or more areas with increased (22 %) or decreased discharge rate (2 %, Figure 21B, 22B). Those excitation patterns were not considered primary-like as they exhibited more variable and less distinct shapes than excitation patterns of afferents. In the study by Mogdans and Kröther (2001), non primary-like excitation patterns of MON units were characterized by rate increases (23 %), rate decreases (7 %), or both rate increases and decreases (36 %). Some patterns contained one or more areas in which stimulation with the vibrating sphere caused a change in discharge rate, while others were broad extending along the entire length of the fish.

Most of the units in the present study exhibited phase-locking (71.6 %). With regard to phase-locking and phase angles, the excitation patterns of MON units were different from those of primary lateral line afferents. While the excitation patterns of afferent fibres are characterized by distinct 180° shifts in phase angle, only 26 % of the MON units with non primary-like spatial excitation patterns exhibited 180° shifts in phase angle (see e.g. Figure 21C, 27). Another 14 % of the units had excitation patterns that were characterized by systematic increases and/or decreases of phase angles in small steps without steep shifts (see e.g. Figure 22A, 26). In the majority of the units, however, the distribution of phase angles across the spatial excitation

pattern did not follow any specific pattern (60 %, see e.g. Figure 22B, 28). These findings lead to the assumption that phase information is not necessarily important for particular MON units. Possibly, these units are only involved in object localisation without consideration of source parameters like phase angle (compare page 83).

Primary-like excitation patterns

In the present study only 8 % of the MON units exhibited excitatory excitation patterns similar to those of primary afferent nerve fibres (see e.g., Münz 1985, Coombs and Montgomery 1992, Kroese and Schellart 1992, Coombs et al. 1996, Coombs et al. 1998, Montgomery and Coombs 1998, Mogdans and Bleckmann 1999, Scholze et al. unpublished). This number is different from those reported in previous studies. Mogdans and Kröther (2001) found that 34 % of MON units had excitation patterns similar those of primary afferents, and Coombs et al. (1998) reported an even higher percentage of 67 % of MON units with primary-like excitation patterns. The causes for this discrepancy are not readily apparent. One possible explanation is that different stimulus amplitudes were used in the different studies. For instance, in the present study the displacement amplitude of the sphere was between 200-500 µm peak-to-peak, while Mogdans and Kröther (2001) used a stimulus amplitude of 2000 µm. In the current study the displacement amplitude was adjusted to the units' dynamic ranges. However, stimulation amplitudes in the current study might have been too small to evoke exact primary like excitation patterns. This could have resulted in the low number of units exhibiting primary-like excitation patterns. Another possible cause for the different numbers may by the type of stimulation and data analysis. In the present study and in the study by Mogdans and Kröther (2001), responses were recorded to a vibrating sphere that was placed successively at different stationary locations. In contrast, Coombs et al. (1998) used a roving sphere, i.e., a sphere that was slowly moved alongside the fish while it was either vibrating or not vibrating and the responses to these two stimuli were compared in order to distinguish responses to a vibrating from a moving source. There is the possibility that with this approach non primary-like excitation patterns, in particular those that are characterized by weak and non phase-locked increases in discharge rate or by slight decreases in discharge rate are easily overlooked and the data sample therefore gets biased towards primary-like responses.

Modelling data suggest that primary-like excitation patterns in the MON are

generated by the processing of peripheral lateral line information through a neural network based on lateral inhibition (Coombs et al. 1998). Excitation patterns with a central excitatory or inhibitory area, bordered rostrally and caudally by inhibitory or excitatory areas, are indicative of a centre-surround organization. Excitation patterns with an excitatory area located near the head and an inhibitory area near the trunk or vice versa (Group 3, see e.g. Figure 23, 26) indicate that inputs from rostral and caudal parts of the fish, i.e., the head and trunk lateral line, are converging onto a medullary unit with opposite sign. Excitatory and inhibitory inputs as those observed here among MON neurons may lead to contrast enhancement, to increased sensitivity or may subserve stimulus localization. For instance, inputs converging with opposite sign from different parts of the lateral line periphery, e.g., from the animal's front and rear, create transitions from excitation to inhibition that could be used in the computation of source location.

Excitation patterns of midbrain units

Excitation patterns of midbrain units in the torus semicircularis were investigated in a study of Plachta et al. (1999). He distinguished two types of excitation patterns, (i) single or double peaked, well defined small excitation patterns and (ii) multi peaked patterns covering large parts of the fish`s body. However, since excitation patterns were not the main subject of that study, their properties were not precisely assessed and investigated. Meyer et al. (unpublished) also investigated spatial excitation patterns of midbrain units. They found excitation patterns consisting of small (18.75 %, n = 3) or broad (62.5 %, n = 10) excitatory areas and patterns like those obtained from lateral line afferents (18.75 %, n = 3). Excitation patterns with areas from which stimulation caused a decrease in discharge rate were not found. This, however, may be a consequence of the fact that midbrain units have a very low or no spontaneous discharge rate, i.e., reductions in discharge rates are not readily apparent. Voges (2008) measured spatial excitation patterns of goldfish midbrain units in two dimensions, i.e., he measured their vertical and horizontal extent. Depending on their alignment and extension four different types of patterns with were distinguished, round (n = 2), horizontally elongated (n = 2), vertically elongated (n = 3) and complex (n = 2). Units with broad excitation patterns that extended along the whole fish body were not found. As in the study of Meyer et al. (unpublished), units that could code for the exact sphere location were not found by Voges (2008).

Except for the lower amount of units that responded with phase-locked discharges in response to stimulation (25 %, Meyer et al. unpublished), midbrain units showed similar spatial excitation patterns (see above). A possible explanation for similarity is that recorded midbrain responses could have originated from MON projections at the midbrain level. That could suppose to mean that those responses are originated in secondary MON units and not in midbrain units. Intracellular recordings should be executed followed by subsequent staining of these units, in order to anatomically ascertain the recording site.

Effects of changing vibration direction

Data of the effects of changing sphere vibration direction on neuronal responses have been obtained only from the lateral line periphery (Scholze et al. unpublished) and from modelling studies (Sand 1981, Coombs et al. 1996, Curcic-Blake and van Netten 2006). To date, no data have been published on the responses of central lateral line units to different sphere vibration directions. The only other study assessing effects of sphere vibration direction that is currently underway is the study by Meyer et al. (unpublished), who is recording responses from lateral line units in the midbrain torus semicircularis.

The present data show that changing sphere vibration angle can have effects on the spatial excitation patterns of brainstem neurons. The effects were highly variable from one neuron to the next and were expressed in terms of the shapes of the excitation patterns, discharge rates, phase locking and/or phase angle. A small number of MON units (8 %) exhibited modifications in excitation patterns with changing sphere vibration direction that were comparable to the responses observed among primary afferent fibres (i.e., discharge rate and/or phase locking, see Introduction page 7-10, Figure 25). In most units, however, changes in size and/or shape of the excitation pattern were not comparable to those described for primary afferents (62 %, Figures 26-28, 30, 31). Depending on the vibration angle, the excitation patterns differed in terms of number of response areas, location of excitation pattern maxima/minima, half-maximum width, discharge rate, and/or phase locking. In most cases, two or more of these parameters changed concurrently. Interestingly, excitation patterns of midbrain units were just recently shown to possess response properties comparable to brainstem units (Meyer et al.

unpublished). Midbrain and brainstem units exhibited a similar variability in their excitation patterns when the vibration angle was varied. Moreover, as among MON units, only a small number of 18.75 % of the midbrain units showed excitation patterns similar to those of primary afferents.

The majority of MON units exhibited spatial excitation patterns that were not suitable for an exact coding of object location and vibration direction. The minority of MON response patterns had distinct, narrow peaks of increased or decreased discharge rates, which were more appropriate for localization. It more likely that not only the particular properties of single spatial excitation patterns will code for object location but the combined information of many units with different spatial excitation patterns (see page 90).

Widths of spatial excitation patterns

Half maximum widths (HMW) of the spatial excitation patterns were determined for seventeen units. More than two thirds (71%) of these units exhibited a ≥ 15% shift of the location of the response maximum alongside the fish's body when vibration direction was varied (Figure 29A). The shifts were not found to be systematic in half of these HMWs. The other half of exhibited a shift towards more rostral locations with reference to the location of the peak determined with parallel stimulation (Figure 29A Right).

In about one thirds of the units (29 %), the shifts of the response maxima of the remaining HMWs were below 15 % of body length (Figure 29B). Units, in which HMWs shift systematically with changing sphere vibration direction, can encode vibration direction due to the fact that the location of maximum response is dependent on the vibration angle but not stimulus location. In contrast, units in which HMW locations are constant, i.e., independent of sphere vibration direction, may encode the exact stimulus location independent of vibration direction. Especially if such a unit was to receive input from a spatially restricted array of receptors, or from primary lateral line afferents with single small excitation areas, an accurate determination of location would be possible. In conclusion of these findings it is very well possible, that different channels of information processing exist already at the level of the lateral line brainstem. One channel may potentially code for stimulus presence, whereas another channel codes for stimulus location and a further channel is specialized on moving objects.

Effects of varying source distance

Ten units were recorded while varying the distance between the fish and the sphere. In these experiments, the general shape of the excitation pattern in terms of discharge rate and phase-locking remained constant for different distances (Figure 32). Modelling data show, that for primary afferent nerve fibres increasing source distance leads to decreasing peak amplitude and broadening of the peripheral spatial excitation patterns and to a decrease in the steepness of their slopes. This is due to the fact that differences in the level of stimulation between adjacent lateral line organs are higher for close sources than for more distant sources (Coombs and Patton 2008). Despite large differences in spatial excitation patterns of lateral line afferents and central units, the theoretical predictions for primary afferents with respect to source distance were also applicable to excitation patterns of MON unit, i.e. they preserved their general shape but decreased slopes and amplitudes. Excitation patterns of midbrain units changed in a similar way when stimulation distance was increased (Meyer et al. unpublished). With increasing distance of stimulus both, the physical parameters as well as their biological relevance decrease (compare page 83).

Spatial excitation patterns and fish behaviour

Numerous studies have investigated the behavioural capabilities of fish to detect and discriminate objects with the lateral line (Weissert and von Campenhausen 1981, Teyke 1985, Hassan 1986, Coombs and Janssen 1990, Coombs and Conley 1997, Coombs and Patton 2008). For instance, blind cave fish (*Anoptichtys jordani*) are able to discriminate the size and the orientation of different stationary objects (Weissert and von Campenhausen 1981, Teyke 1985, Hassan 1986). The mottled sculpin is able to detect a vibrating sphere and can also discriminate source location and vibration direction during approach behaviour (Coombs and Janssen 1990). Studies on the approaching behaviour of mottled sculpin found that the fish use the strategy of keeping the source to one side of the body rather than keeping it in front (Conley and Coombs 1998). This behaviour suggests that it is advantageous for the fish to perceive the stimulation with the complete receptor array (neuromasts) so that the complete range of spatial excitation patterns can be used for stimulus coding. These results support the hypothesis that spatial excitation patterns along the lateral

line play a major role in encoding both source direction and distance (Coombs and Conley 1997).

Recently, Coombs and Patton (2008) tested the hypothesis that mottled sculpin use peaks in the neural excitation patterns to determine the location of an artificial prey (vibrating sphere) along the fish's body surface. In this case, excitation patterns with small single areas, in which stimulation caused an increase in discharge rate, would be particularly useful. In that study the initial orienting response towards the vibrating sphere was investigated. Two different sphere vibration directions were presented, parallel and orthogonal to the animal's body axis. Despite a distinct difference in pressure gradient patterns between parallel and orthogonal source orientation (see Introduction and Curcic-Blake and van Netten 2006) the mottled sculpin performed equally well at solving the localisation tasks for parallel and orthogonal vibration. This result argues against the hypothesis that fish use the peaks in the spatial excitation patterns. Coombs and Patton (2008) negated spatial learning independent of lateral line input as a possible explanation for the performance of the fish. They assumed that the midbrain is mainly involved in localization tasks with the aid of topographic maps. The fish must therefore combine somatotopic information about both source distance and source location to determine the direction of the source with respect to the fish's body surface. To generate the required map, information about these two parameters must be computationally transformed from a somatotopic to an egocentric coordinate system. Another possibility considered by Coombs and Patton (2008) is that fish use an array of neural filters tuned to particular combinations of source orientation, distance, and somatotopic location. Such a filter array could classify entire lateral line pressure gradient patterns rather than relying on a few key features.

Coombs and Patton (2008) also studied the effect of source distance on the fish's orienting response. An increase in source distance led to a decrease in orienting performance. This could be attributed to a decreased amplitude and slope steepness of the pressure gradient pattern and/or a reduced behavioural relevance of objects (prey) at larger distances (Coombs and Patton 2008, Coombs and Conley 1997). This also explains the effects of changing sphere distance on spatial excitation patterns in the present study (see above).

Comparison with the electrosensory system

A high complexity in spatial excitation patterns was also found in the electrosensory system of weakly electric fish (e.g. Metzen et al. 2008). Excitation patterns of secondary brainstem units in the electrosensory lateral line lobe (ELL) in *Gnathonemus petersii* were very heterogeneous. They exhibited one or more areas where stimulation caused an increase and/or decrease in discharge rate. Electrosensory excitation patterns were characterised as simple, complex and very complex, while excitation patterns obtained from primary electrosensory afferents are simpler, i.e. they represent the electric image of the stimulus. Thus, the physiological properties of the electrosensory lateral line are similar to those of the mechanosensory lateral line in that the organization of brainstem excitation patterns is much more diverse and complex compared to the relatively simple and predictable patterns obtained from afferent fibres.

Another similarity between mechanosensory and electrosensory spatial excitation patterns was found in paddlefish, *Polyodon spatula*. Excitation patterns of secondary electrosensory units in the dorsal octavolateral nucleus (DON) were found to be large and/or the excitation peak is surrounded by areas in which stimulation caused a decrease in discharge rate (Hofmann et al. 2005).

Neuronal representation of the environment

Behavioural studies have confirmed that fish can unambiguously determine and localize objects (e.g. Coombs and Janssen 1990, Coombs and Patton 2008). The question is then how central lateral line units analyze the incoming data so that the animal can eventually obtain an unambiguous image of its environment. One possibility to solve this task is to use a hydrodynamic topographic neuronal map. In other sensory systems several parallel pathways are used to process stimulus information, and within each, information is processed in topographically arranged maps or in maps derived from neuronal computation (e.g. Schellart et al. 1987, Northcutt and Wullimann 1988, Udin 1988, Kaas 1997, Chagnaud et al. 2008). Fish as well as other animals have a visual topographical map in the optic tectum (review: Northcutt and Wullimann 1988) and a computed topographical acoustic map in the midbrain (e.g., Schellart et al. 1987). Computed lateral line maps have been found in several aquatic animals like the clawed frog, *Xenopus laevis* (Zittlau et al. 1986), and the Axolotl, *Ambystoma mexicanum* (Bartels et al. 1990). In these animals, the

directions of water surface waves are represented systematically in the optic tectum. While stimulating the lateral line with a stationary vibrating sphere, Knudsen (1977) and Bleckmann et al. (1989b) have discovered a topographic lateral line map in the midbrain of catfish and rays, respectively. There is also evidence that the torus semicircularis in the midbrain of goldfish is topographically organized (Plachta et al. 2003): lateral line units in the rostral midbrain responded to a stimulus moving from anterior to posterior body areas and units in the caudal midbrain were found to respond to the reverse motion direction. Physiological evidence that such a topographic hydrodynamic map already exists at the level of the brainstem is not at hand. However, anatomical studies show that lateral line information could be organized topographically at least partly. For instance, Kröther (2002) found that some information from posterior body areas, i.e. from posterior lateral line fibres (PLLN) projected more dorsally in the brainstem than ALLN fibres which are originating in the head region. These findings correlate with physiological data from MON units and with histological reconstructions of lesioned recording sites (Kröther 2002). The maxima of excitation patterns obtained from units located in the lateral part of the brainstem were found to be centred on the head and the rostral part of the fish's trunk. This suggests also that units located in the medial part of the MON receive input from afferents that innervate neuromasts on the caudal part of the trunk (Kröther 2002). Such a dual somatotopy (head and trunk) in the lateral line brainstem has also been found in zebrafish larvae (Alexandre and Ghysen 1999). Puzdrowski (1989) also report a crude brainstem somatotopy in which the fish's trunk is represented dorsally to the fish's head.

Another possibility how information about the spatial location of a source could be encoded centrally is with the aid of a population vector code. In population vector coding a single unit displays a distribution of responses over some set of inputs, and the combined responses of many units determine the relevance of each input (Rieke et al. 1997). Sensory information derives from the pattern of activity occurring in populations of neurons. This neuronal principle is known for instance for the representation of motion direction in the mammalian motor cortex (e.g. Georgopoulos et al. 1986). Each neuron fires preferentially when movement occurs in a certain direction but the spatial tuning of an individual neuron is rather weak. Instead, the vector sum of all neurons determines the actual direction of motion. Thus, the

population of neurons, and not a single unit, encodes the signal for motion direction (e.g. Georgopoulos et al. 1986). If the principle of a population code was applied to lateral line processing, it would mean that a point in space would be encoded by an ensemble of neurons instead of a single neuron. Such a mechanism could be implemented already at the level of the lateral line brainstem. To determine whether this neuronal principle is relevant to the central processing of lateral line information, with respects to spatial lateral line information, more needs to be known first about the transmission of information between primary afferents and secondary lateral line units.

The above explanations imply that there is not necessarily a need for a topographic arrangement of neurons in the MON. Instead, at least for a certain population of MON units a strict topography may be broken up in favour of information coding in different channels (compare page 88). Perhaps this population code at the level of the MON is used later for generating a more exact “map-like” representation in the midbrain. This would be possible if inputs from many MON units converge onto particular units in the midbrain. As a consequence, topographic order is restored by the projections from the brainstem to the midbrain, which may be achieved by a learning mechanism where vision is used to obtain spatial information about the source location. This kind of plasticity has been shown to align visual and acoustic maps in the barn owl (Hyde and Knudsen 2001). An interaction between visual and lateral line learning can play a possible role in orientation tasks of the lateral line system.

In summary, the data presented here show that changing sphere vibration angle effects the shape and size of brainstem excitation patterns. The effects were highly variable between units, consisting in alterations in excitation pattern shape, discharge rate, phase locking and/or phase angle. In addition, the observed effects of sphere vibration angle on MON units were different from those observed among primary afferent nerve fibres. Thus, while peripheral lateral line excitation patterns follow pressure gradient patterns (see Introduction pages 7-10, Figure 3B) this is not the case at more central levels. This implies that pressure gradient patterns are not represented by MON neurons as they are by the lateral line periphery. Precise encoding of source orientation, distance, and somatotopic location with the aid of the

observed spatial excitation patterns is difficult. Nevertheless, information about location and vibration direction of a sinusoidally vibrating sphere is present in the responses of brainstem neurons, even though this information is not encoded unambiguously. A neural transmission mechanism is quite likely, but exactly at which brain level this filter operates remains to be determined. Exactly how MON units integrate across peripheral inputs in order to generate the observed excitation pattern types remains to be examined. In this context it is important to determine exactly how lateral line afferents from differently oriented hair cells in different neuromasts are connected onto second order target cells in the MON. This is necessary to explain the observed discharge pattern obtained in the present study.

4.3 Responses of MON units to water flow

In the present study, the responses of MON units to different flow regimes were recorded. Flow was presented either at a constant velocity (pulsed flow) or with continuously rising velocity (ramped flow). About 75 % of the recorded units were classified as flow-sensitive. This number is in agreement with the numbers reported for primary afferent nerve fibres. For instance, Carton and Montgomery (2002) showed that in *Trematomus bernacchii* 70 % of the lateral line afferents were flow-sensitive. Similarly, Chagnaud et al. (2007) found that 71 % of the ALLN fibres and 72 % of the PLLN fibres in goldfish were flow-sensitive. In a study by Voigt et al. (2000) 74 % of ALLN fibres from *Anguilla dieffenbachii* responded to water flow. Engelmann et al. (2002) classified 67 % of goldfish primary afferents as flow-sensitive. The number is also in agreement with those from previous studies in the MON of goldfish in which between 67 % and 69 % of the units were found to be flow-sensitive (Kröther et al. 2002, Engelmann et al. 2002), and in the MON of trout, in which 50 % of the units responded to water flow with a change in discharge rate and/or discharge pattern (Engelmann et al. 2002). In contrast to neurons in the brainstem, only about one third of the midbrain units in goldfish was flow-sensitive (Engelmann 2000, Engelmann and Bleckmann 2004).

Types of responses

Neuronal responses to anterior-posterior flow consisted in 54 % of the cases of an increase and in 21 % of a decrease in discharge rate. Primary lateral line afferents typically increase their rate linearly in response to increasing unidirectional water flow (Voigt et al. 2000; Carton and Montgomery 2002; Engelmann et al. 2002, Engelmann et al. 2000; Chagnaud et al. 2007). Decreases in discharge rate in response to flow have rarely been reported for afferent nerve fibres and if so, then in response to low flow velocities (see e.g., Voigt et al. 2000, Chagnaud et al. 2007). Thus, decreases in discharge rate in response to water flow seem to be a property that is typical for central lateral line neurons. The relative proportions of flow-sensitive MON units with increased and decreased discharge rates found in the present study are comparable to those reported by Kröther (2002 Dissertation). In that study, 42 % of the flow-sensitive units increased their discharge rate while 24 % decreased their rate. In contrast to MON units, midbrain lateral line units responded to water flow similar to primary afferents by exclusively increasing their discharge rates (Hofmann et al. unpublished).

Superficial versus canal neuromasts

The results of the present study as well as previous research (Montgomery and Coombs 1992; Coombs and Montgomery 1994) give reason to consider the possibility that flow-sensitive units correspond to velocity-sensitive superficial neuromasts, while flow-insensitive units correspond to acceleration-sensitive canal neuromasts. This interpretation is supported by behavioural (Janssen et al. 1990, Montgomery et al. 1997, Coombs et al. 2001), physiological (Engelmann et al. 2000, Voigt et al. 2000, Engelmann et al. 2002) and theoretical lateral line studies (Denton and Gray 1988, Denton and Gray 1989). However, it is important to note that Chagnaud et al. (2008) found that a clear separation of flow-sensitive and flow-insensitive fibres is not possible since responses to water flow depend on the flow velocity applied. In other words, even apparently flow-insensitive fibres may be rendered flow-sensitive by a sufficiently high flow velocity. In contrast to flow-sensitive lateral line afferent fibres, which typically respond to water flow with sustained changes in discharge rate, the activity patterns of MON units were more variable (see e.g. Figure 34). Phasic, sustained, as well as a combination of phasic and sustained response patterns were obtained (Figures 35, 44). This is in

agreement with Kröther et al. (2002), who documented comparable patterns. Although there was an increase in the discharge variability of those units that increased their rate in running water, burst-like discharge behaviour, similar to that observed in afferent fibres (Chagnaud et al. 2008) was observed in only three units.

Velocity tuning

One hypothesis that can be derived from the work by Chagnaud et al. (2008) is that brainstem units determine velocity and direction of a water flow from turbulences in the flow. Turbulences result in fluctuations of the local flow on the fish surface that are carried with the flow along the side of the fish, i.e., along the array of lateral line receptors. Chagnaud et al. (2008) speculate that central lateral line units use these fluctuations to compute flow velocity by comparing inputs from two or more neuromasts that are organized in series on the fish surface (see Introduction pages 10-11). These units should function as coincidence detectors, i.e., they should respond only if the inputs from these receptors arrive simultaneously. If this was the case, then central units should be found that respond preferentially to distinct flow velocities and flow directions. In the present study, clear evidence for the aforementioned hypothesis was not found. All MON units that increased their discharge rate in response to stimulation with water flow showed a nonlinear velocity response function, i.e., they did not increase (decrease) discharge rate in response to increasing (decreasing) flow. A linear velocity response function was only observed in units that decreased their discharge. Most velocity response functions did not exhibit a sharp tuning for a particular flow velocity. However, a few velocity functions (n = 5, 19 %) exhibited a response maximum at intermediate velocities (Figures 44C, 45). Even though the tuning was broad, these units are possible candidates for the coding of distinct (in this case intermediate) flow velocities. Similar to MON units, units in the midbrain of goldfish increase their spike frequency with increasing water velocity, while background activity, response patterns and response variance are quite diverse (Hofmann et al. unpublished). Most midbrain units (82%) responded to water flow turbulences and to a broad range of velocities. However, in 18 % of the units the responses were restricted to a narrow velocity range, i.e., the units were tuned to distinct flow velocities (Hofmann et al. unpublished).

Directional sensitivity

Within the flow-sensitive units (n = 48, both stimulation paradigms, intersections considered) 35 % responded to water flow in a direction-dependent manner. Regarding SDI values, less than one tenth of the units (9.1 % for ramp stimulation, 8.5 % for pulse stimulation) was strongly directionally sensitive as indicated by SDI values smaller than -50 or greater than 50. Thus, at least a small number of MON neurons codes for AP and PA stimulus direction.

Afferent nerve fibres have been shown to respond to both AP and PA flow with an increase in discharge rate (e.g., Chagnaud et al. 2007). Nevertheless most of the fibres in this study exhibited a slightly greater increase in response to flow in AP than in PA direction (n = 11, 92 %). However, at least at low flow velocities, all flow-sensitive fibres increased their discharge rates regardless of flow direction. This implies that primary lateral line afferents do not encode bulk flow direction. The most plausible explanation for this observation is that the fibres were responding to flow fluctuations instead of the d.c. component of flow (see discussion above and Chagnaud 2006, Chagnaud et al. 2008). Such flow fluctuations then potentially be used by units in higher lateral line nuclei to determine flow direction. Existence of a cross-correlation mechanism is conceivable but has not been shown for the lateral line, yet. However, an advantageous prerequisite for such a mechanism could be the broad spatial excitation patterns of MON units. These units seem to integrate the input of two or more widely spaced neuromasts (see Results 3.2, Discussion 4.2, Mogdans and Kröther 2001). The data on MON units collected in the present study are comparable to data obtained for flow-sensitive midbrain units (Hofmann et al. unpublished), where 24 % of the units were found to be directional sensitive.

The lateral line is also involved in rheotaxis, a behavioural orientation to water currents (Montgomery et al. 1997, Baker and Montgomery 1999, Engelmann 2002, Kanter and Coombs 2003), for which it would be highly advantageous to determine the direction of water flow.

Comparison with responses to moving objects

This is the first study in which brainstem lateral line units were stimulated with water flow in both directions. Most of the previous studies assessing directional sensitivity of the lateral line used a moving object (primary afferents: Mogdans and Bleckmann 1998, Montgomery and Coombs 1998, Engelmann et al. 2003, Mogdans and Geisen

2009; primary afferents and central lateral line units: Bleckmann and Zelick 1993, Engelmann et al. 2003; central lateral line units: Müller et al. 1996, Mogdans et al. 1997, Wojtenek et al. 1998, Mogdans and Goenechea 2000, Montgomery et al. 2000, Engelmann and Bleckmann 2004). Measures of directional sensitivity varied within these studies. Primary lateral line afferent fibres represent the direction of object motion by the temporal pattern of discharge. When motion direction is reversed, the response is inversed (Bleckmann and Zelick 1993, Mogdans and Bleckmann 1998, Montgomery and Coombs 1998, Engelmann et al. 2003). In the PLLN of goldfish, about 96 % of the units responded to a moving object with directional-dependent patterns (Mogdans and Bleckmann 1998), whereas in the ALLN, only 40 % of the units were direction sensitive (Mogdans and Geisen 2009). An inversion of the response pattern with a reversal of motion direction is expected as a consequence of the intrinsic directional sensitivity of the hair cells (Flock 1971, Görner 1963). Hair cell orientations on the goldfish head are fairly homogeneously distributed (Schmitz et al. 2008). Thus, the probability of mirror image responses to AP and PA object motion is substantially reduced for ALLN fibers compared to PLLN fires.

Most of the brainstem units in *Apteronotus* responded equally well to a moving object in AP and PA direction but some units showed a clear direction preference (Bleckmann and Zelick 1993, Engelmann et al. 2003). Engelmann (2002) and Engelmann et al. (2003) showed that most of the responses of midbrain units to a moving object are independent of movement direction (goldfish: 69 %, trout: 81 %). However, responses of moving objects and responses to water flow as in the current study are difficult to compare, since the moving-object-stimulus is more complex than pure water flow and contains greater pressure gradients and therefore evokes more complex neuronal excitation patterns in the units.

MON unit responses to different types of stimulation

Twenty-six units stimulated with water flow were also stimulated with sine waves generated by a vibrating sphere. More than half of these units (n=15, 58%) were responsive to a vibrating sphere. Most of them increased their discharge rate (n=14) and only one unit showed a decrease in discharge rate in response to sinusoidal stimulation. The remaining units (n=11, 42%) were unresponsive to the vibrating sphere. These data show that a given MON unit does not exclusively responds either

to sinusoidal stimulation or to water flow but that many units respond to both types of stimuli. Thus, that the analysis of different types of stimuli is not strictly separated at the level of the brainstem.

For thirteen units that were stimulated with water flow, in addition the spatial excitation patterns in response to sinusoidal stimulation were obtained. Most excitation patterns were characterized by a broad area from which stimulation caused an increase in discharge rate (n = 11). In two units the excitation pattern consisted of two broad areas from which stimulation caused an increase in discharge rate. This finding supports the idea that units with broad excitation patterns are involved in the processing of global hydrodynamic information like flow or stimuli that are travelling along the fish's body.

Twelve units were stimulated with both a constant and a continuously rising water flow. Most (n = 7) of these units showed similar response behaviour to both stimulation paradigms. Five units responded different to the two stimulation paradigms. Three of these units only showed a change in discharge rate and/or pattern in response to constant water flow but not to continuously rising water flow, the remaining two units differed only in the response to a certain direction (see page 75). The hydrodynamic pattern generated by the constant water flow stimulation differed from the continuously rising water flow stimulation. This was confirmed by anemometer measurements (see Chapter 2.4.3, Figure 9). The greater responses of some MON units to pulsed flow possibly were a result of the steeper slope in increase of flow velocity and greater turbulences. The water acceleration component was clearly higher at the beginning of the constant flow stimulus compared to continuously rising flow. To examine exactly which component of water flow the lateral line units respond to, stimuli have to be characterised in more detail. Stimulation with defined turbulences and/or vortices should be performed in future experiments. Like noted before, histological investigation about the innervations of particular neuromasts will be essential.

5. REFERENCES

ALEXANDRE D and GHYSEN A (1999) Somatotopy of the lateral line projection in larval zebrafish. Proceedings of the National Academy of Sciences of the United States of America 96: 7558-7562.

ALI R (2008). Response of the Medial Octavolateral Nucleus (MON) in the Goldfish, *Carassius auratus*, to constant-amplitude and amplitude-modulated water wave stimuli. Institute of Zoology. Bonn, Rheinische Friedrich-Wilhelms-Universität.

BAKER C F and MONTGOMERY J C (1999) Lateral line mediated rheotaxis in the Antarctic fish Pagothenia borchgrevinki. Polar Biology 21: 305-309.

BAKER C F and MONTGOMERY J C (1999) The sensory basis of rheotaxis in the blind Mexican cave fish, Astyanax fasciatus. Journal of Comparative Physiology a-Sensory Neural and Behavioral Physiology 184: 519-527.

BARTELS M, MUNZ H and CLAAS B (1990) Representation of Lateral Line and Electrosensory Systems in the Midbrain of the Axolotl, Ambystoma-Mexicanum. Journal of Comparative Physiology a-Sensory Neural and Behavioral Physiology 167: 347-356.

BATSCHELET E (1981) The Rayleigh test, Circular statistics in biology. Academic press: 54-58.

BLAXTER J H S and FUIMAN L A (1990) The role of the sensory systems of herring larvae in evading predatory fishes. J. mar. biol. Ass. U.K. 70: 413–427.

BLECKMANN H (1986). Role of the lateral line in fish behaviour. The behaviour of teleost fishes. T. J. Pitcher, Croon Helm, London, Sydney**:** 177-202.

BLECKMANN H (1994). Reception of Hydrodynamic Stimuli in Aquatic and Semiaquatic Animals, Gustav Fischer Verlag, Stuttgart; Jena; New York.

BLECKMANN H (2004) 3-D-orientation with the octavolateralis system. Journal of Physiology-Paris 98: 53-65.

BLECKMANN H, BREITHAUPT T, BLICKHAN R and TAUTZ J (1991) The Time Course and Frequency Content of Hydrodynamic Events Caused by Moving Fish, Frogs, and Crustaceans. Journal of Comparative Physiology a-Sensory Neural and Behavioral Physiology 168: 749-757.

BLECKMANN H, MOGDANS J and FLECK A (1996) Integration of hydrodynamic information in the hindbrain of fishes. Marine and Freshwater Behaviour and Physiology 27: 77-94.

BLECKMANN H and TOPP G (1981) Surface-Wave Sensitivity of the Lateral Line Organs of the Topminnow Aplocheilus-Lineatus. Naturwissenschaften 68: 624-625.

BLECKMANN H, WALDNER I and SCHWARTZ E (1981) Frequency Discrimination of the Surface-Feeding Fish Aplocheilus-Lineatus - a Prerequisite for Prey Localization. Journal of Comparative Physiology 143: 485-490.

BLECKMANN H, WEISS O and BULLOCK T H (1989) Physiology of Lateral Line Mechanoreceptive Regions in the Elasmobranch Brain. Journal of Comparative Physiology a-Sensory Neural and Behavioral Physiology 164: 459-474.

BLECKMANN H and ZELICK R (1993) The Responses of Peripheral and Central Mechanosensory Lateral Line Units of Weakly Electric Fish to Moving-Objects. Journal of Comparative Physiology a-Sensory Neural and Behavioral Physiology 172: 115-128.

CAIRD D M (1978) Simple Cerebellar System - Lateral Line Lobe of Goldfish. Journal of Comparative Physiology 127: 61-74.

CAMPENHAUSEN C V, RIESS I and WEISSERT R (1981) Detection of Stationary Objects by the Blind Cave Fish Anoptichthys-Jordani (Characidae). Journal of Comparative Physiology 143: 369-374.

CARTON A G and MONTGOMERY J C (2002) Responses of lateral line receptors to water flow in the Antarctic notothenioid, Trematomus bernacchii. Polar Biology 25: 789-793.

CHAGNAUD B P (2006). Electrophysiological investigations of the anterior and posterior lateral line nerve of the Goldfish, *Carassius auratus*, to running water and oscillatory stimuli. Bonn, Rheinische Friedrich-Wilhelms-Universität.

CHAGNAUD B P, BLECKMANN H and ENGELMANN J (2006) Neural responses of goldfish lateral line afferents to vortex motions. Journal of Experimental Biology 209: 327-342.

CHAGNAUD B P, BLECKMANN H and HOFMANN M H (2007) Karman vortex street detection by the lateral line. Journal of Comparative Physiology a-Neuroethology Sensory Neural and Behavioral Physiology 193: 753-763.

CHAGNAUD B P, BLECKMANN H and HOFMANN M H (2008) Lateral line nerve fibers do not code bulk water flow direction in turbulent flow. Zoology 111: 204-217.

CHAGNAUD B P, BRUCKER C, HOFMANN M H and BLECKMANN H (2008) Measuring flow velocity and flow direction by spatial and temporal analysis of flow fluctuations. Journal of Neuroscience 28: 4479-4487.

CONLEY R A and COOMBS S (1998) Dipole source localization by mottled sculpin. III. Orientation after site-specific, unilateral denervation of the lateral line system. J. Comp Physiol A 183: 335-344.

COOMBS S (1999) Signal detection theory, lateral-line excitation patterns and prey capture behaviour of mottled sculpin. Animal Behaviour 58: 421-430.

COOMBS S, BRAUN C B and DONOVAN B (2001) The orienting response of Lake Michigan mottled sculpin is mediated by canal neuromasts. Journal of Experimental Biology 204: 337-348.

COOMBS S and CONLEY R A (1997) Dipole source localization by mottled sculpin 1. Approach strategies. Journal of Comparative Physiology a-Sensory Neural and Behavioral Physiology 180: 387-399.

COOMBS S and CONLEY R A (1997) Dipole source localization by the mottled sculpin .2. The role of lateral line excitation patterns. Journal of Comparative Physiology a-Sensory Neural and Behavioral Physiology 180: 401-415.

COOMBS S, HASTINGS M and FINNERAN J (1996) Modeling and measuring lateral line excitation patterns to changing dipole source locations. Journal of Comparative Physiology a-Sensory Neural and Behavioral Physiology 178: 359-371.

COOMBS S and JANSSEN J (1990) Behavioral and Neurophysiological Assessment of Lateral Line Sensitivity in the Mottled Sculpin, Cottus-Bairdi. Journal of Comparative Physiology a-Sensory Neural and Behavioral Physiology 167: 557-567.

COOMBS S, JANSSEN J and WEBB J F (1988). Diversity of lateral line systems: evolutionary and functional considerations. Sensory Biology of Aquatic Animals. J. Atema, R. R. Fay, A. N. Popper and W. N. Tavolga, Springer, New York**:** 553-593.

COOMBS S, MOGDANS J, HALSTEAD M and MONTGOMERY J (1998) Transformation of peripheral inputs by the first-order lateral line brainstem nucleus. Journal of Comparative Physiology a-Neuroethology Sensory Neural and Behavioral Physiology 182: 609-626.

COOMBS S and MONTGOMERY J (1992) Fibers Innervating Different Parts of the Lateral Line System of an Antarctic Notothenioid, Trematomus-Bernacchii, Have Similar Frequency Responses, Despite Large Variation in the Peripheral Morphology. Brain Behavior and Evolution 40: 217-233.

COOMBS S and MONTGOMERY J (1994) Function and Evolution of Superficial Neuromasts in an Antarctic Notothenioid Fish. Brain Behavior and Evolution 44: 287-298.

COOMBS S and PATTON P (2008) Lateral line stimulation patterns and prey orienting behavior in the Lake Michigan mottled sculpin (Cottus bairdi). Journal of Comparative Physiology a-Neuroethology Sensory Neural and Behavioral Physiology 195: 279-297.

CURCIC-BLAKE B and VAN NETTEN S M (2006) Source location encoding in the fish lateral line canal. Journal of Experimental Biology 209: 1548-1559.

DENTON E J and GRAY J A B (1988). Mechanical factors in the excitation of the lateral line of fishes. Sensory Biology of Aquatic Animals. J. Atema, R. R. Fay, A. N. Popper and W. N. Tavolga, New York: Springer-Verlag**:** 595–617.

DENTON E J and GRAY J A B (1989). Some observations on the forces acting on neuromasts in fish lateral line canals. In :The mechanosensory lateral line. Neurobiology and evolution. S. Coombs, G. Görner and H. Münz, Springer, Berlin Heidelberg New York**:** 218-229.

DISLER N N (1977) Organy chuvstt sisteny bokovoi linii i ikh znachneie v povedenii ryb. (Lateral line sense organs and their importance in fish behavior.). zd Akad Nauk SSSR (Translated by Israel Program Sci Transl, 1971, avail. Natl Tech Inf Serv Springfield, VA, as TT): 70–54021.

ELEPFANDT A (1986) Wave Frequency Recognition and Absolute Pitch for Water-Waves in the Clawed Frog, Xenopus-Laevis. Journal of Comparative Physiology a-Sensory Neural and Behavioral Physiology 158: 235-238.

ELEPFANDT A and WIEDEMER L (1987) Lateral-Line Responses to Water-Surface Waves in the Clawed Frog, Xenopus-Laevis. Journal of Comparative Physiology a-Sensory Neural and Behavioral Physiology 160: 667-682.

ENGELMANN J (2002). Einfluß von Fließwasser auf die mechano-sensorische Seitenlinie des Goldfisches, *Carassius auratus*, und der Regenbogenforelle, *Oncorhynchus mykiss*. Insitute of Zoology. Bonn, Rheinische Friedrich-Wilhelms-Universität.

ENGELMANN J and BLECKMANN H (2004) Coding of lateral line stimuli in the goldfish midbrain in still and running water. Zoology 107: 135-151.

ENGELMANN J, HANKE W and BLECKMANN H (2002) Lateral line reception in still- and running water. Journal of Comparative Physiology a-Neuroethology Sensory Neural and Behavioral Physiology 188: 513-526.

ENGELMANN J, KROTHER S, BLECKMANN H and MOGDANS J (2003) Effects of running water on lateral line responses to moving objects. Brain Behavior and Evolution 61: 195-212.

ENGELMANN J, MOGDANS J and BLECKMANN H (2000) The influence of hydrodynamic noise on the response of the peripheral lateral line system of the goldfish, carassius auratus, to vibrating sphere stimuli. European Journal of Neuroscience 12: 493-493.

FEST S (2003). Elektrophysiologische und histologische Charakterisierung von Seitenlinienneuronen im Hirnstamm der Goldfisches, *Carassius auratus*. Bonn, Rheinische Friedrich-Wilhelms-Universität.

FLOCK A (1971). The lateral line organ mechanoreceptors. Fish physiology. W. Hoar and D. Randall, New York: Academic Press 5: 241–263.

FLOCK A and WERSALL J (1962) A Study of Orientation of Sensory Hairs of Receptor Cells in Lateral Line Organ of Fish, with Special Reference to Function of Receptors. Journal of Cell Biology 15: 19-27.

FRÜHBEIS B (1984). Verhaltensphysiologische Untersuchungen zur Frequenzunterscheidung und Empfindlichkeit durch das Seitenlinienorgan des blinden Höhlenfisches *Anoptichthys jordani*. Dissertation. University of Mainz.

GEORGOPOULOS A P, SCHWARTZ A B and KETTNER R E (1986) Neuronal Population Coding of Movement Direction. Science 233: 1416-1419.

GOENECHEA L (1998). Antworten medullärer Seitenlinienneurone des Goldfisches, *Carassius auratus*, auf einfache und komplexe hydrodynamische Reize. Institute of Zoology. Bonn, Rheinische Friedrich-Wilhelms-Universität.

GOLDBERG J M and BROWN P B (1969) Response of Binaural Neurons of Dog Superior Olivary Complex to Dichotic Tonal Stimuli - Some Physiological Mechanisms of Sound Localization. Journal of Neurophysiology 32: 613-636.

GORNER P (1963) Untersuchungen Zur Morphologie Und Elektrophysiologie Des Seitenlinienorgans Vom Krallenfrosch (Xenopus-Laevis Daudin). Zeitschrift Für Vergleichende Physiologie 47: 316-338.

GOULET J, ENGELMANN J, CHAGNAUD B P, FRANOSCH J M P, SUTTNER M D and VAN HEMMEN J L (2008) Object localization through the lateral line system of fish: theory and experiment. Journal of Comparative Physiology a-Neuroethology Sensory Neural and Behavioral Physiology 194: 1-17.

HASSAN E S (1986) On the Discrimination of Spatial Intervals by the Blind Cave Fish (Anoptichthys-Jordani). Journal of Comparative Physiology a-Sensory Neural and Behavioral Physiology 159: 701-710.

HENSEL H, BROMM B and NIER K (1975) Effect of Ethyl Meta-Aminobenzoate (Ms-222) on Ampullae of Lorenzini and Lateral-Line Organs. Experientia 31: 958-960.

HOFMANN M H, CHAGNAUD B and WILKENS L A (2005) Response properties of electrosensory afferent fibers and secondary brain stem neurons in the paddlefish. Journal of Experimental Biology 208: 4213-4222.

HYDE P S and KNUDSEN E I (2001) A topographic instructive signal guides the adjustment of the auditory space map in the optic tectum. Journal of Neuroscience 21: 8586-8593.

JANSSEN J, COOMBS S and PRIDE S (1990) Feeding and Orientation of Mottled Sculpin, Cottus-Bairdi, to Water Jets. Environmental Biology of Fishes 29: 43-50.

JØRGENSEN J M and FLOCK A (1973) The ultrastructure of lateral line sense organs in the adult salamander *Ambystoma mexicanum*. J Neurocytol 2: 133-42.

KAAS J H (1997) Topographic maps are fundamental to sensory processing. Brain Research Bulletin 44: 107-112.

KALMIJN A (1989). Functional evolution of lateral line and inner ear sensory systems. Neurobiology and evolution. S. Coombs, P. Görner and H. Münz, Springer, Berlin, Heidelberg, New York 187–216.

KANTER M J and COOMBS S (2003) Rheotaxis and prey detection in uniform currents by Lake Michigan mottled sculpin (Cottus bairdi). Journal of Experimental Biology 206: 59-70.

KNUDSEN E I (1977) Distinct Auditory and Lateral Line Nuclei in Midbrain of Catfishes. Journal of Comparative Neurology 173: 417-431.

KROESE A and NETTEN S V (1989). The Mechanosensory Lateral Line. Sensory transduction in lateral line hair cells. Neurobiology and Evolution. S. Coombs, P. Görner and H. Münz, Springer - Verlag, New York.

KROESE A B A and SCHELLART N A M (1992) Velocity-Sensitive and Acceleration-Sensitive Units in the Trunk Lateral Line of the Trout. Journal of Neurophysiology 68: 2212-2221.

KROESE A B A, VANDERZALM J M and VANDENBERCKEN J (1978) Frequency-Response of Lateral-Line Organ of Xenopus-Laevis. Pflugers Archiv-European Journal of Physiology 375: 167-175.

KRÖTHER S (2002). Influence of Running Water on the Responses of Brainstem Lateral Line Units of the Goldfish, *Carassius auratus*, and the Rainbow Trout, *Oncorhynchus mykiss*. Institute of Zoology. Bonn, Rheinische Friedrich-Wilhelms-Universität.

KROTHER S, MOGDANS J and BLECKMANN H (2002) Brainstem lateral line responses to sinusoidal wave stimuli in still and running water. Journal of Experimental Biology 205: 1471-1484.

MCCORMICK C A and BRADFORD M R J (1994) Organization of Inner Ear Endorgan Projections in the Goldfish, Carassius auratus. Brain Behav Evol 43: 189-205.

MCCORMICK C A and HERNANDEZ D V (1996) Connections of octaval and lateral line nuclei of the medulla in the goldfish, including the cytoarchitecture of the secondary octaval population in goldfish and catfish. Brain Behavior and Evolution 47: 113-137.

METZEN M G, ENGELMANN J, BACELO J, GRANT K and VON DER EMDE G (2008) Receptive field properties of neurons in the electrosensory lateral line lobe of the weakly electric fish, Gnathonemus petersii. Journal of Comparative Physiology a-Neuroethology Sensory Neural and Behavioral Physiology 194: 1063-1075.

MOGDANS J and BLECKMANN H (1998) Responses of the goldfish trunk lateral line to moving objects. Journal of Comparative Physiology a-Sensory Neural and Behavioral Physiology 182: 659-676.

MOGDANS J and BLECKMANN H (1999) Peripheral lateral line responses to amplitude-modulated sinusoidal wave stimuli. Journal of Comparative Physiology a-Sensory Neural and Behavioral Physiology 185: 173-180.

MOGDANS J and BLECKMANN H (2001). The mechanosensory lateral line of jawed fishes. Sensory Biology of Jawed Fishes. H. T. E. Kapoor BG, Enfield: Science Publishers**:** 181–213.

MOGDANS J, BLECKMANN H and MENGER N (1997) Sensitivity of central units in the goldfish, Carassius auratus, to transient hydrodynamic stimuli. Brain Behavior and Evolution 50: 261-283.

MOGDANS J and GEISEN S (2009) Responses of the goldfish head lateral line to moving objects. Journal of Comparative Physiology a-Neuroethology Sensory Neural and Behavioral Physiology 195: 151-165.

MOGDANS J and GOENECHEA L (2000) Responses of medullary lateral line units in the goldfish, Carassius auratus, to sinusoidal and complex wave stimuli. Zoology-Analysis of Complex Systems 102: 227-237.

MOGDANS J and KROTHER S (2001) Brainstem lateral line responses to sinusoidal wave stimuli in the goldfish, Carassius auratus. Zoology-Analysis of Complex Systems 104: 153-166.

MONTGOMERY J, BODZNICK D and HALSTEAD M (1996) Hindbrain signal processing in the lateral line system of the dwarf scorpionfish Scopeana papillosus. Journal of Experimental Biology 199: 893-899.

MONTGOMERY J, CARTON G, VOIGT R, BAKER C and DIEBEL C (2000) Sensory processing of water currents by fishes. Philosophical Transactions of the Royal Society of London Series B-Biological Sciences 355: 1325-1327.

MONTGOMERY J and COOMBS S (1992) Physiological Characterization of Lateral Line Function in the Antarctic Fish Trematomus-Bernacchii. Brain Behavior and Evolution 40: 209-216.

MONTGOMERY J, COOMBS S and HALSTEAD M (1995) Biology of the Mechanosensory Lateral-Line in Fishes. Reviews in Fish Biology and Fisheries 5: 399-416.

MONTGOMERY J C, BAKER C F and CARTON A G (1997) The lateral line can mediate rheotaxis in fish. Nature 389: 960-963.

MONTGOMERY J C and COOMBS S (1998) Peripheral encoding of moving sources by the lateral line system of a sit-and-wait predator. Journal of Experimental Biology 201: 91-102.

MONTGOMERY J C and MACDONALD J A (1987) Sensory Tuning of Lateral Line Receptors in Antarctic Fish to the Movements of Planktonic Prey. Science 235: 195-196.

MONTGOMERY J C, MACDONALD J A and HOUSLEY G D (1988) Lateral Line Function in an Antarctic Fish Related to the Signals Produced by Planktonic Prey. Journal of Comparative Physiology a-Sensory Neural and Behavioral Physiology 163: 827-833.

MULLER H M, FLECK A and BLECKMANN H (1996) The responses of central octavolateralis cells to moving sources. Journal of Comparative Physiology a-Sensory Neural and Behavioral Physiology 179: 455-471.

MUNZ H (1979) Morphology and Innervation of the Lateral Line System in Sarotherodon-Niloticus (L) (Cichlidae, Teleostei). Zoomorphologie 93: 73-86.

MUNZ H (1985) Single Unit-Activity in the Peripheral Lateral Line System of the Cichlid Fish Sarotherodon-Niloticus L. Journal of Comparative Physiology a-Sensory Neural and Behavioral Physiology 157: 555-568.

NAUROTH I (2008). Verhaltensphysiologische Untersuchungen zur Detektion von Dipolreizen an Cypriniden und Cichliden. Bonn, RheinischeFriedrich-Wilhelms-Universität.

NEW J G, COOMBS S, MCCORMICK C A and OSHEL P E (1996) Cytoarchitecture of the medial octavolateralis nucleus in the goldfish, Carassius auratus. Journal of Comparative Neurology 366: 534-546.

NEW J G, FEWKES L A and KHAN A N (2001) Strike feeding behavior in the muskellunge, *Esox masquinongy*: contributions of the lateral line and visual sensory systems. J Exp Biol 204: 1207-21.

NORTHCUTT R G (1989). The phylogenetic distribution and innervation of craniate mechanoreceptive lateral lines. The mechanosensory lateral line: Neurobiology and evolution. S. Coombs, P. Görner and H. Münz, Springer-Verlag, New York, Berlin, Heidelberg, London, Paris, Tokyo**:** 17-78.

NORTHCUTT R G and WULLIMANN M F (1988). The visual system in teleost fishes. Sensory Biology of Aquatic Animals. J. Atema, R. R. Fay, A. N. Popper and W. N. Tavolga, Springer, New York**:** 515-552.

PARTRIDGE B L and PITCHER T J (1980) The sensory basis of fish schools: Relativ roles of lateral line and vision. J. Comp. Physiol. A 135: 315-325.

PAUL D H and ROBERTS B L (1977) Studies on a Primitive Cerebellar Cortex .1. Anatomy of Lateral-Line Lobes of Dogfish, Scyliorhinus-Canicula. Proceedings of the Royal Society of London Series B-Biological Sciences 195: 453-466.

PLACHTA D, MOGDANS J and BLECKMANN H (1999) Responses of midbrain lateral line units of the goldfish, Carassius auratus to constant-amplitude and amplitude-modulated water wave stimuli. Journal of Comparative Physiology a-Sensory Neural and Behavioral Physiology 185: 405-417.

PLACHTA D T T, HANKE W and BLECKMANN H (2003) A hydrodynamic topographic map in the midbrain of goldfish Carassius auratus. Journal of Experimental Biology 206: 3479-3486.

POHLMANN K, ATEMA J and BREITHAUPT T (2004) The importance of the lateral line in nocturnal predation of piscivorous catfish. Journal of Experimental Biology 207: 2971-2978.

PUZDROWSKI R L (1989) Peripheral Distribution and Central Projections of the Lateral-Line Nerves in Goldfish, Carassius-Auratus. Brain Behavior and Evolution 34: 110-131.

RIEKE F, WARLAND D, DE RUYTER VAN STEVENINCK RR, BIALEK W (1997) Spikes: Exploring the neural code. Computational neuroscience. Cambridge (Massachusetts): The MIT Press.

SAND O (1981). The lateral line and sound reception. Hearing and sound communication in fishes. W. N. Tavolga, A. N. Popper and R. R. Fay, Springer, Berlin Heidelberg New York**:** 459-480.

SATOU M, TAKEUCHI H-A, NISHII J, TANABE M, KITAMURA S, OKUMOTO N and IWATA M (1994) Behavioral and electrophysiological evidences that the lateral line is involved in the inter-sexual vibrational communication of the himé salmon (landlocked red salmon, *Oncorhynchus nerka*). Journal of Comparative Physiology A Neuroethology Sensory Neural and Behavioral Physiology 174: 539-549.

SCHELLART N A M, KAMERMANS M and NEDERSTIGT L J A (1987) An Electrophysiological Study of the Topographical Organization of the Multisensory Torus Semicircularis of the Rainbow-Trout. Comparative Biochemistry and Physiology a-Physiology 88: 461-469.

SCHELLART N A M, PRINS M and KROESE A B A (1992) The pattern of trunk lateral line afferents and efferents in the rainbow trout (*Salmo gairdneri*). Brain Behav. Evol. 39: 317-380.

SCHELLART N A M and WUBBELS R J (1998). The Auditory and Mechanosensory Lateral Line System. The physiology of fishes. D. H. Evans. New York, CRC Press**:** 245-282.

SCHMITZ A, BLECKMANN H and MOGDANS J (2008) Organization of the superficial neuromast system in goldfish, Carassius auratus. Journal of Morphology 269: 751-761.

SIMMONS A M, COSTA L M and GERSTEIN H B (2004) Lateral line-mediated rheotactic behavior in tadpoles of the African clawed frog (*Xenopus laevis*). J Comp Physiol A Neuroethol Sens Neural Behav Physiol 190: 747-58.

SONG J K and NORTHCUTT R G (1991) Morphology, Distribution and Innervation of the Lateral-Line Receptors of the Florida Gar, Lepisosteus-Platyrhincus. Brain Behavior and Evolution 37: 10-37.

SPATH M and SCHWEICKERT W (1977) Effect of Metacaine (Ms-222) on Activity of Efferent and Afferent Nerves in Teleost Lateral-Line System. Naunyn-Schmiedebergs Archives of Pharmacology 297: 9-16.

TEYKE T (1985) Collision with and Avoidance of Obstacles by Blind Cave Fish Anoptichthys-Jordani (Characidae). Journal of Comparative Physiology a-Sensory Neural and Behavioral Physiology 157: 837-843.

UDIN S B and FAWCETT J W (1988) Formation of Topographic Maps. Annual Review of Neuroscience 11: 289-327.

VAN NETTEN S M and KROESE A B A (1987) Laser Interferometric Measurements on the Dynamic Behavior of the Cupula in the Fish Lateral Line. Hearing Research 29: 55-61.

VOGEL D and BLECKMANN H (1997) Water wave discrimination in the surface-feeding fish Aplocheilus lineatus. Journal of Comparative Physiology a-Sensory Neural and Behavioral Physiology 180: 671-681.

VOGES K (2008). 2-dimensionale rezeptive Felder und Sensitivität für unterschiedliche Schwingrichtungen eines Dipolreizes von Seitenlinienneuronen im Torus semicircularis des Goldfisches, *Carassius auratus*. Bonn, Rheinische Friedrich-Wilhelms-Universität.

VOIGT R, CARTON A G and MONTGOMERY J C (2000) Responses of anterior lateral line afferent neurones to water flow. Journal of Experimental Biology 203: 2495-2502.

WAGNER H and TAKAHASHI T (1992) Influence of temporal cues on acoustic motion-direction sensitivity of auditory neurons in the owl. J Neurophysiol 68: 2063 - 2076.

WEBB J F (1989) Neuromast Morphology and Lateral Line Trunk Canal Ontogeny in 2 Species of Cichlids - an Sem Study. Journal of Morphology 202: 53-68.

WEEG M S and BASS A H (2002) Frequency response properties of lateral line superficial neuromasts in a vocal fish, with evidence for acoustic sensitivity. Journal of Neurophysiology 88: 1252-1262.

WEISSERT R and VON CAMPENHAUSEN C (1981) Discrimination between Stationary Objects by the Blind Cave Fish Anoptichthys-Jordani (Characidae). Journal of Comparative Physiology 143: 375-381.

WEISSTEIN E W (1998). The CRC Concise Encyclopedia of Mathematics, CRC Press.

WOJTENEK W, MOGDANS J and BLECKMANN H (1998) The responses of midbrain lateral line units of the goldfish, *Carassius auratus*, to objects moving in the water. Zoology-Analysis of Complex Systems 101: 69-82.

WUBBELS R J (1991) Phase Reversal in the Lateral Line of the Ruff (Acerina-Cernua) as Cue for Directional Sensitivity. Comparative Biochemistry and Physiology a-Physiology 100: 571-573.

WUBBELS R J, KROESE A B A and SCHELLART N A M (1993) Response Properties of Lateral-Line and Auditory Units in the Medulla-Oblongata of the Rainbow-Trout (Oncorhynchus-Mykiss). Journal of Experimental Biology 179: 77-92.

WULLIMANN M F and NORTHCUTT R G (1989) Afferent Connections of the Valvula Cerebelli in 2 Teleosts, the Common Goldfish and the Green Sunfish. Journal of Comparative Neurology 289: 554-567.

ZITTLAU K E, CLAAS B and MUNZ H (1986) Directional Sensitivity of Lateral Line Units in the Clawed Toad Xenopus-Laevis Daudin. Journal of Comparative Physiology a-Sensory Neural and Behavioral Physiology 158: 469-477.

6. APPENDIX

6.1. Physiological Salt Solution for fresh water fishes (after Oakley and Schafer 1978)

- Dissolve in 700 ml Aqua dest.:

NaCl	5.902 g
KCl	0.261 g
$NaHCO_3$	2.1 g
Na_2HPO_4	0.179 g
Tris-Buffer	0.121 g
$MgSO_4$	0.296 g

- Fill up with Aqua dest. to 750 ml
- Set pH to 7.2

$CaCl_2$	0.277 g

- Fill up with Aqua dest. to 1000 ml
- Set pH to 7.2

6.2 Vibrating sphere calibration

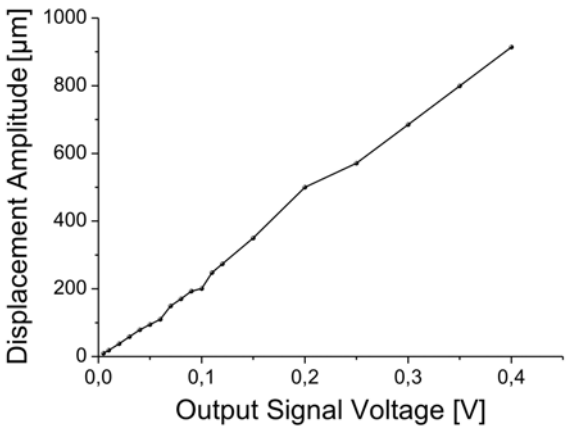

Figure 49: Vibrating sphere calibration. Displacement amplitude of the vibrating sphere (peak to peak) as a function of PC output signal.

6.3 Flow calibration

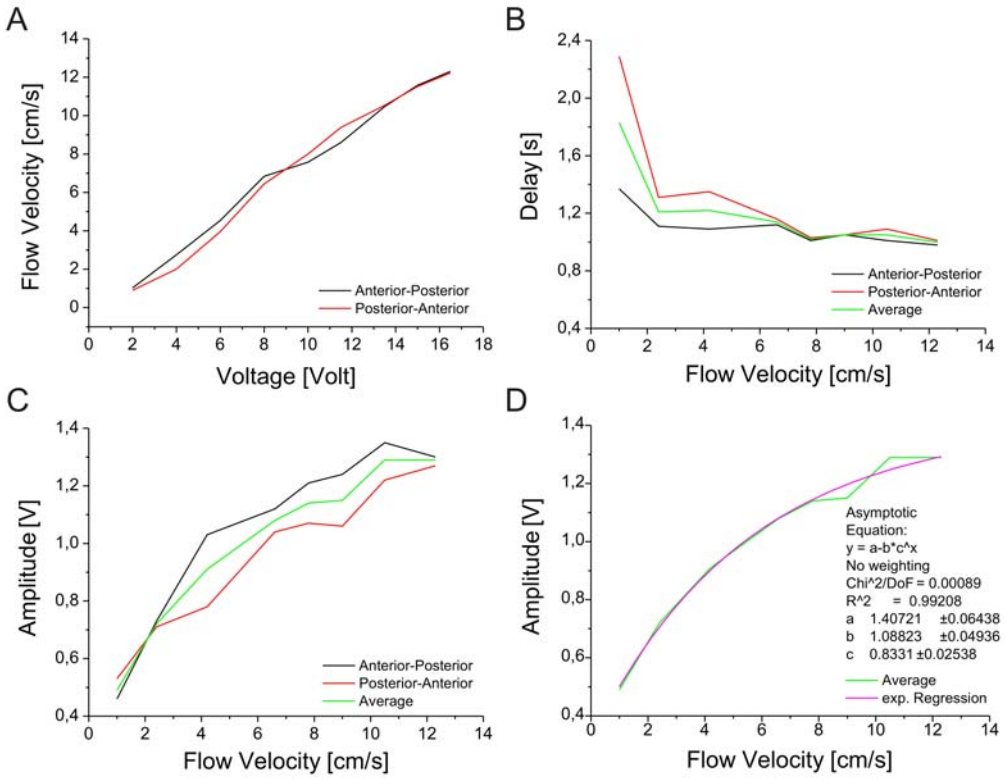

Figure 50: Flow Calibration and Quantification with Particle Imaging Velocimetry (PIV) and Hot Wire Anemometry. A: PIV measurement of flow. Flow velocity as a function of Voltage (Amplifier signal for propeller). Black: Flow in AP direction. Red: Flow in PA direction. Green: Average across both lines. **B**: Time past until Flow maximum is reached (delay) as a function of flow velocity (see A). Black: Flow in AP direction. Red: Flow in PA direction. Green: Average across both lines. **C**: Amplitude of Voltage (anemometer) as a function of flow velocity. Black: Flow in AP direction. Red: Flow in PA direction. Green: Average across both lines. **D**: Exponential regression across average (Graph in C). Green: Average. Pink: Regression curve. Equation is shown in graph.

6.4 Excitation patterns of MON neurons

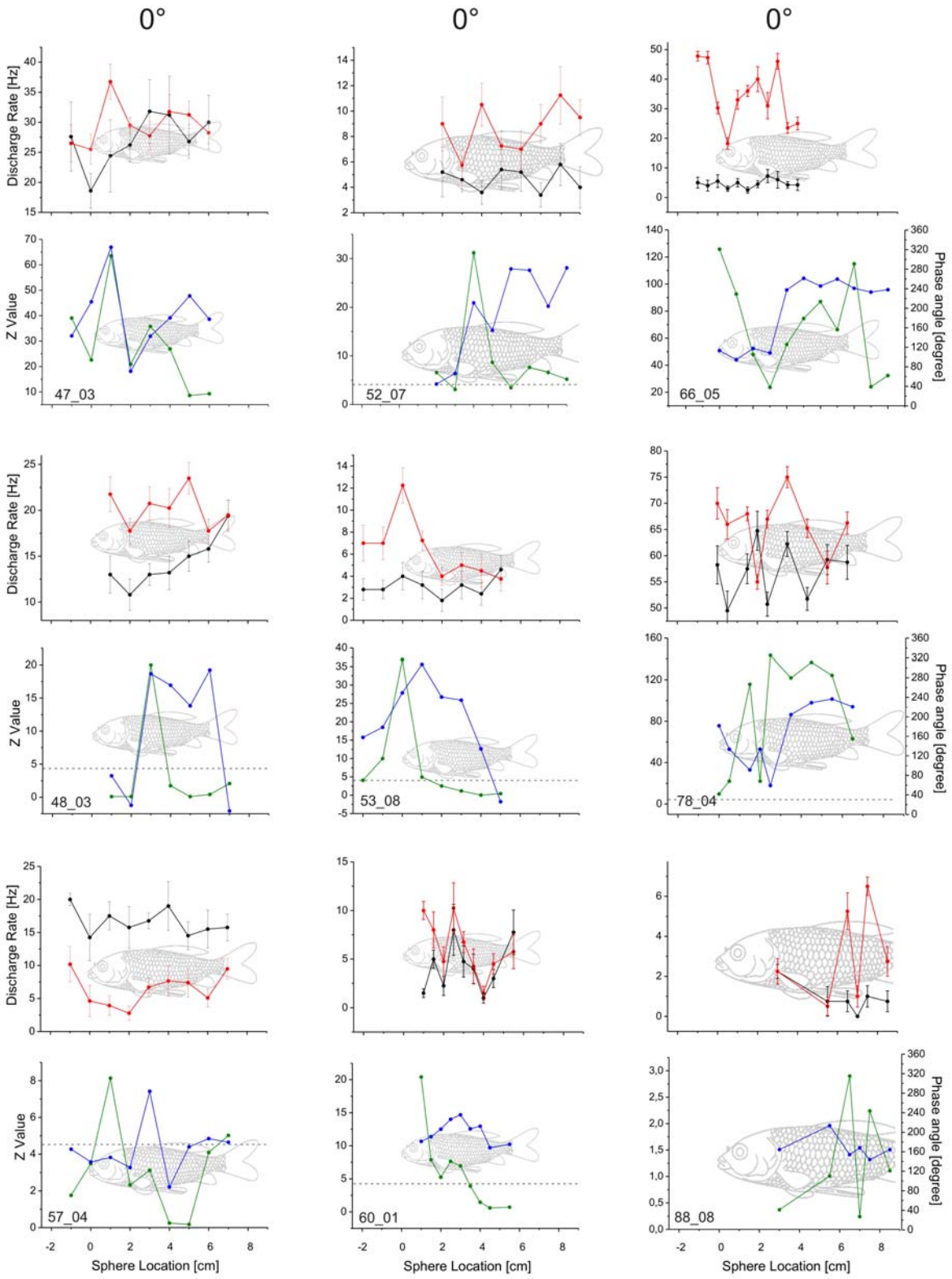

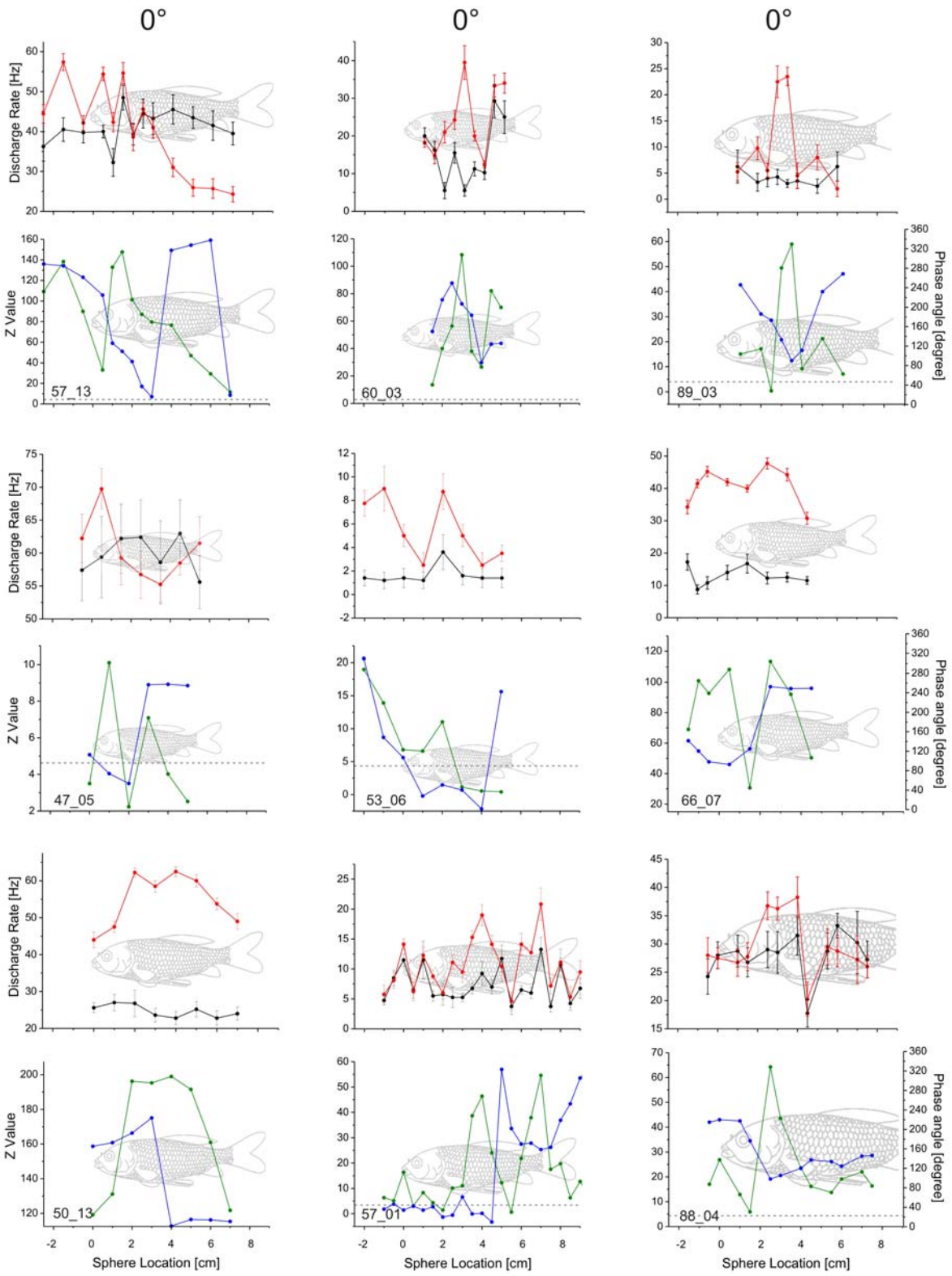
0°
0°
0°
Discharge Rate [Hz]
Z Value
Phase angle [degree]
57_13
60_03
89_03
47_05
53_06
66_07
50_13
57_01
88_04
Sphere Location [cm]

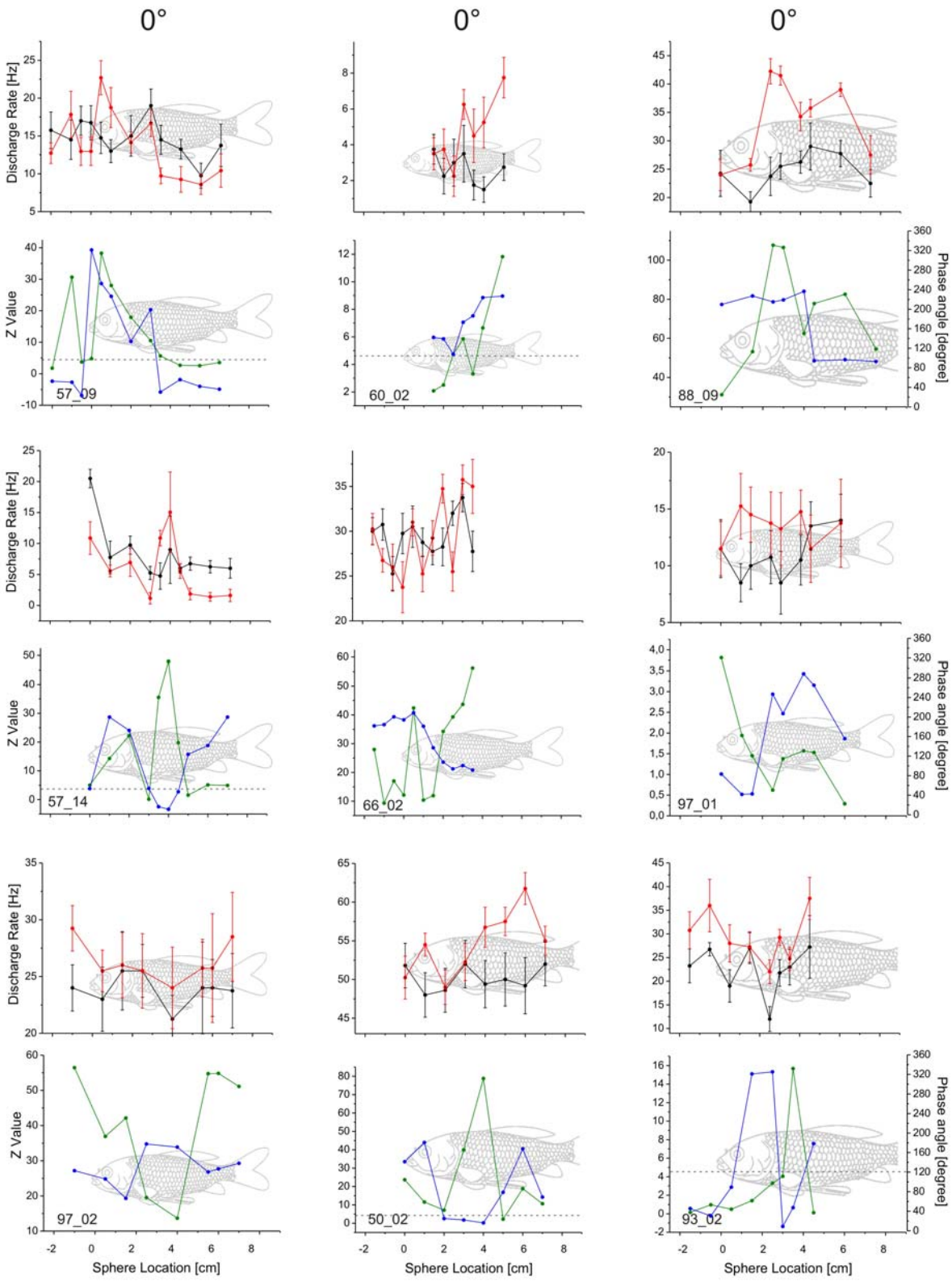
0°
0°
0°
Discharge Rate [Hz]
Z Value
Phase angle [degree]
57_09
60_02
88_09
57_14
66_02
97_01
97_02
50_02
93_02
Sphere Location [cm]

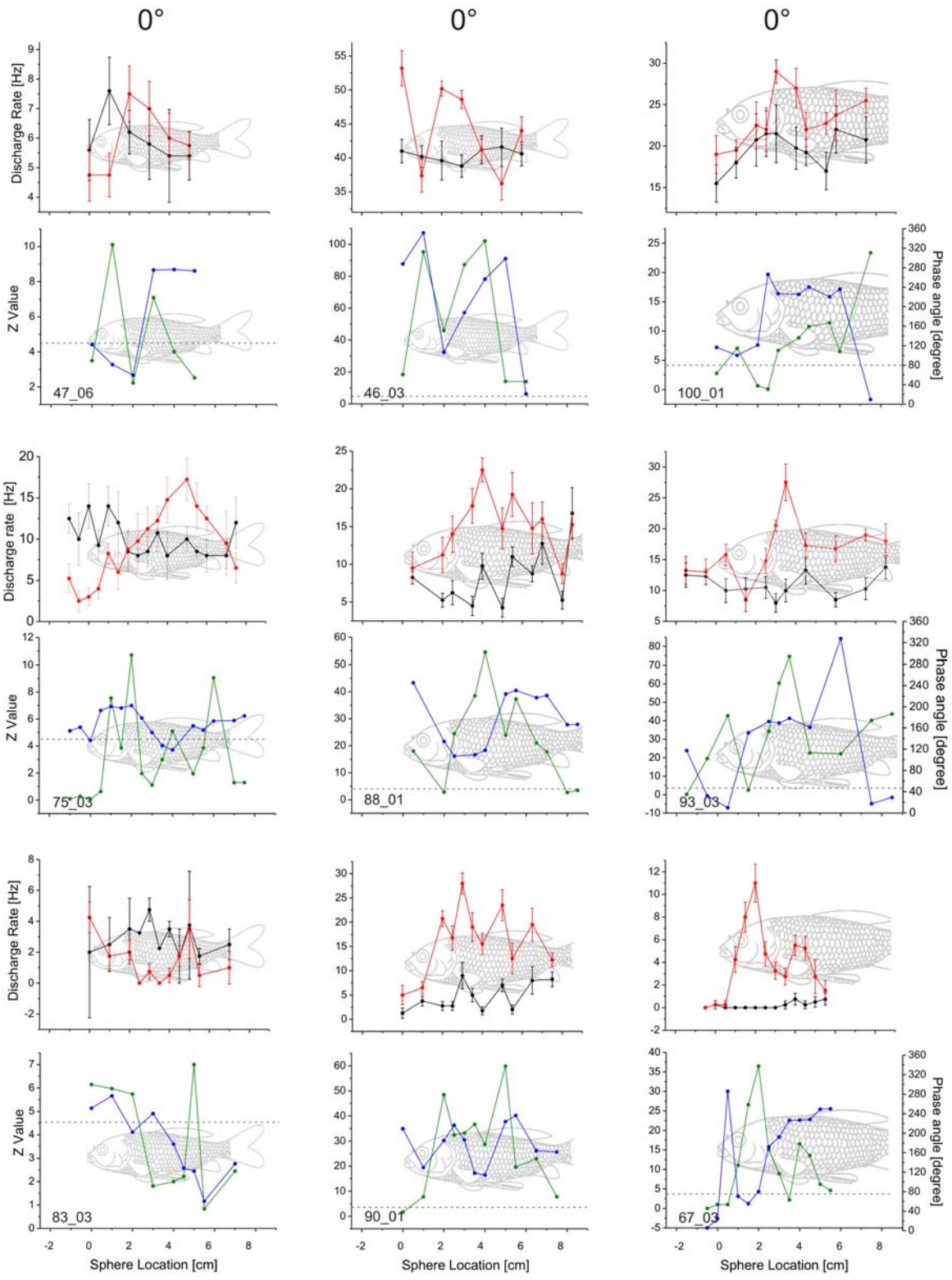
0°
0°
0°
Discharge Rate [Hz]
Z Value
Phase angle [degree]
47_06
46_03
100_01
Discharge rate [Hz]
75_03
88_01
93_03
83_03
90_01
67_03
Sphere Location [cm]

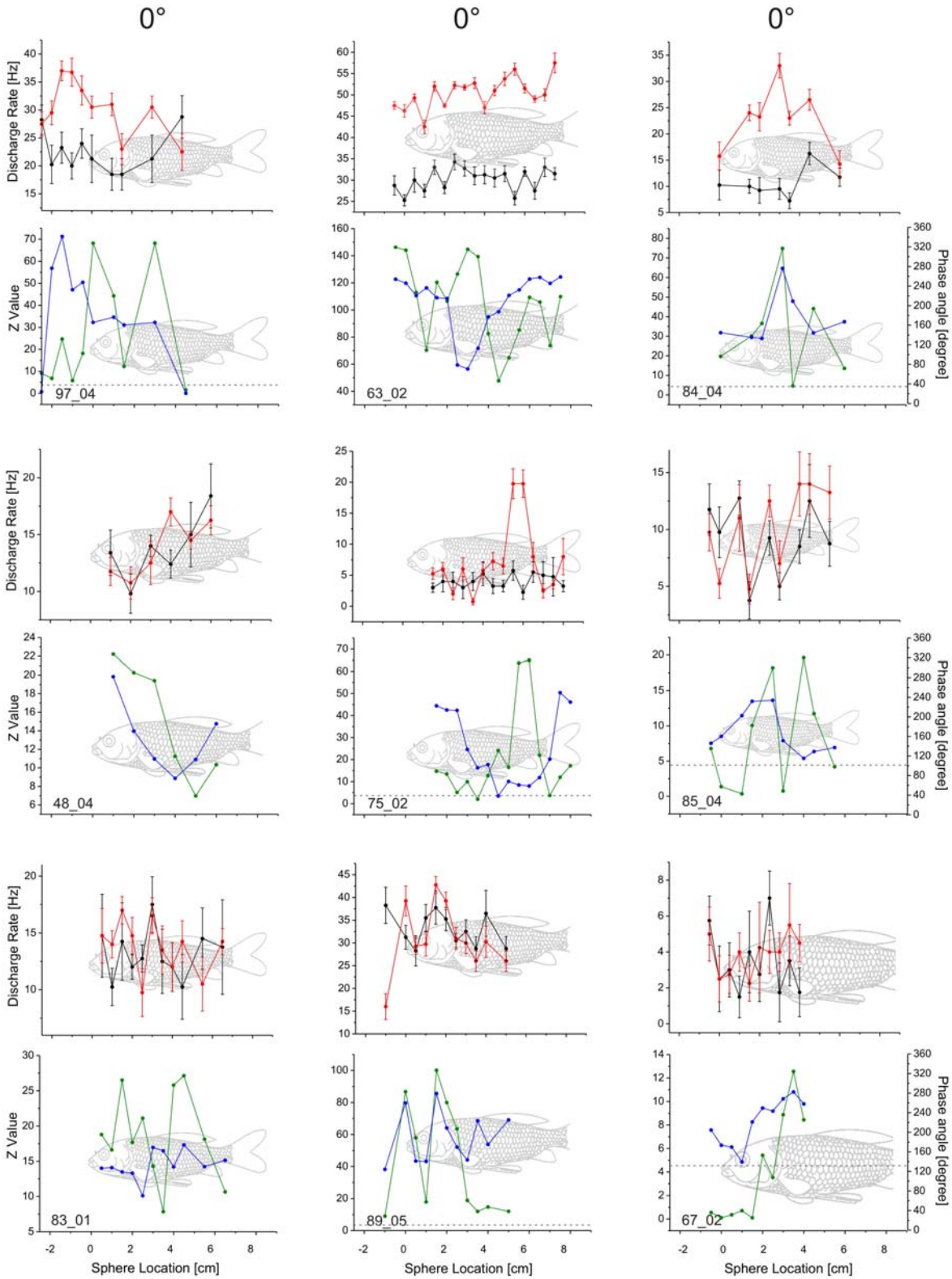
0°
0°
0°
Discharge Rate [Hz]
Z Value
Phase angle [degree]
97_04
63_02
84_04
48_04
75_02
85_04
83_01
89_05
67_02
Sphere Location [cm]

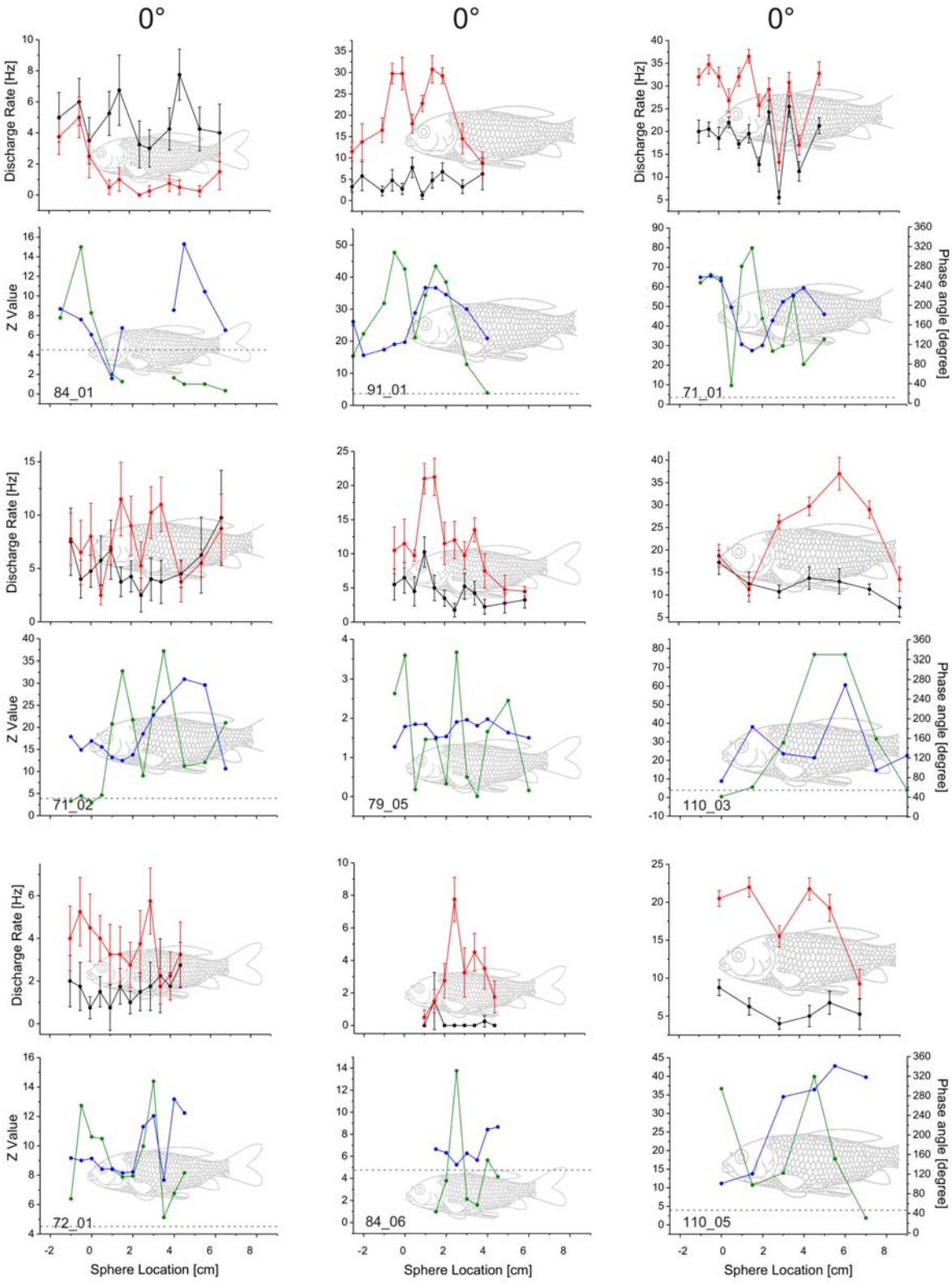
0°
0°
0°
Discharge Rate [Hz]
Z Value
Phase angle [degree]
84_01
91_01
71_01
71_02
79_05
110_03
72_01
84_06
110_05
Sphere Location [cm]

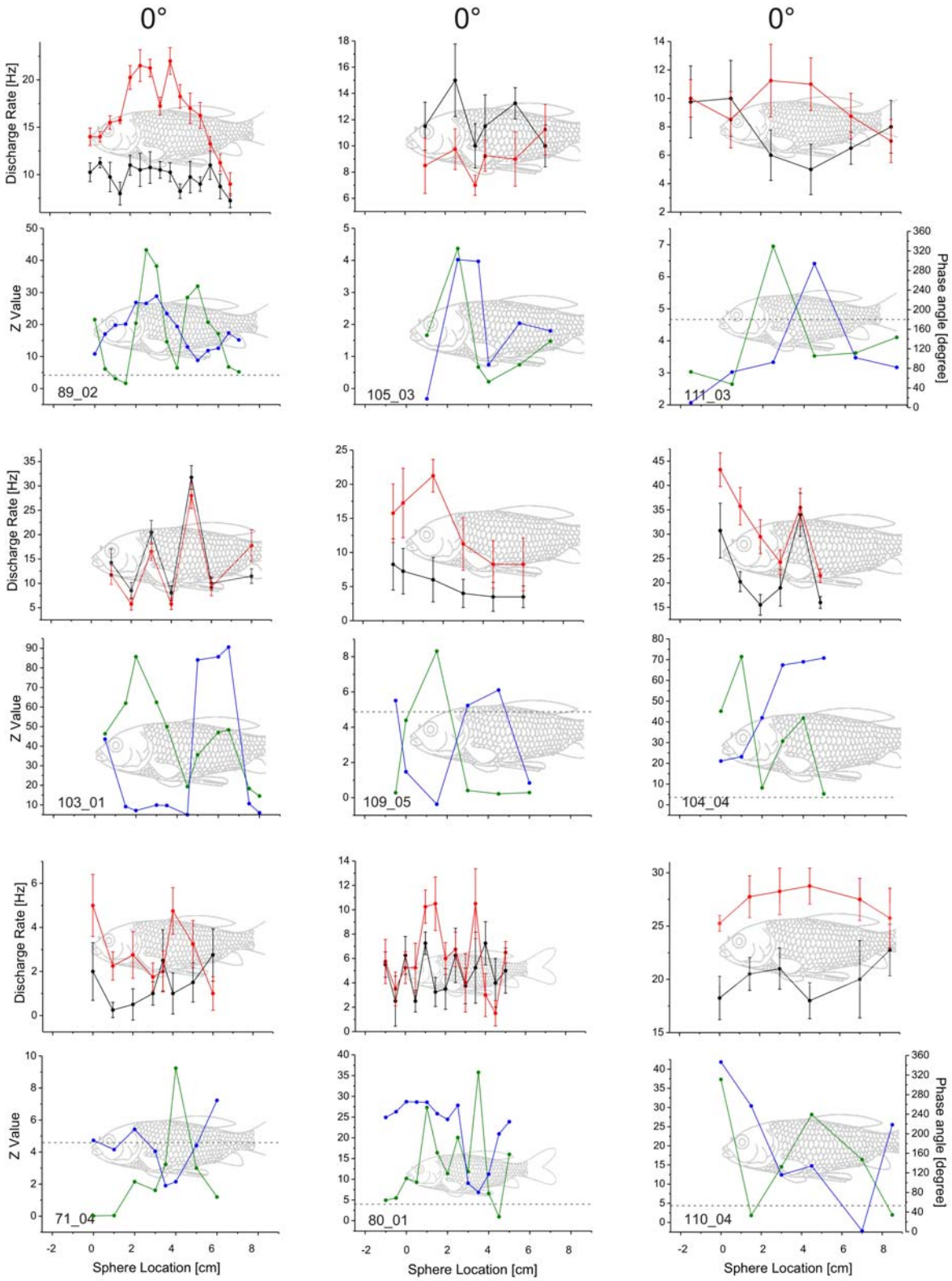
0°
0°
0°
Discharge Rate [Hz]
Z Value
Phase angle [degree]
89_02
105_03
111_03
103_01
109_05
104_04
71_04
80_01
110_04
Sphere Location [cm]
Sphere Location [cm]
Sphere Location [cm]

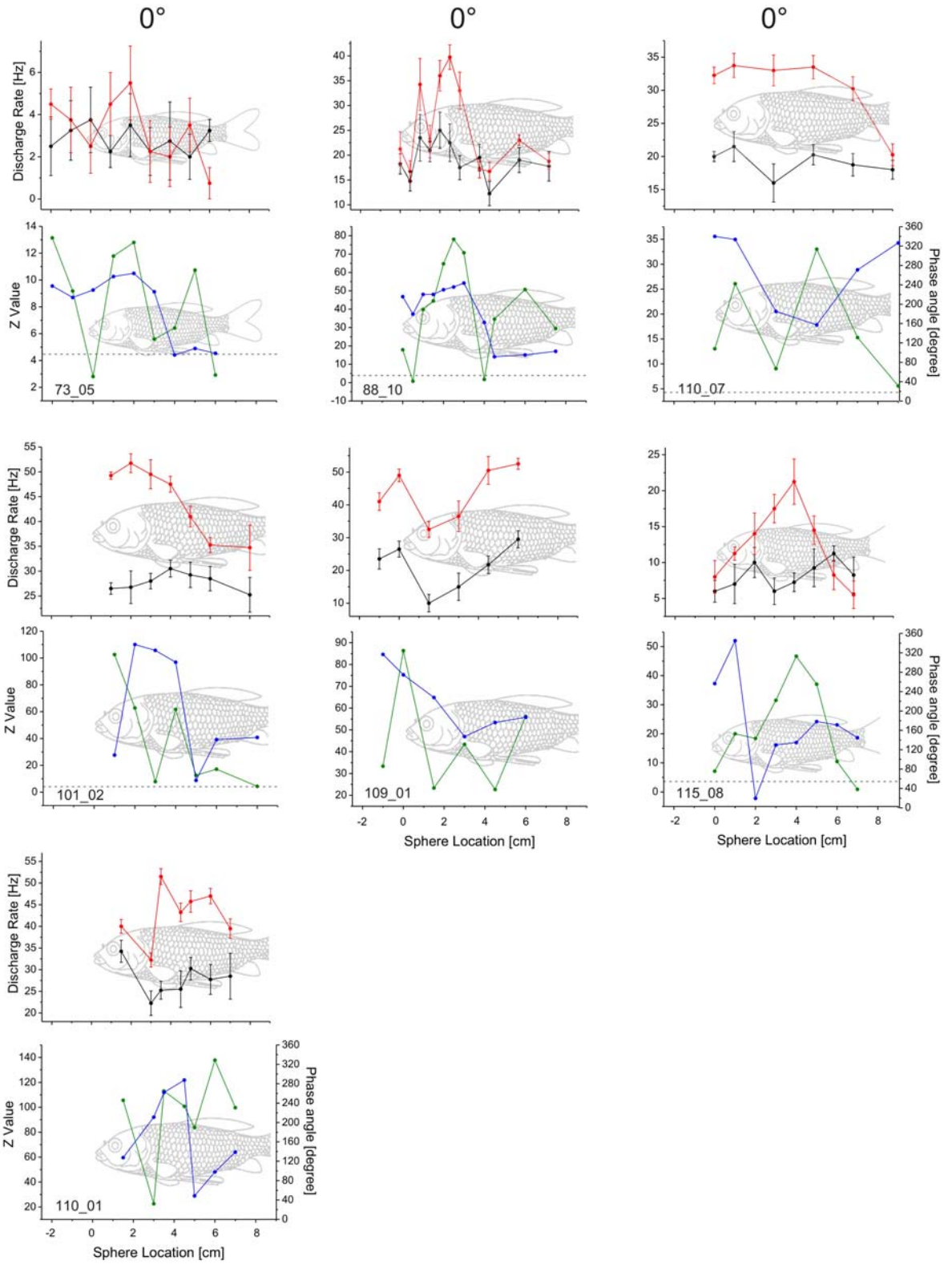

Figure 51: Spatial excitation patterns of MON units obtained by stimulating the lateral line with a sphere creating sinusoidal vibrations parallel to the fish (angle of vibration 0°, sphere radius 8 mm, frequency 50 Hz, sphere displacements between 200 and 650 µm, 1 cm distance between sphere and fish). **Upper graphs**: Ongoing discharge rates (black lines) and evoked rates (red lines) as a function of sphere location along the side of the fish. Vertical bars represent standard deviation. **Lower graphs**: Z-values (green lines, left Y-axis) and mean phase angles (blue lines, right Y-axis) as a function of sphere location along the side of the fish. The horizontal grey dashed line indicates the Z-value criterion ($Z \geq 4.6$). The fish in the background is drawn to scale. The numeral (bottom left) indicates experiment number.

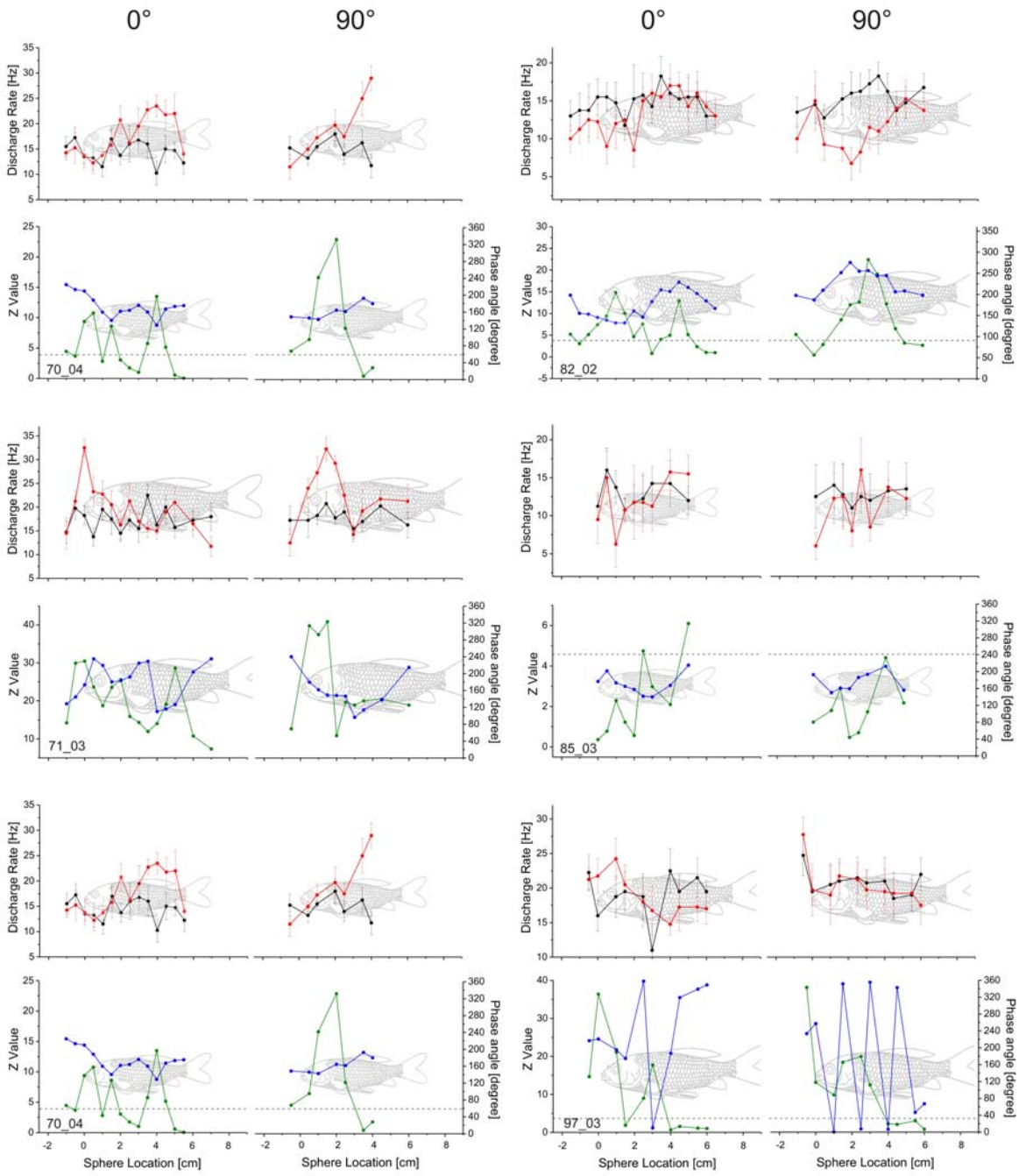
0°
90°
0°
90°
Discharge Rate [Hz]
Z Value
Phase angle [degree]
70_04
82_02
71_03
85_03
70_04
97_03
Sphere Location [cm]

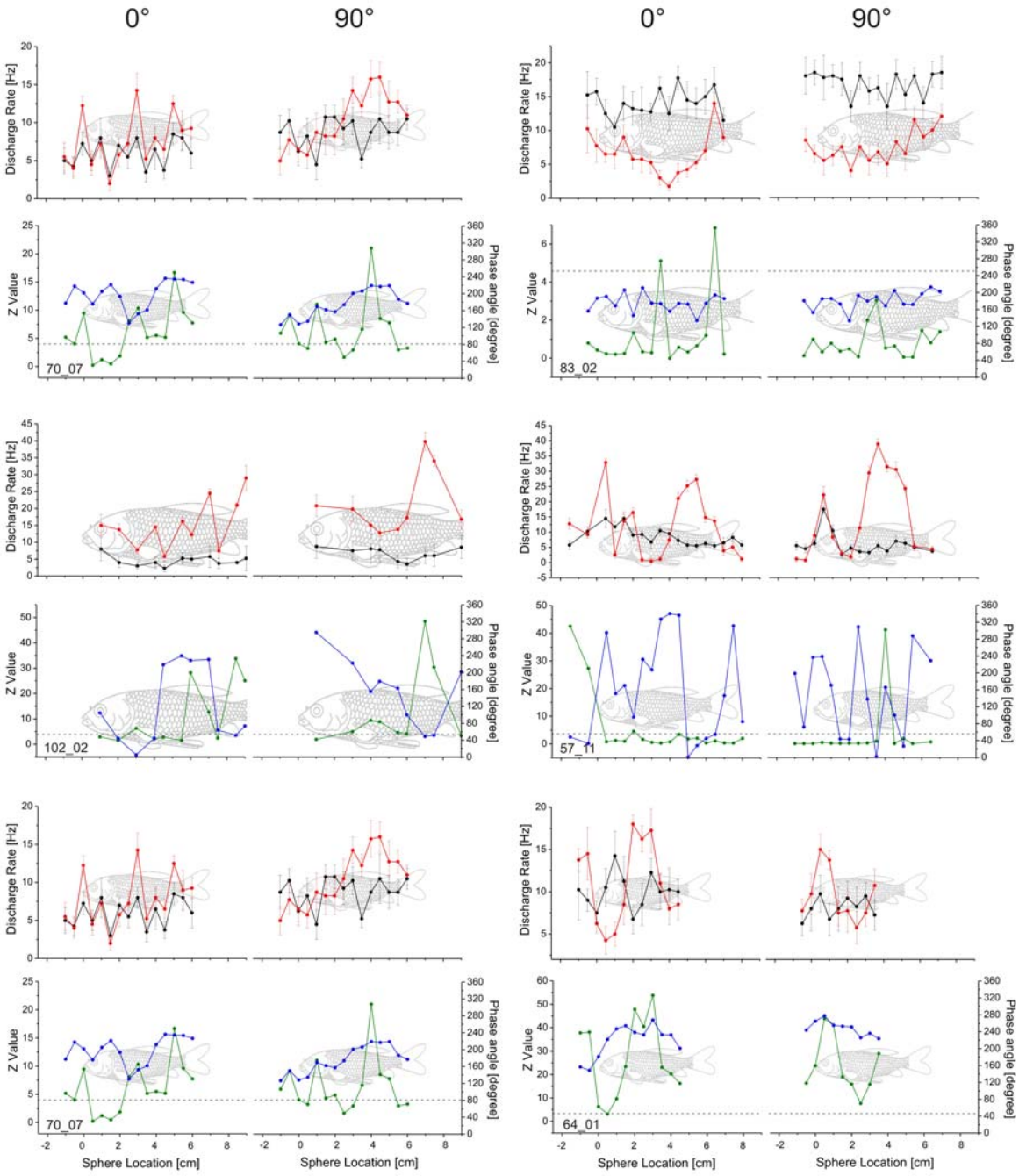

Figure 52: Spatial excitation patterns of MON units obtained by stimulating the lateral line with a sphere creating sinusoidal vibrations parallel and perpendicular to the fish (angle of vibration 0° and 90°, sphere radius 8 mm, frequency 50 Hz, sphere displacements between 200 and 650 µm, 1 cm distance between sphere and fish). **Upper graphs**: Ongoing discharge rates (black lines) and evoked rates (red lines) as a function of sphere location along the side of the fish. Vertical bars represent standard deviation. **Lower graphs**: Z-values (green lines, left Y-axis) and mean phase angles (blue lines, right Y-axis) as a function of sphere location along the side of the fish. The horizontal grey dashed line indicates the Z-value criterion ($Z \geq 4.6$). The fish in the background is drawn to scale. The numeral (bottom left) indicates experiment number.

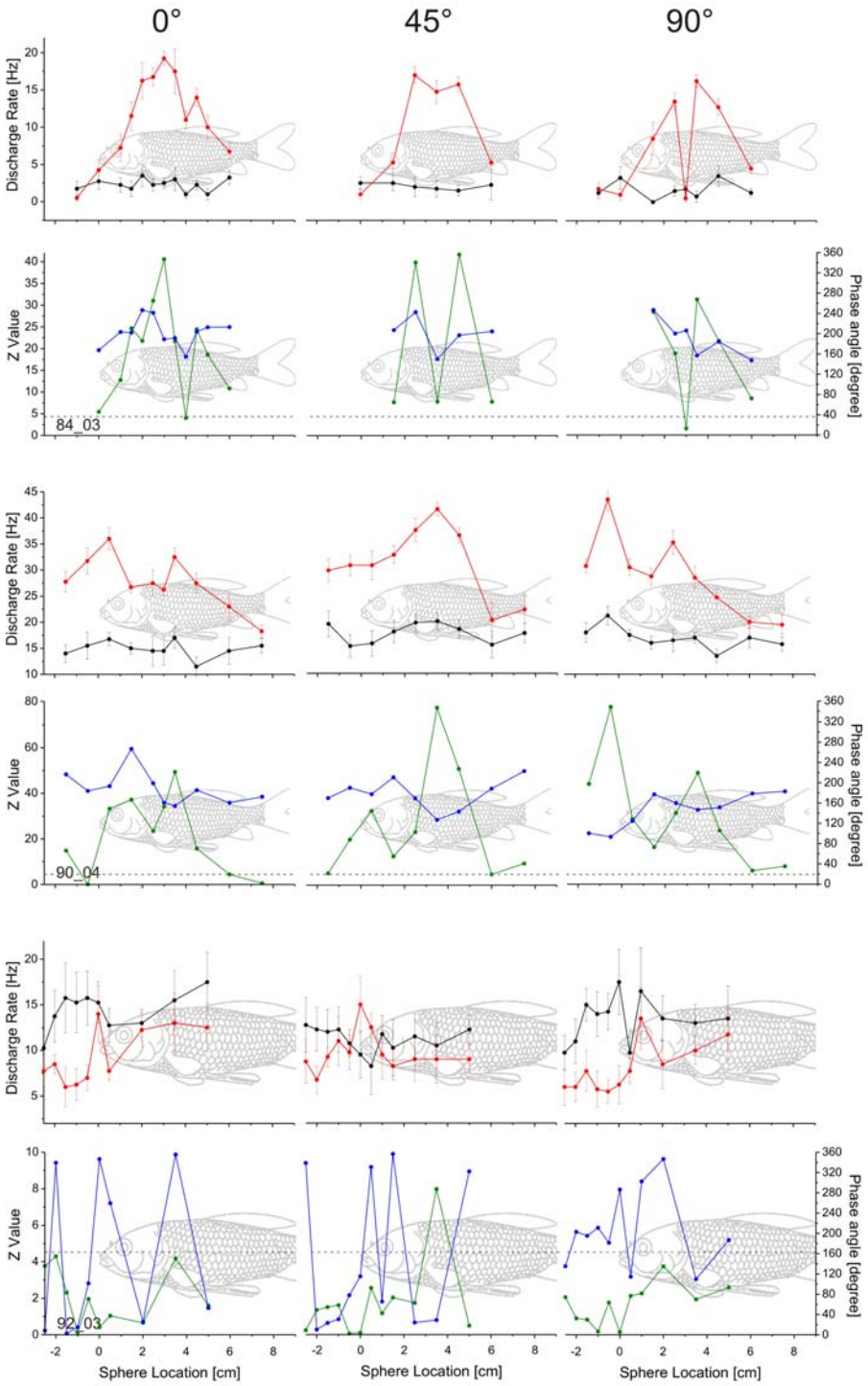
0°
45°
90°
Discharge Rate [Hz]
Z Value
Phase angle [degree]
84_03
90_04
92_03
Sphere Location [cm]

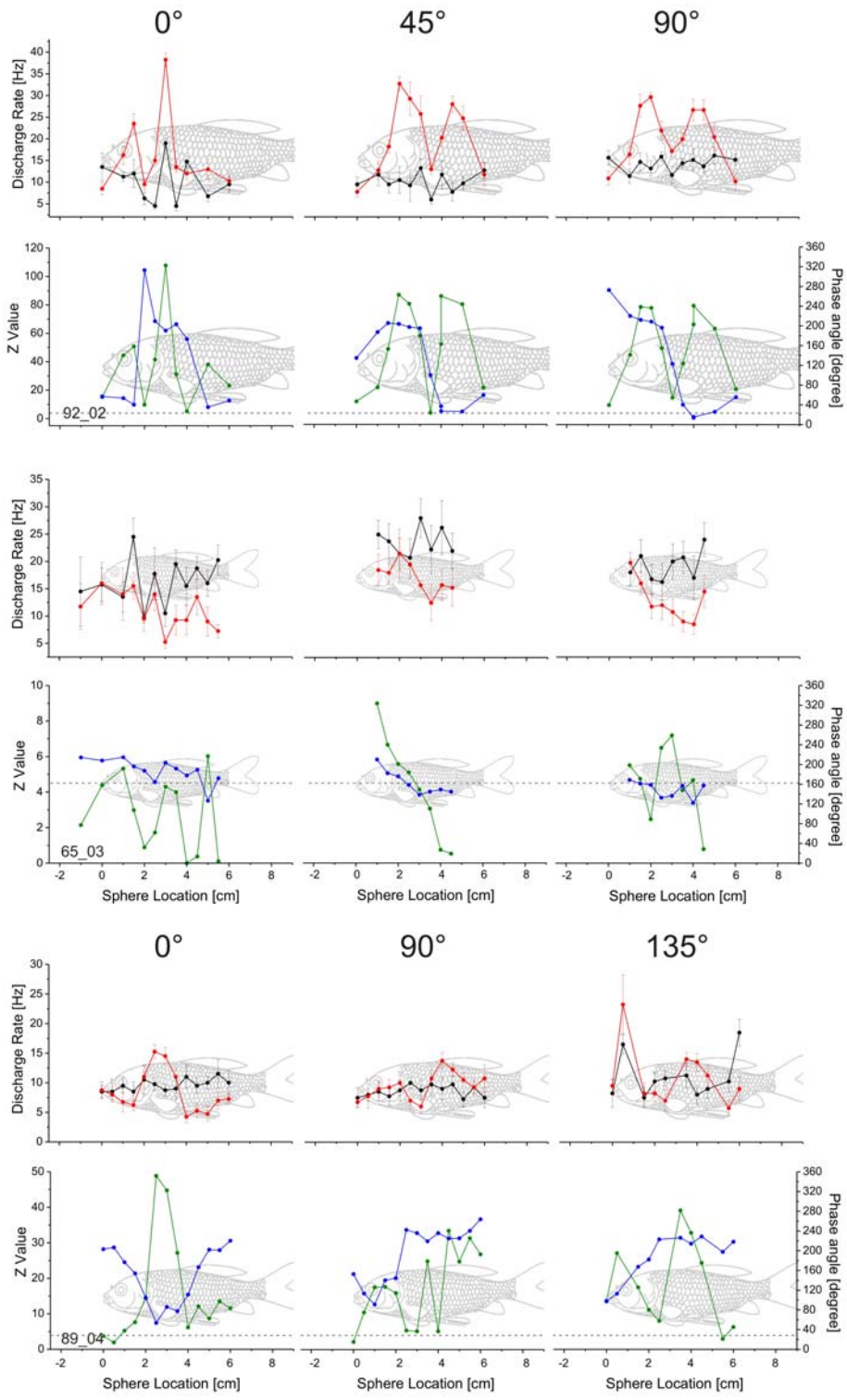

Figure 53: Spatial excitation patterns of MON units obtained by stimulating the lateral line with a sphere creating sinusoidal vibrations in three different angles (angle of vibration 0°, 45°, 90° and/or 135°, sphere radius 8 mm, frequency 50 Hz, sphere displacements between 200 and 650 µm, 1 cm distance between sphere and fish). **Upper graphs:** Ongoing discharge rates (black lines) and evoked rates (red lines) as a function of sphere location along the side of the fish. Vertical bars represent standard deviation. **Lower graphs:** Z-values (green lines, left Y-axis) and mean phase angles (blue lines, right Y-axis) as a function of sphere location along the side of the fish. The horizontal grey dashed line indicates the Z-value criterion ($Z \geq 4.6$). The fish in the background is drawn to scale. The numeral (bottom left) indicates experiment number.

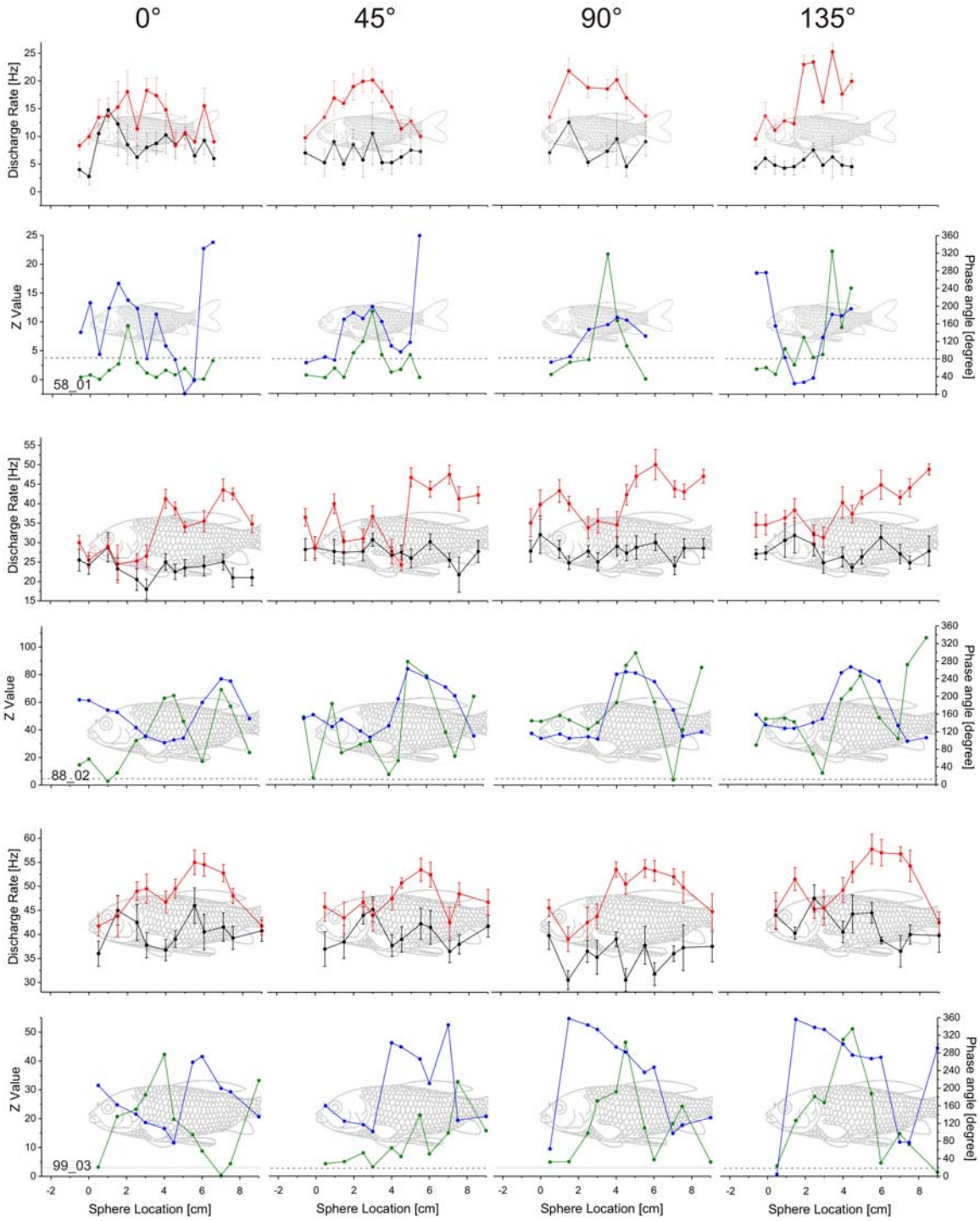
0°
45°
90°
135°
Discharge Rate [Hz]
Z Value
Phase angle [degree]
58_01
88_02
99_03
Sphere Location [cm]

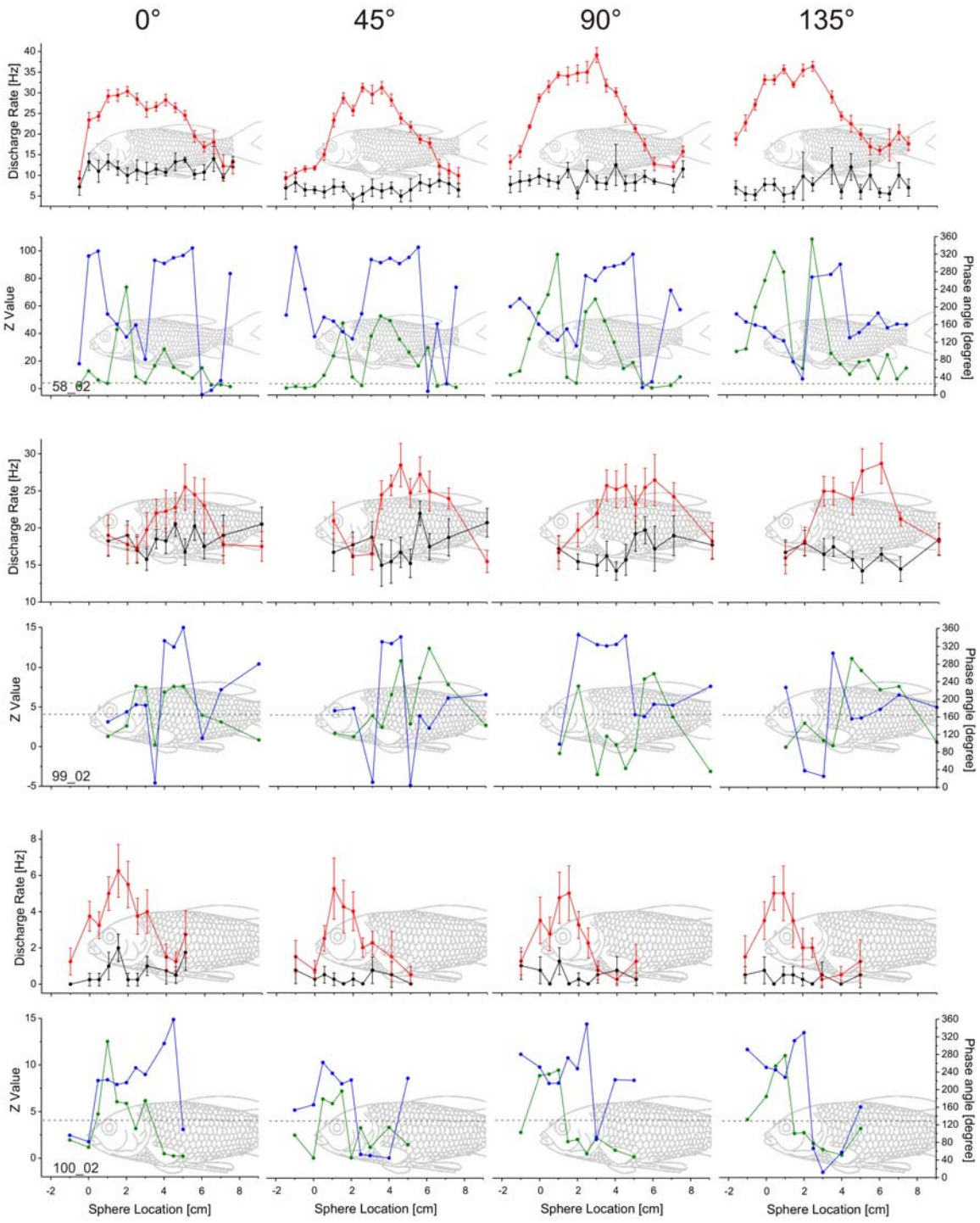
0°
45°
90°
135°
Discharge Rate [Hz]
Z Value
Phase angle [degree]
58_02
99_02
100_02
Sphere Location [cm]

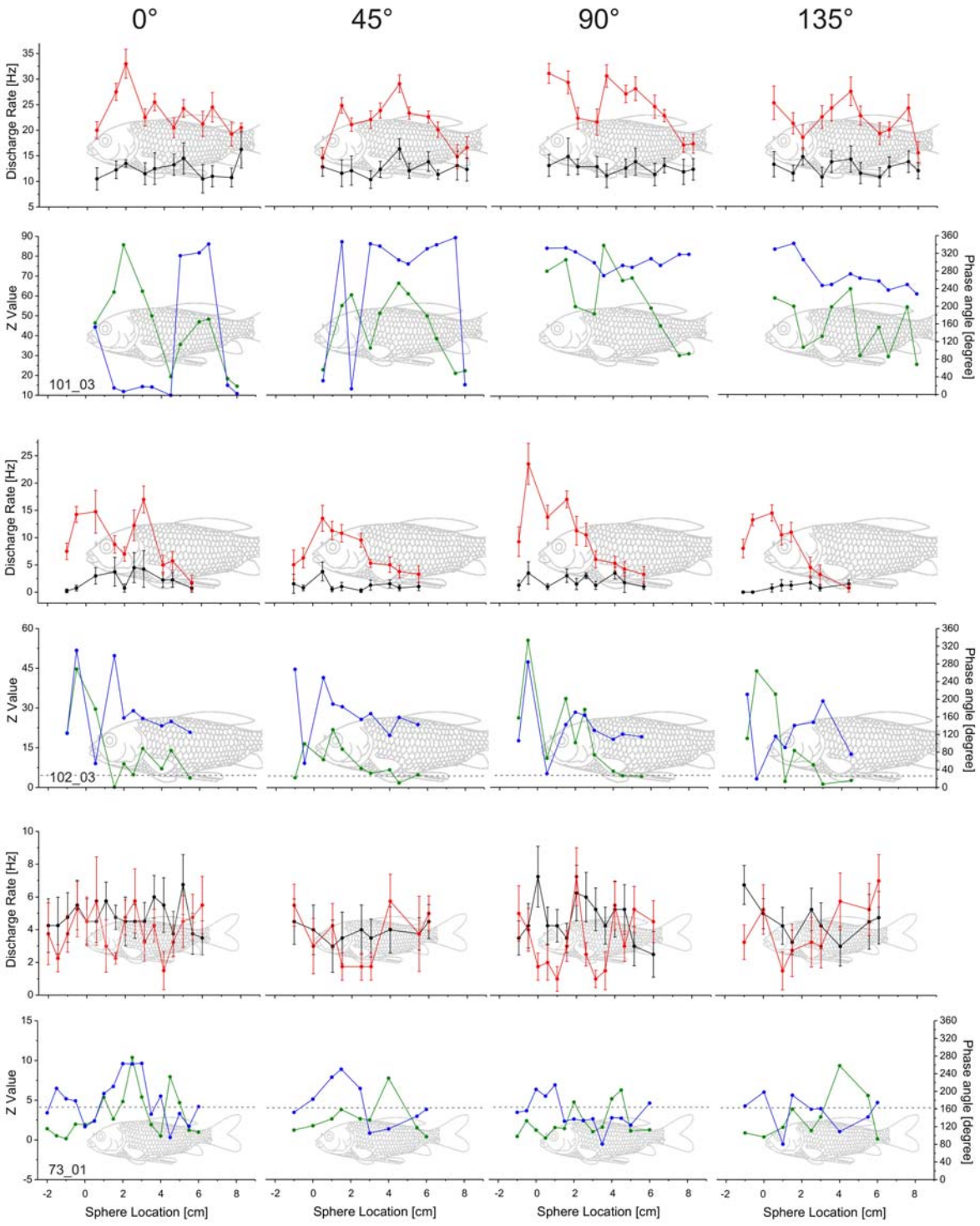
0°
45°
90°
135°
Discharge Rate [Hz]
Z Value
Phase angle [degree]
101_03
102_03
73_01
Sphere Location [cm]

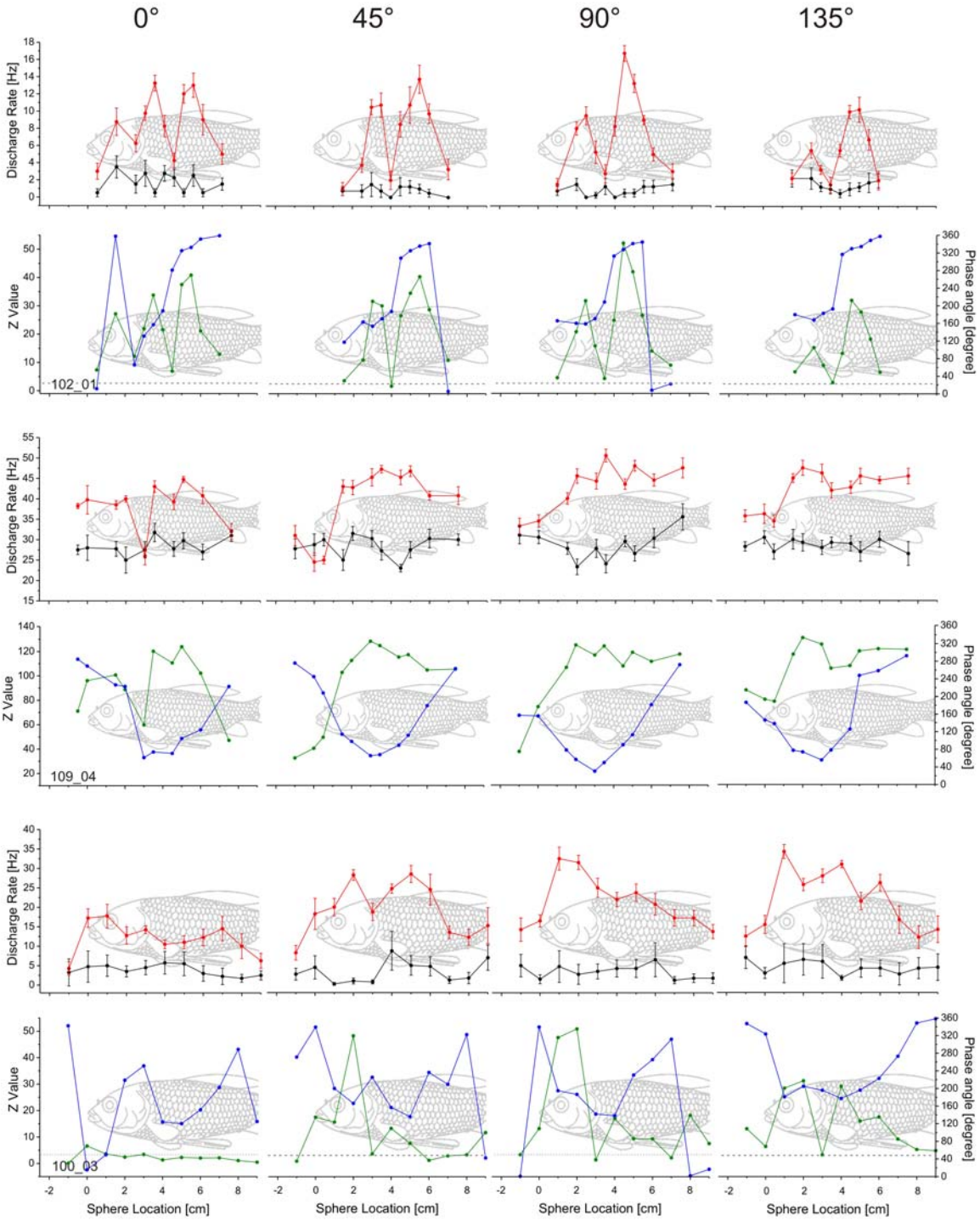
0°
45°
90°
135°
Discharge Rate [Hz]
Z Value
Phase angle [degree]
102_01
109_04
100_03
Sphere Location [cm]

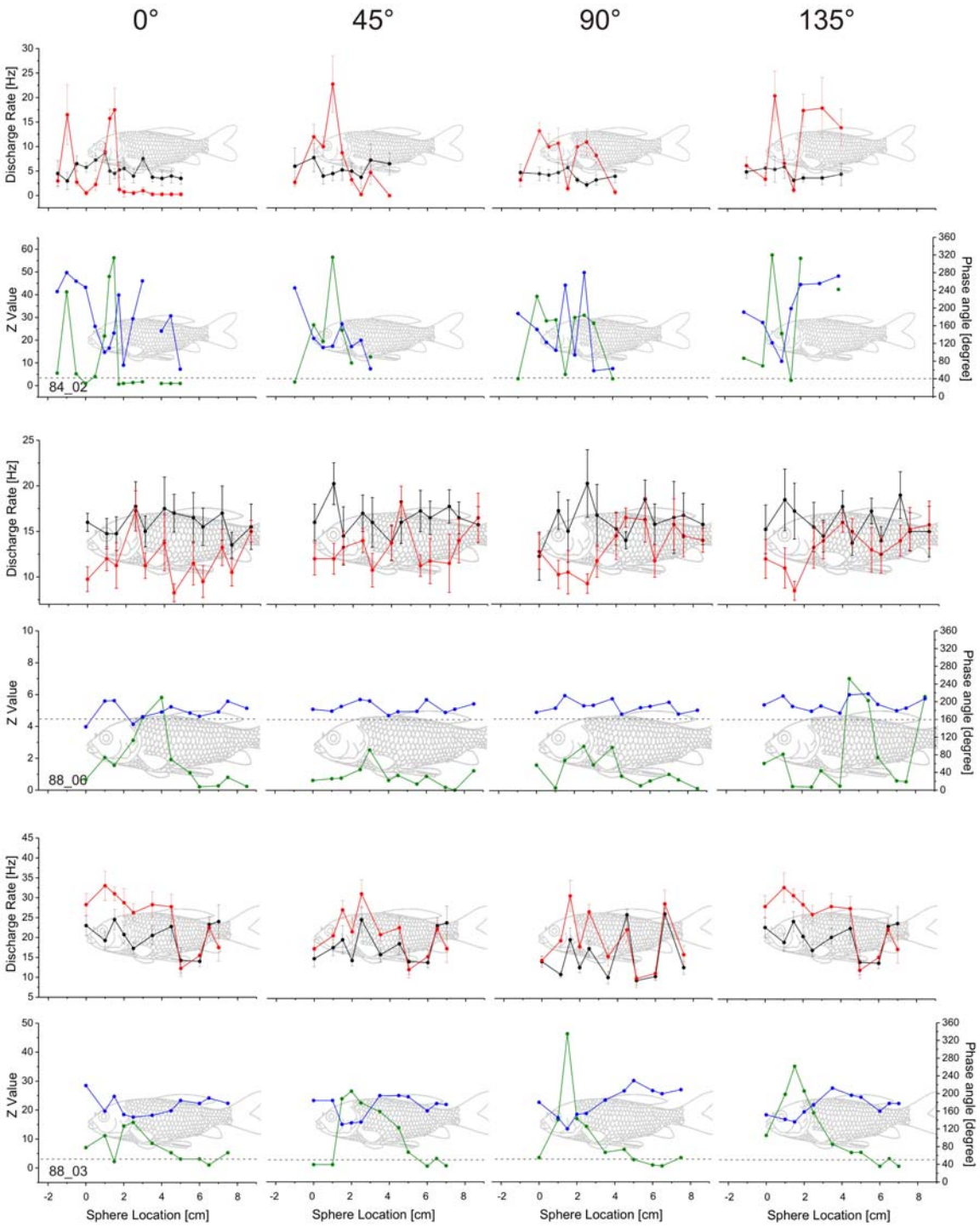
0°
45°
90°
135°
Discharge Rate [Hz]
Z Value
Phase angle [degree]
84_02
88_00
88_03
Sphere Location [cm]

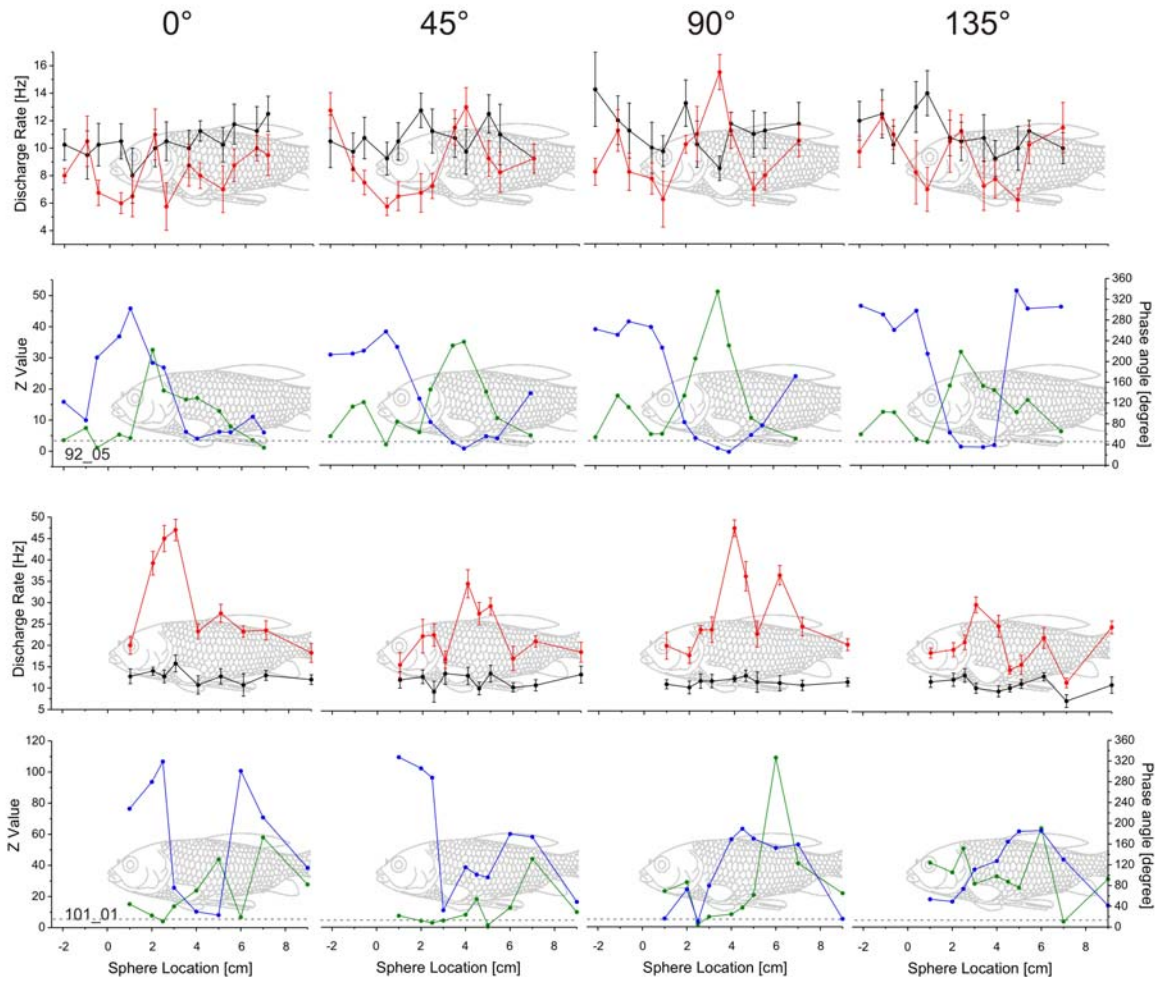

Figure 54: Spatial excitation patterns of MON units obtained by stimulating the lateral line with a sphere creating sinusoidal vibrations in different angles (angle of vibration 0°, 45°, 90° and/or 135°, sphere radius 8 mm, frequency 50 Hz, sphere displacements between 200 and 650 µm, 1 cm distance between sphere and fish). **Upper graphs:** Ongoing discharge rates (black lines) and evoked rates (red lines) as a function of sphere location along the side of the fish. Vertical bars represent standard deviation. **Lower graphs:** Z-values (green lines, left Y-axis) and mean phase angles (blue lines, right Y-axis) as a function of sphere location along the side of the fish. The horizontal grey dashed line indicates the Z-value criterion ($Z \geq 4.6$). The fish in the background is drawn to scale. The numeral (bottom left) indicates experiment number.

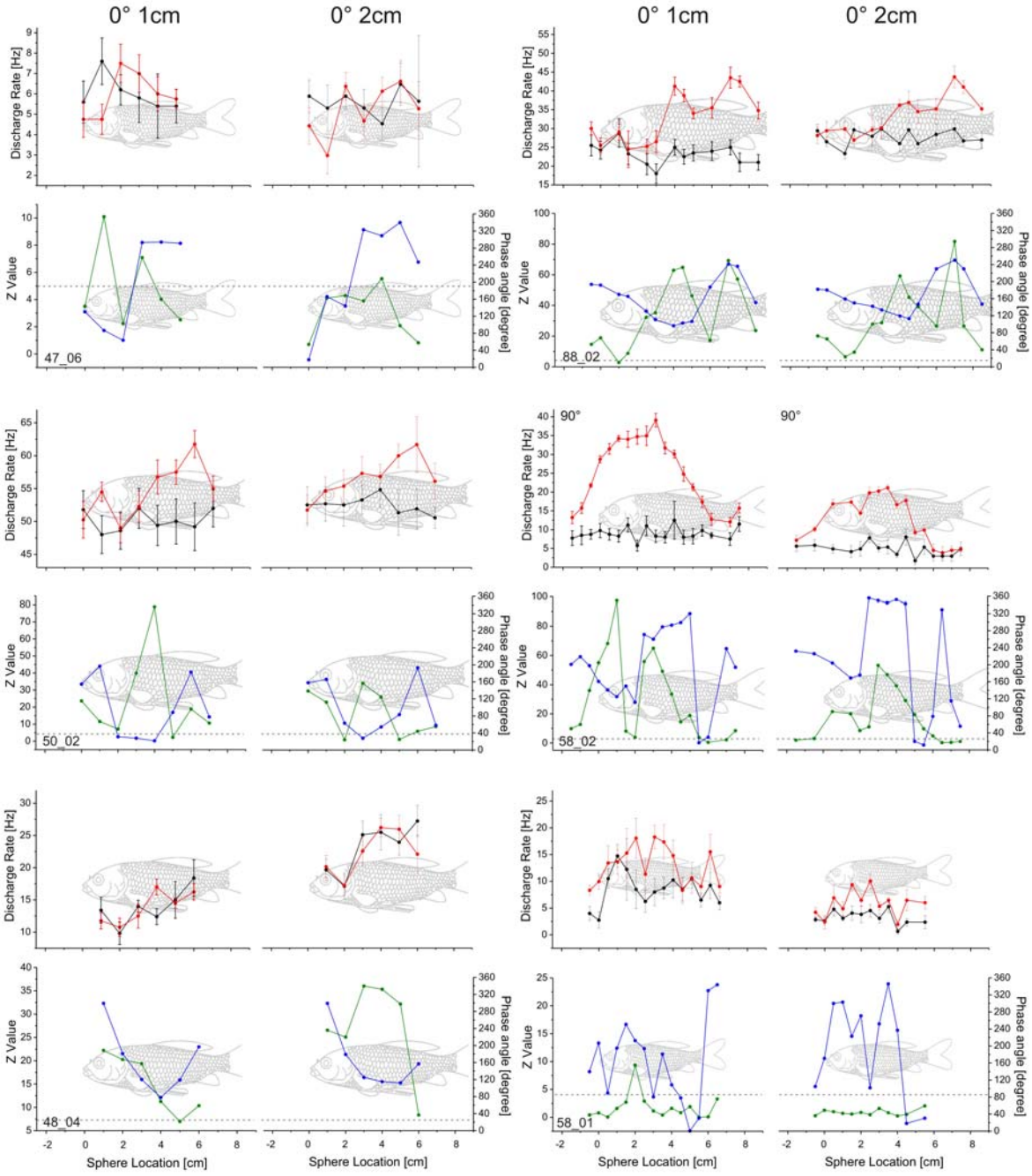

Figure 55: Spatial excitation patterns of MON units obtained by stimulating the lateral line with a sphere creating sinusoidal vibrations parallel to the fish (angle of vibration 0°, sphere radius 8 mm, frequency 50 Hz, sphere displacements between 200 and 650 µm, 1 and 2 cm distance between sphere and fish). **Upper graphs:** Ongoing discharge rates (black lines) and evoked rates (red lines) as a function of sphere location along the side of the fish. Vertical bars represent standard deviation. **Lower graphs:** Z-values (green lines, left Y-axis) and mean phase angles (blue lines, right Y-axis) as a function of sphere location along the side of the fish. The horizontal grey dashed line indicates the Z-value criterion ($Z \geq 4.6$). The fish in the background is drawn to scale. The numeral (bottom left) indicates experiment number.

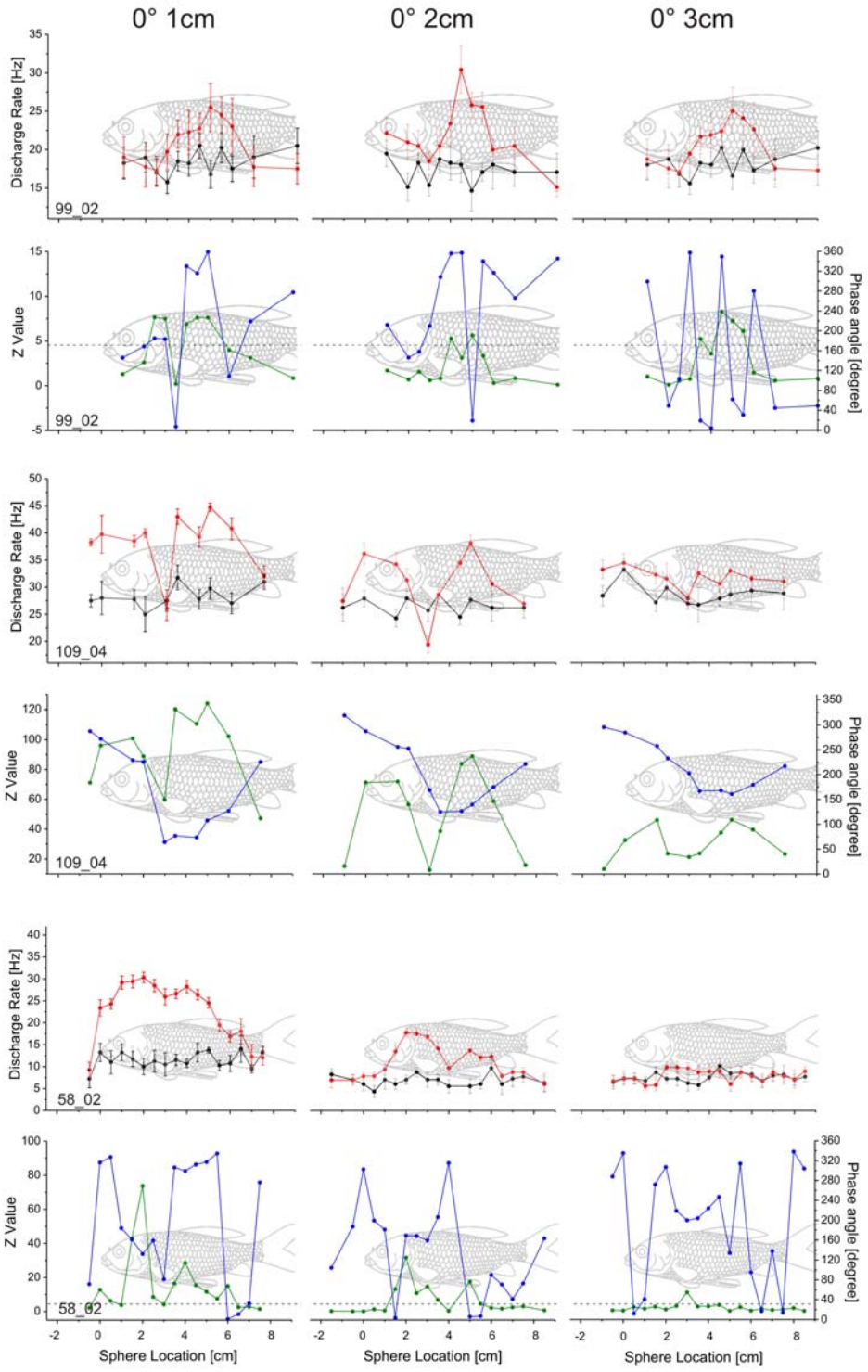
0° 1cm
0° 2cm
0° 3cm
Discharge Rate [Hz]
99_02
Z Value
Phase angle [degree]
109_04
58_02
Sphere Location [cm]

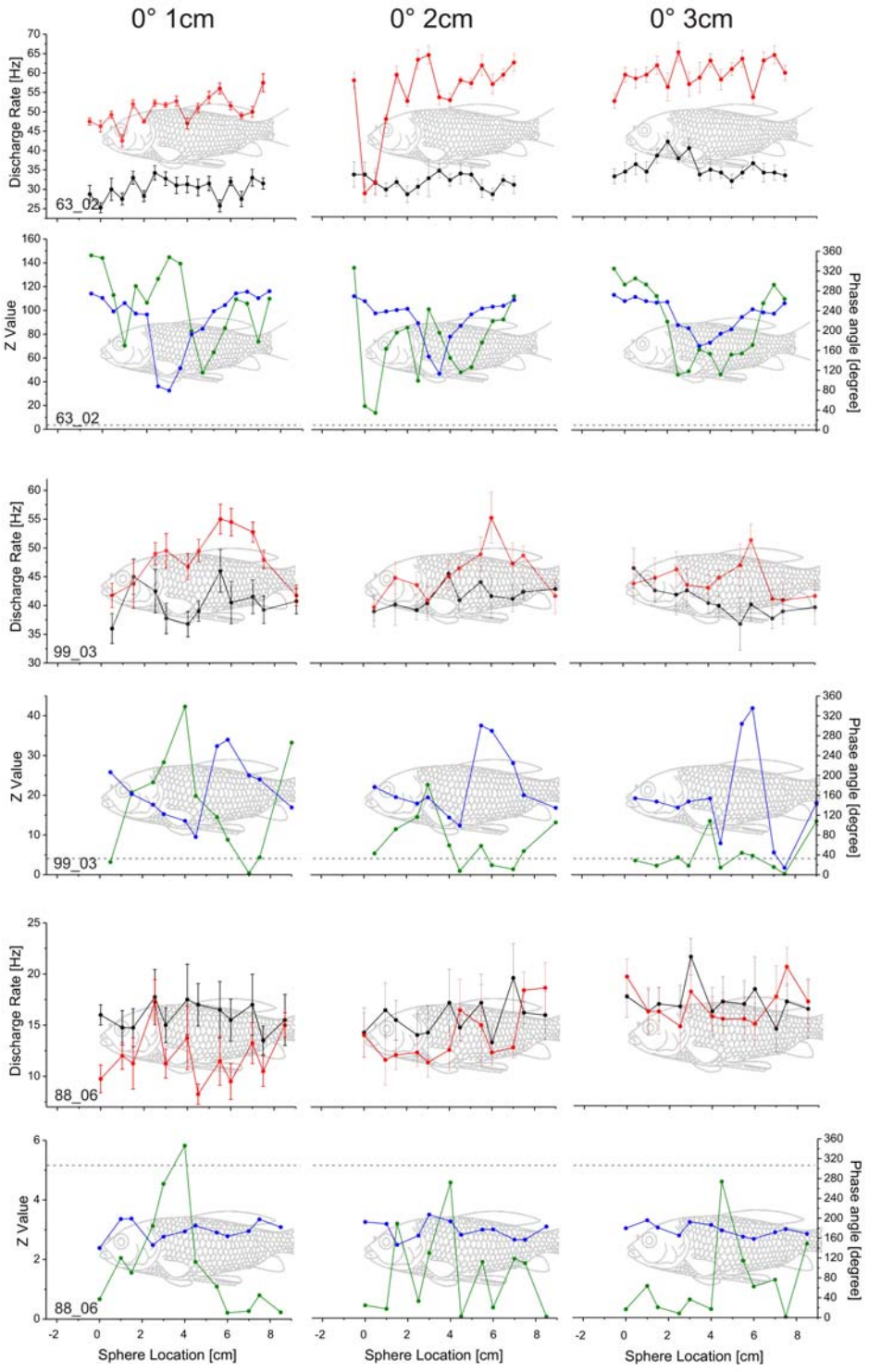

Figure 56: Spatial excitation patterns of MON units obtained by stimulating the lateral line with a sphere creating sinusoidal vibrations in three different distances parallel to the fish (angle of vibration 0°, sphere radius 8 mm, frequency 50 Hz, sphere displacements between 200 and 650 µm, 1 , 2 and 3 cm distance between sphere and fish). **Upper graphs:** Ongoing discharge rates (black lines) and evoked rates (red lines) as a function of sphere location along the side of the fish. Vertical bars represent standard deviation. **Lower graphs:** Z-values (green lines, left Y-axis) and mean phase angles (blue lines, right Y-axis) as a function of sphere location along the side of the fish. The horizontal grey dashed line indicates the Z-value criterion ($Z \geq 4.6$). The fish in the background is drawn to scale. The numeral (bottom left) indicates experiment number.

ERKLÄRUNG

Hiermit erkläre ich an Eides statt, dass ich für die vorliegende Arbeit keine anderen als die angegebenen Hilfsmittel benutzt habe, und dass die inhaltlich und wörtlich aus anderen Werken entnommenen Stellen und Zitate als solche gekennzeichnet sind.

Silke Künzel

Bonn, Oktober 2009